Scaling Analysis for US-APWR Small Break LOCAs

Non-Proprietary Version

October 2010

PREFACE

M-RELAP5, which is applied to US-APWR Small Break LOCA (SBLOCA) analyses, has been developed in conformance to the Regulatory Guide 1.203, “Transient and Accident Analysis Methods.” In the process of the code development, the regulatory guide requires verification of the adequacy of the experimental test data used for the code assessment. In particular, scalability of the experimental test facilities to the actual plant shall be examined, if the facility is a scaled one.

This report addresses evaluations of the scalability of the experimental test facilities, which are used for the M-RELAP5 code assessment in its application to US-APWR SBLOCA analyses. In addition, scale-up capabilities of the code governing equations, models and correlations are also investigated in the present report.

The present material is a revised scaling analysis report for US-APWR SBLOCAs from the report submitted to the US Nuclear Regulatory Commission (NRC) enclosed in the letter UAP-HF-09568 in December 2009. Primary changes and modifications are followings:

(1) It is clearly stated that the objective of the present scaling analysis, in particular the top-down scaling analysis, is limited to confirming a similarity between the US-APWR SBLOCA and the corresponding integral effects test (IET) data which were obtained using the test facility simulating the existing 4-loop PWRs. The similitude was judged by comparing the nondimensionalized governing parameter and the relative magnitude of other parameters against the governing one between the US-APWR and the IETs. This approach is reasonably acceptable since the US-APWR SBLOCA is similar to that occurring in the existing 4-loop PWRs, and there is no thermal-hydraulic phenomena, processes and system interactions that should be newly addressed for the US-APWR SBLOCA.
(2) Data from the recently performed ROSA/LSTF (Rig of Safety Assessment, Large Scale Test Facility) IB-CL-02 (17% break) IET are included in the scaling analysis. This test is selected because the break size is scaled to the US-APWR 1-ft^2 break where the boil-off PCT occurs.
(3) Code applicability in terms of the break flow and the secondary system behavior is directly investigated in the code assessment using the IET data.
(4) A reduced model examining the blowdown phase from the top-down approach is modified such that the thermal-hydraulic behaviors in the subcooled and saturated regions of the reactor coolant system (RCS) are appropriately represented.
(5) A computer program examined in the present code scale-up capability is updated to the latest version of M-RELAP5 that is explained in Topical Report of MUAP-07013-P (R1) ‘Small Break LOCA Methodology for US-APWR’.

TABLE OF CONTENTS

LIST OF TABLES

LIST OF FIGURES

LIST OF ACRONYMS

ACC	Accumulator
APWR	Advanced Pressurized-Water Reactor
BD or BLD	Blowdown
BO	Boil-off
CCFL	Counter-Current Flow Limitation
CHF	Critical Heat Flux
CL	Cold Leg
CLB	Cold Leg Break
CSAU	Code Scaling Applicability and Uncertainty
CSS	Containment Spray System
CV	Containment Vessel
CVCS	Chemical and Volume Control System
DNB	Departure from Nucleate Boiling
DVI	Direct Vessel Injection
ECCS	Emergency Core Cooling System
EFWS	Emergency Feedwater System
EMDAP	Evaluation Model Development and Assessment Process
ESF	Engineered Safety Feature
FLECHT	Full-Length Emergency Core Heat Transfer
HHIS	High Head Injection System
HL	Hot Leg
ICIS	Incore Instrumentation System
IET	Integral Effects Test
INL	Idaho National Laboratory
JAERI	Japan Atomic Energy Research Institute
LBLOCA	Large Break Loss-of-Coolant Accident
LOCA	Loss-of-Coolant Accident
LOOP	Loss of Offsite Power
LP	Lower plenum of reactor vessel
LSC	Loop Seal Clearance
LSTF	Large Scale Test Facility
MHI	Mitsubishi Heavy Industry, Ltd.
NC	Natural Circulation
NR	Neutron Reflector
ORNL	Oak Ridge National Laboratory
PCT	Peak Cladding Temperature
PIRT	Phenomena Identification and Ranking Table
PWR	Pressurized-water Reactor
PZR	Pressurizer
RAI	Request for Additional Information
RCCA	Rod Cluster Control Assembly
RCP	Reactor Coolant Pump
RCS	Reactor Coolant System
REC	Recovery
RHR	Residual Heat Removal
RHRS	Residual Heat Removal System
ROSA	Rig of Safety Assessment
RV	Reactor Vessel

RVH	Reactor Vessel Head
RVI	Reactor Vessel Internal
RWSP	Refueling Water Storage Pit
SBLOCA	Small Break Loss-of-Coolant Accident
SEASET	Separate Effects and Systems Effects Tests
SET	Separate Effects Test
SG	Steam Generator
SI	Safety Injection
SIP	Safety Injection Pump
SRP	Standard Review Plan
SRV	Safety Relief Valve
T_{COLD}	Cold Leg Temperature
T_{HOT}	Hot Leg Temperature
THTF	Thermal Hydraulic Test Facility
UP	Upper Plenum of Reactor Vessel
USNRC	United States Nuclear Regulatory Committee

NOMENCLATURE

d	diameter
e	energy per unit mass
f	friction factor
g	gravitational acceleration
h	specific enthalpy
l	length or characteristic dimension
$\dot{m}$	mass flow
P	pressure
q	heat
r	radius
t	time
u	internal energy
v	velocity
x	quality
A	area
C	coefficient for nondimensional equations
C_p	specific heat
D	diameter or characteristic dimension
G	mass flux
H	height or elevation
K	loss coefficient
L	pipe length or level (tanks)
LHS	left hand side
M or m	mass
P	pressure
Q	volumetric flow
R	ideal gas constant or radius
R'	line resistance parameter
RHS	Right hand side
T	temperature
V	volume
Y	elevation or elevation difference
Z	elevation difference

Greek symbols

α	void fraction
β	thermal expansion coefficient
γ	specific heat ratio
ε	specific energy
Ψ	nondimensional coefficient
Δ	difference (as in ΔT)
ρ	density
ν	specific volume
μ	viscosity

ξ	perimeter

Subscripts

ℓ	liquid
v	vapor
m	mixture
0	reference

Superscript

*	normalized value

1. INTRODUCTION

1.1 Background

The US-APWR[1-1] is an advanced pressurized water reactor with a rated thermal output of 4451MWt. The most important aspect of the US-APWR design philosophy is utilization of proven technologies accompanied with well-balanced safety systems. Significant experience in the design, fabrication, installation, construction, and operation of 4-loop PWRs has resulted in proven technologies being developed by MHI, which have been incorporated into the design of US-APWR. Therefore, the system configurations of the reactor internals, components, piping system and engineered safety features (ESFs) are mostly identical between the US-APWR and the 4-loop PWR, while thermal-hydraulic volume, flow area, and diameter of each reactor component are appropriately enlarged from the 4-loop PWR so as to accommodate the larger thermal output of the US-APWR.

The M-RELAP5 code[1-2] has been developed to evaluate the adequacy of the US-APWR safety design against postulated small break loss-of-coolant accidents (SBLOCAs) in conformance with Appendix K to 10 CFR 50 specified by the USNRC[1-3]. The basis of M-RELAP5 is the best-estimate thermal-hydraulic system analysis code RELAP5-3D[1-4] which has been used extensively for safety analyses including SBLOCAs, and differences between these two codes appear only in several evaluation models required for the licensing safety analysis.[1-2] Although the thermal-hydraulic models, correlations, numerical solution methods, and code structure have been sufficiently validated and assessed using the various experimental test data in the past few decades, MHI independently evaluated their adequacy in M-RELAP5 application to US-APWR SBLOCAs according to the Evaluation Model Development and Assessment Process (EMDAP) specified in Regulatory Guide 1.203[1-5]. In the process of M-RELAP5 code assessment, important phenomena and processes occurring during US-APWR SBLOCAs were identified and summarized in a Phenomena Identification and Ranking Table (PIRT). Then, a code assessment matrix was established to validate the code, particularly for the identified important phenomena and processes, based on the various experimental test data obtained in several Separate Effects Test (SET) and Integral Effects Test (IET) facilities. The code validation using the test data demonstrated that M-RELAP5 is sufficiently applicable to US-APWR SBLOCAs.[1-2]

A feature of the M-RELAP5 code assessment matrix is that many of the SET and IET facilities providing the experimental test data were designed by referring to the existing Westinghouse-designed 4-loop PWRs. No test facility has been newly constructed to obtain experimental data simulating US-APWR SBLOCAs except for the advanced accumulator[1-6], since the US-APWR design is very similar to the existing 4-loop PWR. In fact, the primary plant transient behaviors and the identified important phenomena and processes occurring in SBLOCAs are almost identical between the US-APWR and the 4-loop PWR. However, quantitative evaluations with respect to the scalability of these test facilities have not been explicitly addressed, although qualitative scaling investigations were given in the topical report[1-2]. In addition, it is also necessary to examine the code scale-up capabilities based upon the code validations using the experimental data to complete the code development and assessment process required in the regulatory guide.

1.2 Objectives

In this report, quantitative scaling analyses based on the hierarchical two-tiered scaling (H2TS) methodology[1-7] were performed to complete the M-RELAP5 development and assessment which is required in the EMDAP. Specifically, the IET and SET facilities and experimental data are evaluated by the top-down and bottom-up approaches to respond to Step 6 in Element 2 of EMDAP "*Perform Scaling Analysis and Identify Similarity Criteria*", which demonstrates whether similar thermal-hydraulic behaviors expected in the US-APWR are also observed in the scaled test facilities. Here, the top-down scaling approach evaluates the global system behaviors and system interactions from IETs, and addresses the similarity between the IETs and the US-APWR as was done for AP600[1-8]. Due to the inherent similarity of the US-APWR design to the 4-loop Westinghouse design the top-down scaling analysis is limited to a confirmatory approach. The adoption of this limitation has been judged based on that the inherent similarity is considered to be possible to select EMDAP Sec.5 "*Graded Approach to Applying the EMDAP Process*". The scope of the top-down scaling study is limited to the SBLOCA scenarios resulting in the highest peak cladding temperatures (PCT). The objective of the top-down scaling analysis is to show that the same phenomena and mechanism are active and dominant in the US-APWR and IET responses. On the other hand, the bottom-up scaling analyses address the issues raised in the plant- and transient-specific PIRT related to localized behaviors, where SETs in the code assessment matrix are examined.

When any scaling distortion is recognized due to differences in the configuration and/or initial/boundary conditions between the IET and US-APWR, the effects will be evaluated according to Step 8(a) in Element 2 of EMDAP "*Evaluate Effects of IET Distortions and SET Scale up Capability*". Furthermore, the scalability of locally important phenomena and processes which are lost through identifying the global behavior in the top-down scaling will be examined by the bottom-up scaling analyses of the SETs (Step 8(b) in Element 2 of EMDAP).

In assessing the evaluation model adequacy, the code scale-up capability will be examined using the bottom-up and top-down approaches. The scalability of the models and/or correlations specific to the locally important phenomena and processes will be evaluated based on the applicable range of SET database. This scalability evaluation is limited to whether the specific model or correlation is appropriate for application to the configuration and conditions of the US-APWR SBLOCAs (Step 15 of Element 4 of EMDAP "*Assess Scalability of Models*"). Simultaneously, scalability of the integrated code predictability both for the US-APWR SBLOCAs and IETs is assessed from the top-down point of view. This evaluation is performed to confirm whether the code calculations for the US-APWR SBLOCA and the IET experiment exhibit otherwise unexplainable differences which may indicate experimental or code scaling distortions (Step 19 in Element 4 of EMDAP "*Assess Scalability of Integrated Calculations and Data for Distortions*"). These code scale-up evaluations were previously conducted for RELAP5 in its application to AP600 SBLOCA analyses.[1-9]

Chapter 2 of the present report describes the methodology applied to the scaling analyses. The US-APWR system, SBLOCA scenarios, PIRT and code assessment matrix developed for M-RELAP5 application to US-APWR SBLOCAs are briefly described in Chapters 3, 4 and 5, respectively. The scaling analyses are given in Chapter 6 and scalability of the selected experimental test facilities and data is examined. In Chapter 7,

M-RELAP5 code scale-up capability is evaluated with respect to the specific model or correlation, and the code integral predictability for the specific transient is also assessed. Overall evaluation results from the present scaling analyses are described in Chapter 8, where the adequacy of the US-APWR SBLOCA PIRT, code assessment matrix, and M-RELAP5 code scale-up capability are judged. In Chapter 9 the results of the analyses are summarized.

1.3 References

1-1 Mitsubishi Heavy Industries, Ltd., 'Design Document Control for US-APWR,' MUAP-DC001 Revision 1, August 2008.

1-2 Mitsubishi Heavy Industries, Ltd., 'Small Break LOCA Methodology for US-APWR,' MUAP-07013-P (R1), May 2010.

1-3 U.S. Nuclear Regulatory Committee, 'Appendix K to Part 50 – ECCS Evaluation Models,' 72 FR 49508, August 28 2007.

1-4 'RELAP5-3D Code Manual Volume I: Code Structure, System Models and Solution Methods,' INEEL-EXT-98-00834, Revision 2.4, June 2005.

1-5 U.S. Nuclear Regulatory Committee, 'Transient and Accident Analysis Methods,' Regulatory Guide 1.203,' December 2005.

1-6 Mitsubishi Heavy Industries, Ltd., 'The Advanced Accumulator,' MUAP-07001-P (R2), September 2008.

1-7 N. Zuber, 'Hierarchical, Two-Tiered Scaling Analysis, Appendix D to An Integrated Structure and Scaling Methodology for Severe Accident Technical Issue Resolution,' NUREG/CR-5809, EGG-2659, November 1991.

1-8 S. Banerjee et al., 'Top-Down Scaling Analyses Methodology for AP600 Integral Tests,' INEL-96/0040, May 1997.

1-9 C. D. Fletcher et al., 'Adequacy Evaluation of RELAP5/MOD3, Version 3.2.1.2 for Simulating AP600 Small Break Loss-of-Coolant Accidents,' INEL-96/0400 (nonproprietary version), April 1997.

2. SCALING ANALYSIS METHODOLOGIES

The scaling analysis methodologies used for the US-APWR SBLOCA follows the hierarchical two-tiered scaling (H2TS) methodology[2-1] composed of the top-down scaling which identifies integral processes important to the system behavior, and the bottom-up scaling to qualify individual phenomena identified as important from the top-down approach. The top-down and bottom-up scaling approaches are briefly described below.

2.1 Top-down Scaling

The top-down approach starts with scaling the entire system as a whole. Since no active part of the system is excluded, the top-down scaling is able to provide a comprehensive understanding of the integral system response occurring during the accident scenario. As pointed out by Zuber[2-1], the top-down scaling approach in the H2TS methodology proceeds from the whole system (reactor and/or plant) to the system components (reactor core, pressurizer, SG, RCP, ECCS, piping and so on), to constituents (fluid), to phases (liquid and vapor), and fields (continuous and dispersed fields). It yields one scaling group for every transfer process between media at every level in the system's hierarchy.

The top-down approach applied here is based on the method embodied by Banerjee et al.[2-2] in the quantitative scaling analysis for AP600 SBLOCA tests. Prior to the quantitative evaluation, the method identifies the system to be addressed, and divides the transient and accident progression into several phases, and further into sub-phases if necessary. A system response of interest in each phase is represented by the governing conservation equations, which account for the primary nature of physics with a (few) simplified and lumped volume(s). Then, the equations are mathematically nondimensionalized and the nondimensional groups, a set of nondimensionalized coefficients characterizing the system response, are defined. In the final step, data from the plant and from the experimental test facilities are used to evaluate the nondimensional groups, which are compared to each other to evaluate the scalability of the test data to the plant behavior quantitatively. The magnitudes of the numerical values of the nondimensional groups are used to determine the relative importance of the associated mechanisms. The scalability evaluation is based on the same mechanisms being dominant in the test facility and the plant, and on the relative ranking of the other important mechanisms.

Another aspect of the top-down scaling is that its evaluation results can be used for assessing adequacy and validity of the Phenomena Identification and Ranking Table (PIRT) established for code development. Since the top-down scaling quantitatively evaluates the importance of phenomena of interest, it can be used to review the ranking for each phenomenon identified in the PIRT.

2.2 Bottom-up Scaling

The bottom-up scaling is the traditional approach to evaluate the similitude for the processes and phenomena of interest between the test facilities and the plant. In many cases, this scaling approach has been applied to assess the applicability of models and correlations implemented into a code, namely the bottom-up scaling is used for the local and/or component levels, not for the system level. Zuber gave comprehensive

descriptions with regard to the several bottom-up scaling techniques, linear scaling, power-to-volume scaling, Ishii-Kataoka scaling and so on, in establishment of the Code Scaling, Applicability, and Uncertainty (CSAU) methodology.[2-3]

One of the techniques used for the present scaling study is the power-to-volume scaling, a well-known geometrical scaling approach, where the most important consideration is to preserve power and flow distribution as well as the time scale of thermal-hydraulic behaviors. Each component of the system is evaluated with a fluid volume ratio between the test facility and plant, and agreement of the volume ratio with the facility-to-plant power ratio provides good scalability from the viewpoints of time scale, fluid mass and energy distributions, velocities, acceleration, and length. This technique was conceived and developed in the LOFT (Loss of Fluid Test) program in the early 1970s[2-4], and many test facilities have been designed and constructed based on the power-to-volume scaling criterion.

However, in application of the power-to-volume scaling, it is necessary to consider several scaling effects and inherent deficiencies of the scaling criterion. In practice, it is generally impossible to simultaneously preserve length, elevation, area, volume, and pressure drop between the test facility and plant. For example, even if the test facility piping is well scaled based on the power-to-volume ratio concurrently with the full length and elevation, the hydraulic diameter differs from the actual plant, resulting in the different hydraulic resistance, and in the different flow regime characteristics.

Therefore, scaling techniques based on the nondimensional parameters representing flow characteristics will occasionally be applied in the bottom-up approach. For example, similitude of the counter-current flow limitation (CCFL) occurring in SG U-tubes between the test facility and plant is scaled with the nondimensional volumetric flowrate.[2-5] Similitude of the flow regime transition from the bubbly to stratified flow occurring in the horizontal piping can be evaluated based on the bottom-up scaling by using the Froude number[2-6]. These nondimensional parameters are suitable to evaluate the scalability in terms of the local thermal-hydraulic phenomena and processes. More comprehensive scaling laws using the nondimensional parameters were derived by Ishii and Kataoka based on different formulations of the conservation equations.[2-7]

In the H2TS methodology, the results obtained by the top-down scaling provide the rational framework for the bottom-up scaling by directing it toward a component where the most important phenomenological processes evolve. The bottom-up scaling addresses the details lost in the averaging at the component level in the top-down scaling, thereby, providing insight into qualitatively different responses between the test facility and plant, and sometimes explaining distortions between the test facility and plant based on the numerical values of nondimensional groups obtained from the top-down scaling.

2.3 Reference

2-1 N. Zuber, 'Hierarchical, Two-Tiered Scaling Analysis, Appendix D to An Integrated Structure and Scaling Methodology for Severe Accident Technical Issue Resolution,' NUREG/CR-5809, EGG-2659, November 1991.

2-2 S. Banerjee et al., 'Top-Down Scaling Analyses Methodology for AP600 Integral Tests,' INEL-96/0040, May 1997.

2-3 N. Zuber et al., 'Evaluation of Scale-Up Capabilities of Best-Estimate Codes, Appendix C to Quantifying Reactor Safety Margins,' NUREG/CR-5249 R4, December 1989.

2-4 L. J. Ybarrando et al., 'Examination of LOFT Scaling,' ASME Annual Meeting, 74-WA/HT-53, New York, November 17-22, 1974.

2-5 G. B. Wallis, 'One Dimensional Two-Phase Flow', McGraw-Hill Inc., NY (1969)

2-6 N. Zuber, 'Problems in Modeling of Small Break LOCA,' NUREG-0724, October 1980.

2-7 M. Ishii and I. Kataoka, 'Similarity Analysis and Scaling Criteria for LWRs under Single-Phase and Two-Phase Natural Circulation,' NUREG/CR-3267, March 1983.

3. US-APWR DESIGN OVERVIEW

3.1 Reactor Coolant System

The general system configuration of US-APWR is identical to that of the Westinghouse-designed 4-loop PWR, while thermal-hydraulic volume, flow area, and diameter of reactor components and their piping are appropriately enlarged from the 4-loop PWR so as to accommodate the larger thermal output of US-APWR. Table 3.1-1 summarizes various scale ratios of the primary plant parameters between the US-APWR and a representative Westinghouse-designed 4-loop PWR. It is noted that the operating conditions for the US-APWR in the table correspond to the initial conditions postulated for the safety analysis.

The reactor core consists of 257 17X17 fuel assemblies, surrounded by the neutron reflector, which is located between the core barrel and the core. Relative to conventional PWR baffle designs, the US-APWR neutron reflector improves neutron utilization and significantly reduces vessel irradiation. The reactor internals provide support and alignment of the core, and direct the amount of coolant flow and its distribution within the reactor vessel. The upper reactor internals consist of the upper core support, upper core plate, upper support columns and control rod guide tubes. The lower core support plate is welded to the bottom of the core barrel, and supports all fuel assemblies, the neutron reflector, the flow diffuser plate and the energy absorber. The reactor internal structure is illustrated in Figure 3.1-1.

The US-APWR fuel assembly utilizes a 17x17 array of 264 fuel rods, 24 control rod guide thimbles and one in-core instrumentation guide tube, as shown in Figure 3.1-2. The fuel rod and thimble components are bundled by grid spacers. The fuel design uses 11 grid spacers that span the 14-ft active fuel length. The grid-to-grid distance for the US-APWR design is basically the same as that for the 12-ft Mitsubishi fuel with a nine grid spacer design, thus ensuring a similar resistance to failures due to fretting wear, and the same proven coolant mixing and DNB performance as the 12-ft fuel design. The fuel assembly top and bottom nozzles provide structural support and alignment within the core. The top nozzle has a function to prevent fuel assembly lift during normal operation and transients, and also to provide alignment for insertion of control and instrumentation components. The bottom nozzle is designed to provide adequate flow and prevent debris from entering the fuel assembly.

The reactor coolant system (RCS) and related piping configuration is basically identical to that of the existing MHI 4-loop PWRs. The RCS provides reactor cooling by transferring the heat from the core to the secondary system to produce steam for the turbine. The major components of the RCS are the reactor vessel (RV), the steam generators (SGs), the reactor coolant pumps (RCPs), the pressurizer, and the reactor coolant pipes and valves. The flow diagram is illustrated in Figure 3.1-3.

The SGs are vertical shell and U-tube heat exchangers with integral moisture separator on the secondary side. The channel head is of hemispherical shape and divided into the inlet and outlet parts separated by a divider plate. The RCPs are vertical single-stage centrifugal pumps, each driven by a three-phase induction motor mounted above the pump. A flywheel attached to the motor provides additional inertia, thereby, preventing a rapid reduction in the reactor coolant flow during a loss of offsite power (LOOP). The

pressurizer, which is a vertical cylindrical vessel with hemispherical top and bottom heads, provides a point in the RCS where liquid and vapor can be maintained in equilibrium under saturated conditions for pressure control purposes. The coolant re-circulates through the hot leg (piping between RV and SG), crossover leg (piping between the SG and RCP suction), and cold leg (piping between the RCP and the RV).

Table 3.1-1 US-APWR Primary Design Parameters

Characteristics	PWR*	US-APWR	US-APWR/ PWR
Pressure (MPa)	15.5	15.5	1.00
Fluid temp. at hot leg (K)	598	598	1.00
Fluid temp. at cold leg (K)	562	561	1.00
Core			
Core power (MW)	3423	4451	1.30
Number of fuel rods	50952	67848	1.33
Number of unheated rods	4825	6425	1.33
Diameter of fuel rod (mm)	9.5	9.5	1.00
Diameter of unheated rod (mm)	12.2	9.7	0.80
Rod pitch (mm)	12.6	12.6	1.00
Hydraulic diameter of core (mm)	10.9		
Core height (m)	3.66		
Power density (MW/m^3)	9.9		
Core flow area (m^2)	4.75		
Core inlet flow rate (ton/s)	16.7		
Pressurizer			
Volume (m^3)	51		
Downcomer			
Downcomer flow area (m^2)	3.38		
Downcomer gap (m)	0.26		
Hot leg			
Diameter (m)	0.737		
Flow area (m^2)	0.427		
Cold leg			
Diameter (m)	0.699		
Flow area (m^2)	0.384		
Steam Generator (SG)			
Number of Tubes per one SG	3382		
Tube inner diameter (mm)	19.6		
Flow area per one SG (m^2)	1.02		
Length of SG tube (average) (m)	20.2		
Height from the top of heated part of core to the top of SG U-tube (m)	14.92		

* W-type 4-loop PWR in JAERI-M84-237 (ROSA-IV System description)

TDF: Thermal Design Flow

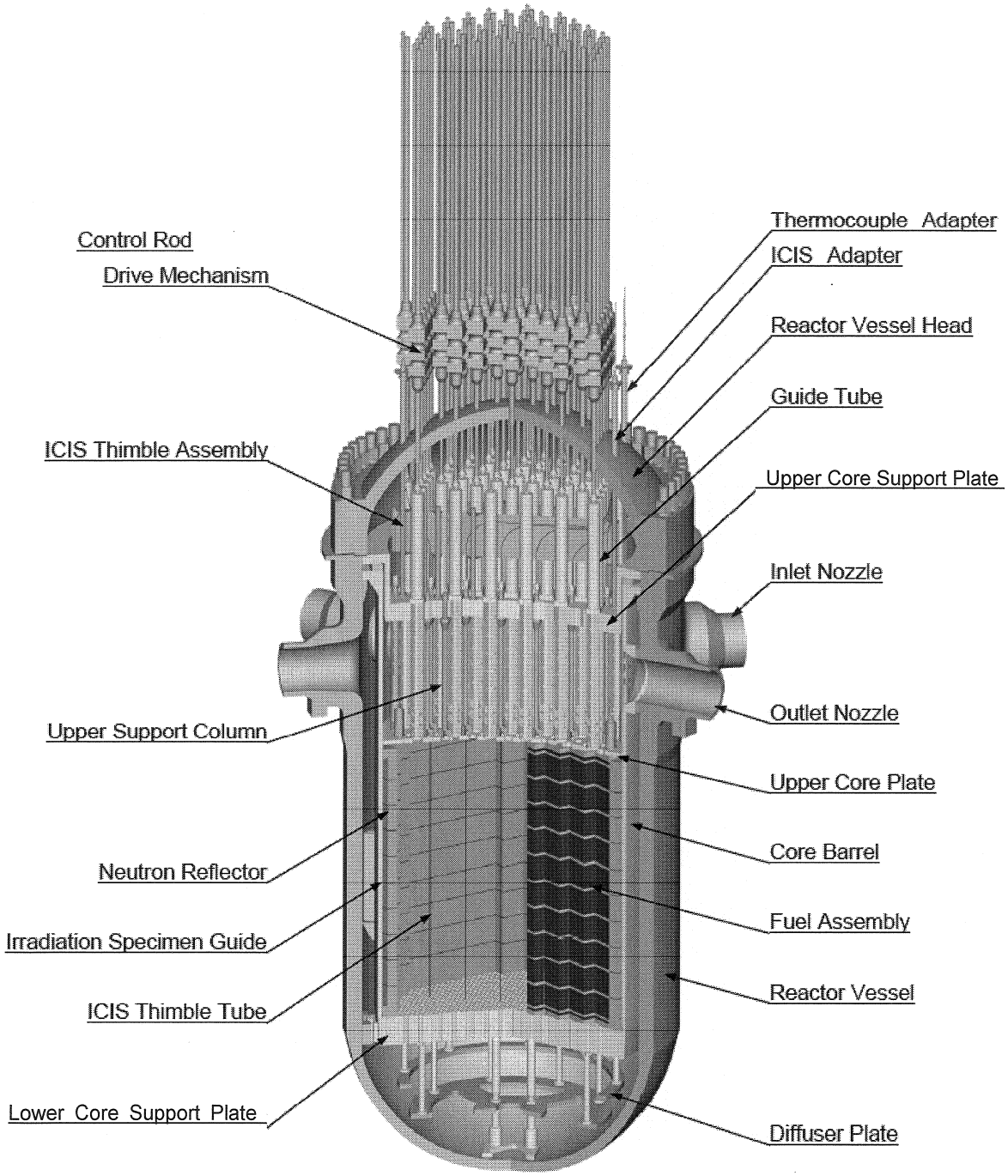

Figure 3.1-1 US-APWR Reactor

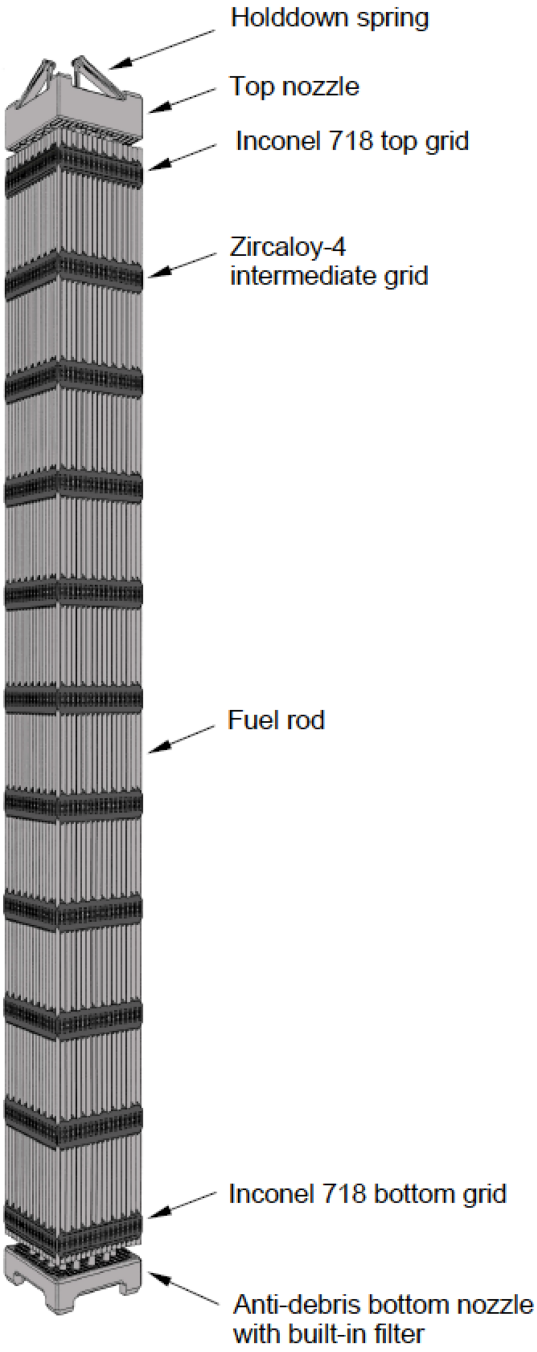

Figure 3.1-2 US-APWR 17X17 Fuel Assembly

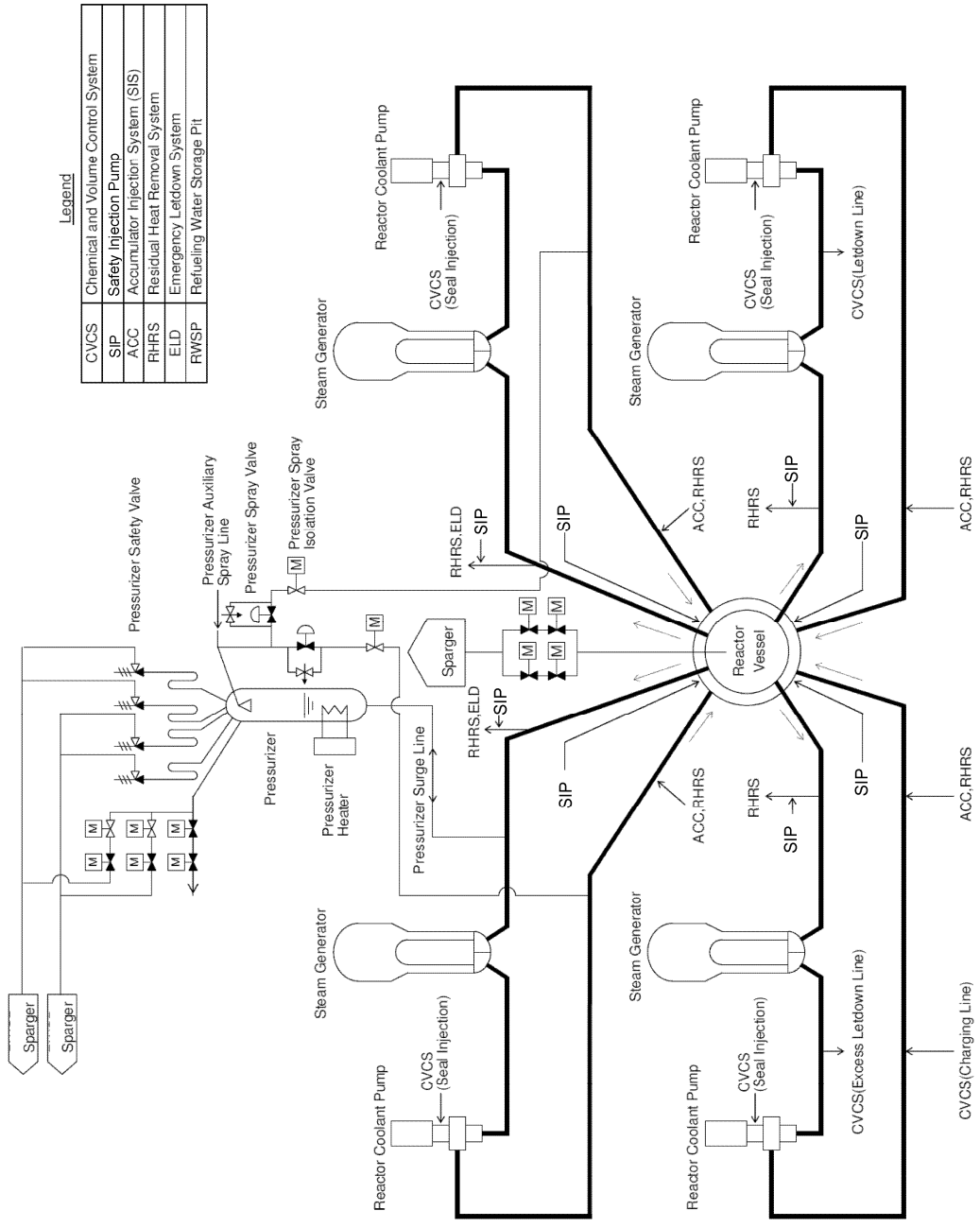

Figure 3.1-3 US-APWR Reactor Coolant System

3.2 Secondary System

The secondary system consists of the main feedwater system, the main steam system, the emergency feedwater system, and the power conversion system.

The main steam system includes the main steam pipes from the steam generator outlets to the turbine inlet steam chests and equipment and piping connected to the main steam pipes. The main steam relief and safety valves are installed upstream of the main steam isolation valve. They prevent excessive steam pressure and maintain cooling of the RCS if the turbine bypass is not available. The total capacity of the main steam safety valves exceeds 100% of the rated main steam flow rate. Branch pipes for driving the turbine-driven emergency feedwater pumps are connected upstream of the main steam isolation valves.

The main feedwater system supplies the steam generators with heated feedwater in a closed steam cycle using regenerative feedwater heating. The system is composed of the condensate subsystem, the feedwater subsystem, and a portion of the steam generator feedwater piping. The feedwater control valves, the feedwater bypass control valves, the steam generator water filling control valves, and the feedwater isolation valves are installed on the feedwater lines.

The emergency feedwater system (EFWS) consists of two motor-driven pumps, two steam turbine-driven pumps, two emergency feedwater pits, and associated piping and valves. The four emergency feedwater pumps take suction from the two emergency feedwater pits.

3.3 Emergency Core Cooling System

The emergency core cooling system (ECCS), shown in Figure 3.3-1, includes the accumulator system[3-1], the high-head safety injection system, and the emergency letdown system. Following a LOCA, the ECCS injects borated water into the reactor coolant system, cools the reactor core, prevents the fuel and fuel cladding from serious damage, and limits the zirconium-water reaction of the fuel cladding to a very small amount.

The ECCS design is based on the following requirements:

- In combination with control rod insertion, the ECCS is designed to shutdown and cool the reactor during the following accidents:
  - LBLOCA and SBLOCA of the primary piping,
  - Control rod ejection,
  - Main steam line break,
  - Steam generator tube rupture.
- The ECCS is designed with sufficient redundancy (four trains) to accomplish the specified safety functions assuming a single failure of an active component in the short term following an accident with one train out of service for maintenance, or a single failure of an active component or passive component for the long term following an accident with one train out of service.
- The ECCS is automatically initiated by a safety injection signal.
- The emergency electrical power to the essential components is provided so that the design functions can be maintained during a loss of offsite power.

The accumulator system, which is a passive safety component, consists of four accumulators, and the associated valves and piping, for each RCS loop. The system is connected to the cold legs of the reactor coolant piping and injects borated water when the RCS pressure falls below the accumulator operating pressure. Pressurized nitrogen gas forces borated water from the tanks into the RCS. The accumulator performs the large flow injection to refill the reactor vessel, and then provides a smaller injection flow during core reflooding in association with the high-head safety injection pumps. The high-head safety injection system provides long term core cooling.

The high-head injection system (HHIS), which is an active safety component, consists of four independent trains, each containing a safety injection pump and the associated valves and piping. The safety coolant is directly injected into the downcomer (Direct Vessel Injection (DVI)). The safety injection pumps start automatically upon receipt of the safety injection signal. One of four independent safety electrical buses is available to each safety injection pump. The safety injection pumps are aligned to take suction from the refueling water storage pit (RWSP) and to deliver borated water to the safety injection nozzles on the reactor vessel. Two safety injection trains are capable of meeting the design cooling function for a large break LOCA. This capability ensures adequate ECC delivery in the case where it is assumed that there is a single failure in one train and a second train is out of service for maintenance.

The RWSP in the containment provides a continuous borated water source for the safety injection pumps. This configuration eliminates the need for realignment from the refueling water storage tank to the containment sump, which is employed in the existing PWR plants.

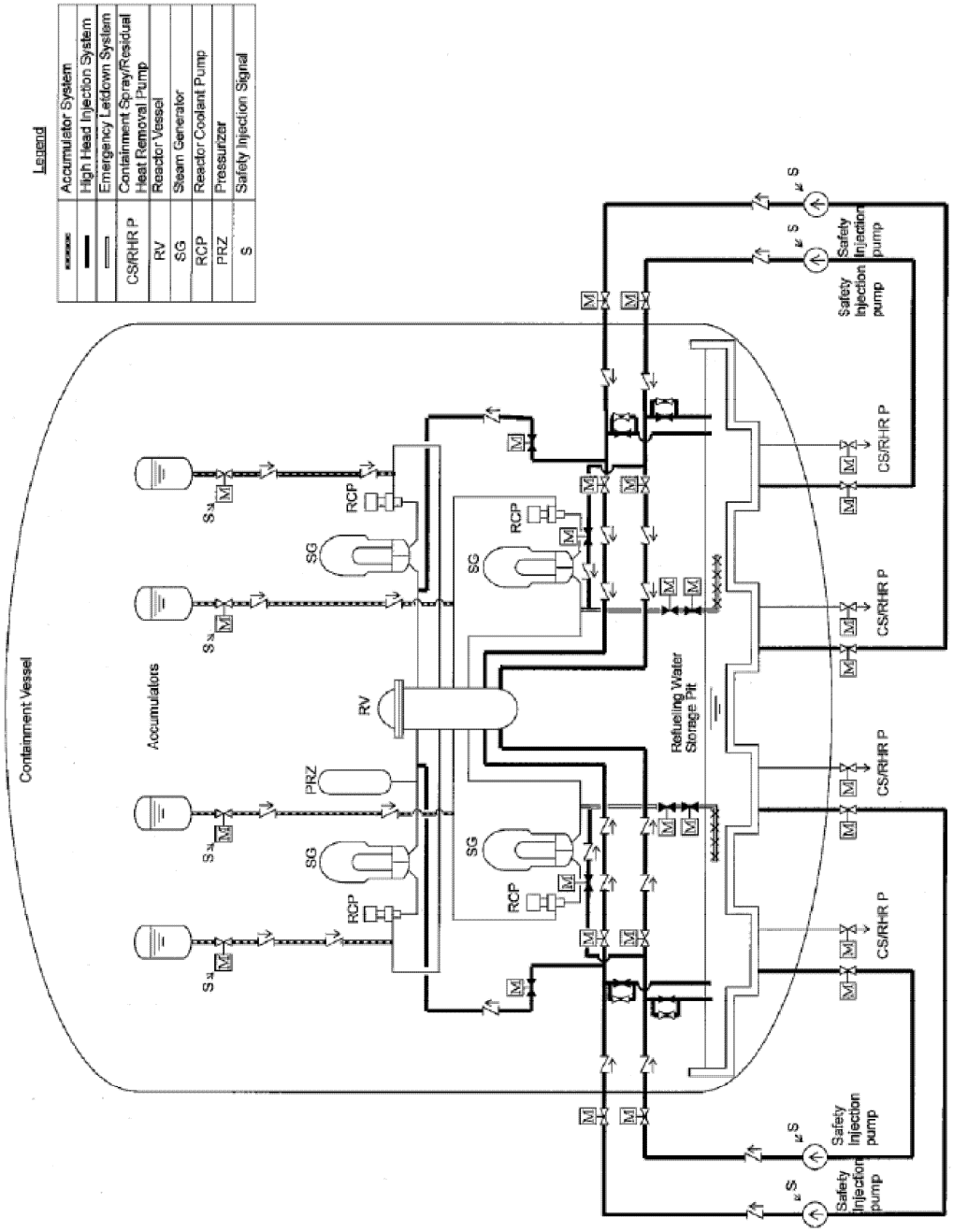

Figure 3.3-1 US-APWR Emergency Core Cooling System

3.4 References

3-1 Mitsubishi Heavy Industry, Ltd., “The Advanced Accumulator,” MUAP-07001-P (R2), September 2008.

4. US-APWR SBLOCA SCENARIOS AND PHASE DESCRIPTION

4.1 Accident Scenario

Here, a small break in the RCS piping is postulated at the normal reactor power operation. During the SBLOCA transient, the RCS primary side rapidly depressurizes upon initiation of the break, and the reactor trip and ECCS actuation signals are generated when pressurizer pressure falls below each set point. Loss of offsite power (LOOP) is assumed which causes all RCPs to trip following the reactor trip. Decrease of the RCS coolant inventory eventually causes core uncovery, resulting in fuel cladding heat-up. After the RCS pressure falls below the accumulator operating pressure or emergency electrical power is established for the active safety trains, the ECCS starts injecting the safety coolant into the RCS, and then the core is refilled and recovered.

Compared with the LBLOCA, the phases of the SBLOCA prior to the core recovery occur over a longer time period. Therefore, various thermal-hydraulic phenomena can be observed during the duration, which affect the progression of the accident. In order to identify the important phenomena, a typical US-APWR SBLOCA is divided into five phases: blowdown, natural circulation, loop seal clearance, boil-off, and core recovery, as illustrated in Figure 4.1-1. The duration of each phase depends on the break size and the performance of the ECCS.

A detailed set of sensitivity calculations for the US-APWR SBLOCA[4-1] revealed that the limiting PCT occurs during the loop seal clearance phase when a break size of 7.5-in is assumed at the top of the cold leg, while a break size of 1.0-ft^2 at the top of the cold leg results in the limiting PCT during the boil-off phase. These two break sizes provide the limiting PCT for SBLOCAs with different mechanisms being active during the cladding temperature excursion and rewetting. In the 7.5-in break the PCT and rewet occur at high pressure (~9 MPa) and prior to the accumulator flow. In the 1-ft^2 break the dryout and rewet occur at low pressure after the accumulator flow begins. The extent and duration of core uncovery was significantly larger in the 1-ft^2 break. Data from tests in the ROSA facility were used in the top-down scaling study.

In the cold leg break scenarios, a single failure of the electrical power to one HHIS train is postulated with the assumption that another HHIS is out of service for maintenance, and that LOOP occurs concurrently with the reactor trip, resulting in the severest PCT during the US-APWR SBLOCA.[4-1]

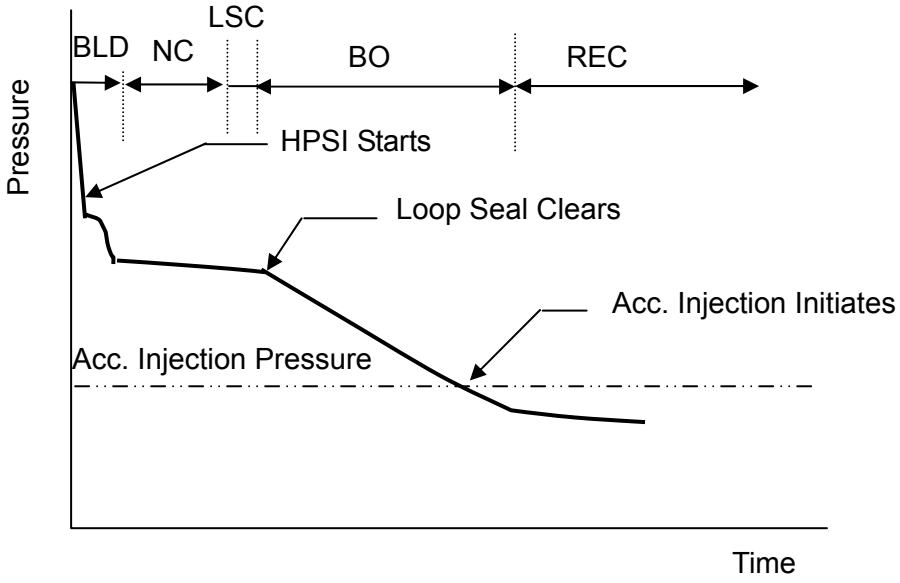

Primary Pressure Response

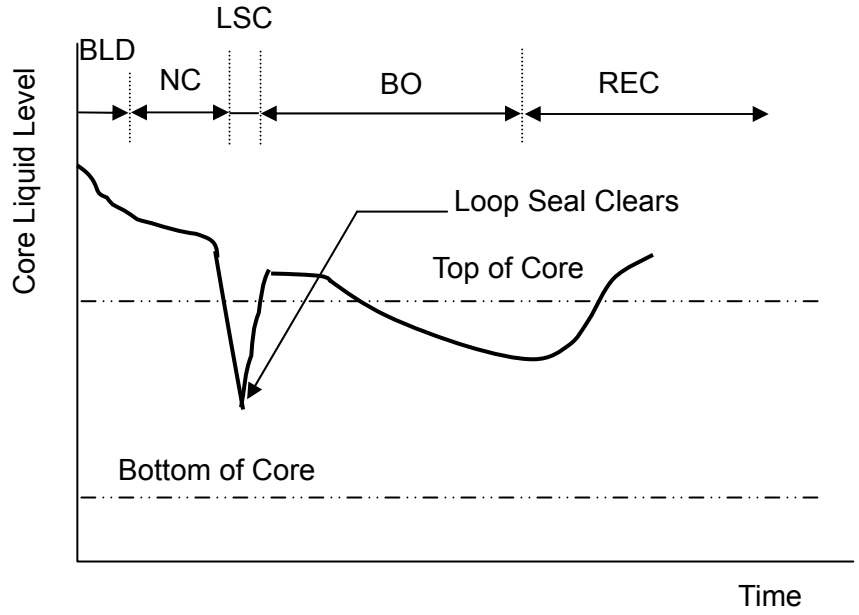

Core Collapsed Liquid Level Response

Figure 4.1-1 Pressure and Core Liquid Level Responses in US-APWR SBLOCA

4.2 Phase Definitions

The typical scenario of the US-APWR SBLOCA can be divided into five phases, and the primary plant transient behaviors are described for each phase. In smaller breaks the five phases are all present and occur in a fairly linear sequence. As the break size increases there is some temporal overlap of the dominant processes in each phase and in some cases the timing of events eliminates certain phases. For the range of break sizes considered in the top-down study the phase boundaries are somewhat different for each break size.

4.2.1 Blowdown

Upon initiation of the break, the RCS primary side rapidly depressurizes until flashing of the hot coolant into steam begins (saturation pressure corresponding the hot channel outlet temperature). Reactor trip is initiated on the low pressurizer pressure set point of 1860 psia. Closure of the condenser steam dump valves isolates the SG secondary side. As a result, the SG secondary side pressure rises to the safety valve set point of 1296 psia, and steam is released through the safety valves. The ECCS actuation signal is generated at the time the pressurizer pressure decreases to the low pressurizer pressure set point of 1760 psia and safety injection initiates, after a time delay. Then the RCPs trip, after a 3 second delay, upon the reactor trip resulting from the low pressurizer pressure.

The rapid depressurization ends when the pressure falls to the saturation pressure of the of the hottest liquid in the RCS, usually in the upper plenum at the hot channel outlet). The break flow in the RCS is single-phase liquid throughout the blowdown period. As the break size increases, the RCS pressure decreases more rapidly to the accumulator operation pressure, which for sufficiently large breaks, can result in the disappearance of the subsequent natural circulation and loop seal clearance phases described below.

4.2.2 Natural Circulation

As the RCPs coast down, two-phase natural circulation is established in the RCS loops if the RCS pressure is higher than the steam generator secondary side pressure. During natural circulation the decay heat is removed by boiling in the core and condensation in the SG tubes. The EFW is initiated to maintain the secondary side inventory. As more coolant is lost from the RCS through the break, steam accumulates in the up-flow side of the SG tubes. The natural circulation phase will continue until there is insufficient driving head on the cold leg side of the loops, due to the accumulation of steam in the loops between the top of the steam generator tubes and the loop seals or when the RCS pressure falls below the steam generator secondary side pressure. Specifically, the natural circulation phase ends when the liquid mass flow at the top of the U-tubes becomes zero or the RCS pressure falls below the steam generator secondary side pressure.

4.2.3 Loop Seal Clearance

The third phase is the loop seal clearance period. The RCS liquid inventory will be increasing or decreasing depending on the relative magnitudes of the break and ECC flows. With liquid in the loop seals, the steam generated in the core cannot escape through the break. Therefore, pressure in the core increases relative to the downcomer

and the core liquid level is depressed by the pressure difference between the core and downcomer. The core level is depressed relative to the downcomer until the pressure difference is large enough to push the liquid out of the pump suction side of the loop seal. If the core mixture level drops below the top of the core during this process, the cladding will experience a dryout and the cladding temperature in the uncovered portion will begin to rise. When the liquid level of the downhill side of the cross over leg is depressed to the elevation of the loop seals, the seals clear and steam in the hot side of the RCS is vented to the cold legs. This venting relieves the backpressure in the core and the core liquid level is re-equalized with the downcomer.

4.2.4 Boil-Off

The reactor vessel mixture level may decrease as a result of the core boiling in this phase if the RCS pressure is too high for the injection system to make up for the boil-off rate. The core might uncover and fuel cladding heat-up may occur before the RCS depressurizes to the point where the SI pumps (and accumulator when the RCS pressure drops to a sufficiently low value) deliver ECCS water to the RCS at a rate higher than the break flow. In the two break sizes considered in the top-down study the loss-of-off site power assumption causes the SI pumps to be delayed about 120 s from the low-pressure initiation signal. The end of the boil-off phase is when the core minimum liquid level occurs.

4.2.5 Core Recovery

As the RCS pressure continues to fall, the ECCS flow rates eventually exceed the break flow. The vessel mass inventory then increases, and core recovery is established, resulting in rewetting and quench of the high temperature cladding. The end of the core recovery phase is when the entire core has rewetted and the cladding temperature returns to saturated liquid temperature. For small cold leg breaks the ECCS are able to re-establish core cooling while the RCS pressure is high enough to maintain choked flow at the break. Therefore, the containment pressure in the small break LOCA does not affect the PCT.

4.3 References

4-1 Mitsubishi Heavy Industry, Ltd., “Small Break LOCA Sensitivity Analyses for US-APWR,” MUAP-07025-P (R1), May 2010.

5. PHENOMENA IDENTIFICATION RANKING TABLE AND ASSESSMENT MATRIX

5.1 Phenomena Identification Ranking Table (PIRT)

The major plant responses and behaviors during US-APWR SBLOCAs are described in the preceding chapter. Each of these major plant behaviors can be decomposed into several fundamental thermal-hydraulic phenomena and processes. Therefore, one of the most important steps in developing an analysis methodology is to identify the phenomena and processes providing the most dominant influence on the specific transient and plant behavior of interest and ultimately on PCT. These significant phenomena and processes are listed and summarized in a Phenomena Identification and Ranking Table (PIRT).

The US-APWR SBLOCA PIRT is specifically developed in the topical report for the US-APWR SBLOCA methodology[5-1]. Important (high-ranked) phenomena and processes from the PIRT are presented in Table 5.1-1. Several important phenomena and processes are addressed with conservative assumptions in the US-APWR SBLOCA methodology: **[**

]. These phenomena and processes are properly excluded from the explicit examination for the code validation and the scaling analysis, since the treatment of these parameters conforms to the requirements prescribed either in Appendix K to 10 CFR 50[5-2] or in the standard review plan[5-3]. As for the break flow, however, the accuracy of M-RELAP5 model has been assessed using IET data[5-1], and the effect of break flow on the system responses are to be addressed in the present scaling analysis.

The PIRT is a useful tool in developing the code assessment matrix described in the succeeding section, since it provides a clear understanding of the phenomena and processes which will be modeled and validated in the code assessment. Similarly, the PIRT supports scaling investigations by identifying important phenomena that must be considered, particularly for the bottom-up scaling approach. Therefore, it is possible to demonstrate the applicability of test facility results for code assessment purposes, by confirming the scalability of experimental data in terms of the important phenomena and processes identified in the PIRT.

Table 5.1-1 Important Processes and Phenomena for US-APWR SBLOCAs (High-Rank)

Location / Processes/Phenomenon	SBLOCA Phase				
	Blowdown	Natural Circulation	Loop Seal Clearance	Boil-off	Recovery
Fuel					
Decay Heat					
Local Power					
Core					
CHF/Dryout					
Uncovered Heat Transfer					
Rewet					
Mixture Level					
3-D Power Distribution					
Steam Generator					
Water Hold-up in SG Inlet Plenum					
Water Hold-up in U-Tube Uphill Side					
Primary Side Heat Transfer					
Secondary Side Heat Transfer					
Crossover Leg					
Water Level in SG Outlet Piping					
Loop Seal Formation/Clearance					
Downcomer/Lower Plenum					
Mixture Level/Void Distribution					
DVI/SI Water/Flow rate					
Break					
Critical Flow					
Break Flow Enthalpy					

5.2 Code Assessment Matrix

Table 5.2-1 lists the experiments to be used for the M-RELAP5 code assessment. This assessment matrix is basically identical to that in the topical report (Table 4.4.2-1) [5-1] except that two separate effects experiments, the FLECHT-SEASET reflood test[5-4] and the UPTF Test 5 (loop seal clearing test)[5-5], were added to the original code assessment matrix to respond to USNRC's Request for Additional Information (RAI). The FLECHT-SEASET test analysis was conducted to demonstrate M-RELAP5 conformance to the requirements specified in Appendix K to 10 CFR 50, particularly for the code applicability under the low pressure and low flooding velocity conditions. The UPTF Test 5 analysis shows the adequacy of M-RELAP5 predictions for water retention during loop seal clearance. In addition one ROSA cold leg break test was added. The IB-CL-02 test simulated a 1-ft^2 break in the US-APWR.

In M-RELAP5 code assessment, the ROSA/LSTF facility provides the integral effects test (IET) data, which represent the major plant responses and behaviors during the typical US-APWR SBLOCA. Therefore, the scalability of the ROSA/LSTF facility is primarily addressed by the top-down approach, and adequacy of the test data obtained in the test facility will be investigated. The separate effect test (SET) data were obtained in the other test facilities listed in Table 5.2-1. Each of the experiments is related to the important phenomena and processes identified in the US-APWR SBLOCA PIRT. The SET data represent the phenomena and processes appearing in some local portions of the plant, of which scalability is evaluated based on the bottom-up approach in the present scaling analysis.

Table 5.2-1 M-RELAP5 Assessment Matrix for US-APWR SBLOCAs

	CHF/Core Dryout	Uncovered core heat transfer	Rewet	Core mixture level	Water hold-up in SG Inlet plenum	Water hold-up in U-tube uphill side	SG primary and secondary heat transfer	Water level in SG outlet piping	Loop seal formation and clearance	Downcomer mixture level/void distribution
ROSA/LSTF Void Profile Test				X						
ORNL/THTF Void Profile Test				X						
ORNL/THTF Uncovered Heat Transfer Test	X	X								
ORNL/THTF Reflood Test		X	X							
FLECHT-SEASET Reflood Test*		X	X							
UPTF SG plenum CCFL Test					X					
Dukler Air-Water Flooding Test						X				
UPTF Test 5*								X	X	
ROSA/LSTF small break (5%) LOCA test	X	X	X	X	X	X	X	X	X	X
ROSA/LSTF small break (1-ft^2) LOCA test*	X	X	X	X	X	X	X	X		X

* New experiments added to the original M-RELAP5 code assessment[5-1]

5.3 References

5-1 Mitsubishi Heavy Industry, Ltd., 'Small Break LOCA Methodology for US-APWR,' MUAP-07013-P (R1), May 2010.

5-2 USNRC, 'Appendix K to Part 50 – ECCS Evaluation Models,' 72 FR 49508, August 28 2007.

5-3 USNRC, 'Standard Review Plan 15.6.5 Loss-of-Coolant Accidents Resulting from Spectrum of Postulated Piping Breaks within the Reactor Coolant Pressure Boundary,' NUREG-0800.

5-4 M. J. Loftus et al., 'PWR FLECHT-SEASET Unblocked Bundle, Forced and Gravity Reflood Task Data Report,' NUREG/CR-1532, June 1980.

5-5 J. Liebert and R. Emmerling, 'UPTF experiment Flow Phenomena during Full-scale Loop Seal Clearing of a PWR,' Nucl. Eng. Design, 179, pp. 51-64, 1998.

6. SCALING ANALYSIS FOR TEST FACILITIES

As described in Chapter 5, in the M-RELAP5 code assessment matrix the IET data are from two ROSA/LSTF SBLOCA tests. The scalability of these test data is evaluated by the top-down approach for each transient phase defined in Chapter 4. When any significant scaling distortion occurs due to differences in the configuration and/or initial/boundary conditions between the US-APWR and ROSA/LSTF, the effect is to be evaluated based on the bottom-up scaling approach. Similarly, the bottom-up scaling will support the top-down scaling when the local phenomena and processes significantly affect the global behavior.

The 8 SET data are supplied from the 6 test facilities to assess the M-RELAP5 applicability to the important thermal-hydraulic phenomena and processes. The scalability of each SET facility is evaluated by the bottom-up approach, and the results are to be used not only in assessing the code scale-up capability, but also in completing the quantitative scaling evaluation associated with the top-down approach.

Design specifications of the IET and SET facilities are described in the topical report for the US-APWR SBLOCA methodology[6-1].

ROSA/LSTF is an integral test facility which is a volumetrically 1/48-scaled and full height model of the Westinghouse-type 3423 MWt 4-loop PWR[6-2]. The test facility was designed to reproduce thermal-hydraulic phenomena peculiar to SBLOCAs and operational transients in the reference plant. The ROSA/LSTF is reasonably applicable for investigation of the SBLOCA behavior occurring in the US-APWR, since the US-APWR design is very similar to the Westinghouse 4-loop PWR as mentioned in Section 3.1. Appendix A of the present report provides a comparison of the primary design parameters between the US-APWR and ROSA/LSTF. The SB-CL-18 test simulated a 5% cold leg break (CLB) in the reference PWR which is close to the US-APWR 7.5-in CLB (**[ ]** in a precise sense from the volumetric scaling ratio) [6-3]. The IB-CL-02 test was specifically for the US-APWR program and simulated a 1-ft^2 break in the US-APWR[6-4]. These ROSA tests correspond to the break sizes producing the highest PCT in US-APWR SBLOCAs. Therefore, all the major plant behaviors, and important phenomena and processes occurring during the representative US-APWR SBLOCA scenario can be observed in the test data.

6.1 Blowdown

6.1.1 Phenomena and Applied Test Facilities

The blowdown phase starts from the break initiation and proceeds through several steps. Initially the RCS fluid outside the pressurizer is subcooled. Very rapidly rarefaction waves propagate from the break to the upper plenum where the liquid at the outlet of the hottest channels begins to flash. The rapid depressurization ends when the pressure reaches the saturation pressure corresponding to the fluid temperature at the hot channel outlet. At this time the cold leg break flow is subcooled liquid. The break flow causes the system to depressurize by removing mass and energy from the system. When the pressure falls to the saturation pressure of the cold leg liquid, the break flow transitions to saturated liquid with a corresponding reduction in flow rate. When the system void fraction is large enough vapor begins to flow out the break resulting in a further reduction in the break mass flow rate.

The RCS depressurization initiated by the break is a dominant global behavior during the blowdown phase. The discharge flow out the break determines the initial decrease of RCS inventory, which affects the depressurization rate and the duration of blowdown. In the US-APWR system, particularly, transient behavior of the pressurizer pressure determines the timing for the reactor trip (scram) and the safety injection. Therefore, the primary system mass and depressurization are addressed as significant parameters of interest for the blowdown phase. In the M-RELAP5 code assessment, data from the two ROSA/LSTF tests are used in the top-down analysis.

6.1.2 Top-Down Scaling Analysis

Results for each of the two break sizes are discussed separately.

6.1.2.1 Transient Behavior of Interest

7.5-in cold leg break

Figure 6.1-1 shows the calculated pressure transient in the pressurizer during the US-APWR 7.5-in CLB. The pressure monotonically decreases until the pressurizer becomes empty. The timing of important events related to the safety system is included in the figure. After about 36 seconds, the pressure stabilizes slightly above the SG secondary pressure level, which indicates the beginning of the natural circulation phase as discussed in Section 6.2.

The pressurizer pressure transient during the ROSA/LSTF SB-CL-18 test is shown in Figure 6.1-2, where the time of pressurizer emptying is almost the same as calculated in the US-APWR. Rapid depressurization ends at about 30 seconds, and then the pressure decreases much more slowly. This slow depressurization continues until about 80 seconds after the break initiation when the primary system pressure equalizes with the secondary system pressure. Both transients are compared in Figure 6.1-3. By taking account of the slightly larger break size in the US-APWR under the volumetric scaling, it can be concluded that the two depressurization behaviors look similar to each other until about 36 seconds, corresponding to the end of the blowdown phase for the US-APWR

7.5-in CLB.

The break flow rate is compared in Figure 6.1-4. The break flow rate for the US-APWR tends to decrease with time in the first about 36 seconds, while that for the ROSA/LSTF indicates almost constant trend. Since the measured break flow rate was estimated from the change of liquid level in a huge storage tank located far from the break location, the early transient of break flow is expected to be smoothed in time. The different transients of break flow rate between the US-APWR and the ROSA/LSTF affect the results for the top-down scaling analysis in the next section. Since the different transients provoke an uncertainty of the break flow model of the M-RELAP5, the applicability of the break flow model for the US-APWR will be discussed in the bottom-up scaling section 6.1.3.

The void fractions at various locations are compared in Figure 6.1-5 through Figure 6.1-8. The void generation occurs in US-APWR just after the break initiation, which is due to the steam production in core and to flashing following depressurization. The ROSA/LSTF response was also calculated by M-RELAP5, showing similar void behaviors. These indicate that a saturated two-phase region can be assumed in the primary system even just after the break initiation. The two-phase hot region is supposed to be most of the core, the upper plenum, the upper head, the hot leg, the pressurizer and the steam generator upflow sides.

1-ft^2 cold leg break

Figure 6.1-9 shows the calculated pressure transient in the pressurizer during the US-APWR 1-ft^2 CLB. The pressure monotonically decreases until the pressurizer becomes empty. The timing of important events related to the safety system is included in the figure. After about **[ ]**, the pressure stabilizes slightly above the SG secondary pressure level, which relates to the beginning of the natural circulation phase as discussed in Section 6.2.

[

]

[

]

[

]

Figure 6.1-1 Pressurizer Pressure for US-APWR 7.5-in CLB (Calculation)

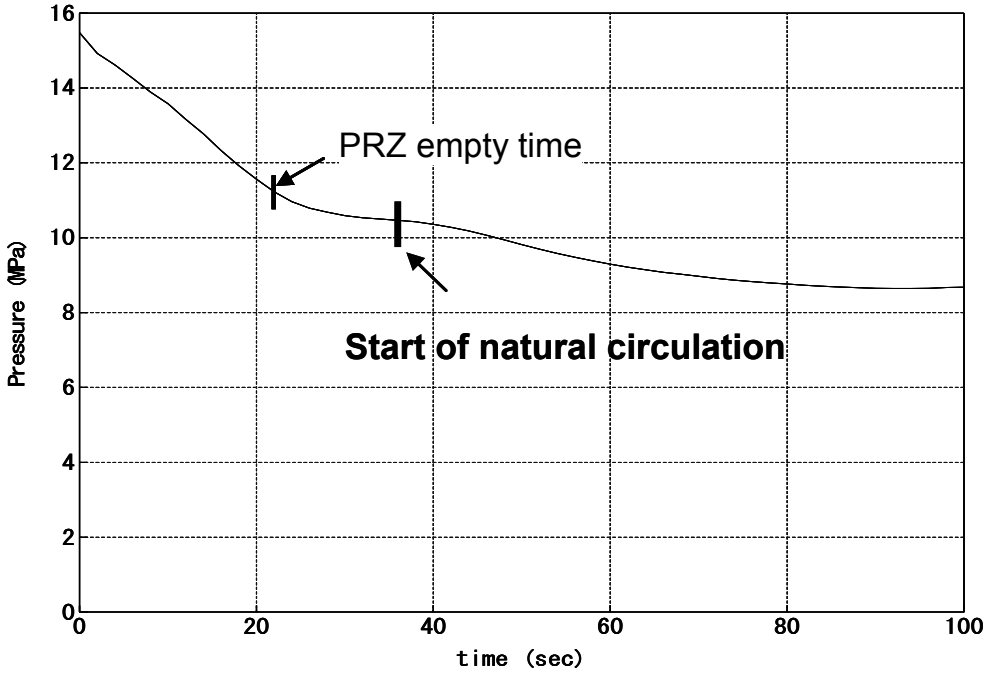

Figure 6.1-2 Pressurizer Pressure for ROSA/LSTF SB-CL-18 (Measurement)

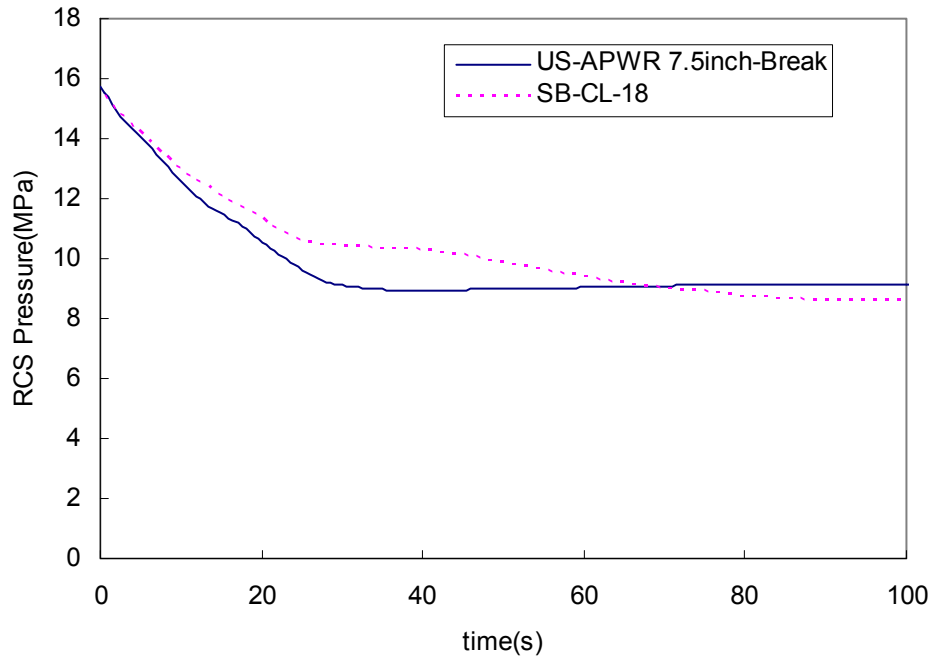

Figure 6.1-3 Comparison of RCS Pressure between US-APWR 7.5-in CLB (Calculation) and ROSA/LSTF SB-CL-18 (Measurement)

Figure 6.1-4 Comparison of Mass Flow rate at Break between US-APWR 7.5-in CLB (Calculation) and ROSA/LSTF SB-CL-18 (Measurement)

Figure 6.1-5 Comparison of Core Void Fractions between US-APWR 7.5-in CLB and ROSA/LSTF SB-CL-18 (Calculations)

Figure 6.1-6 Comparison of Upper Plenum Void Fractions between US-APWR 7.5-in CLB and ROSA/LSTF SB-CL-18 (Calculations)

Figure 6.1-7 Comparison of Hot Leg Void Fractions between US-APWR 7.5-in CLB and ROSA/LSTF SB-CL-18 (Calculations)

Figure 6.1-8 Comparison of SG (Inlet Plenum to U-Tube Uphill Side) Void Fractions between US-APWR 7.5-in CLB and ROSA/LSTF SB-CL-18 (Calculations)

Figure 6.1-9 Pressurizer Pressure for US-APWR 1-ft^2 CLB (Calculation)

Figure 6.1-10 Pressurizer Pressure for ROSA/LSTF IB-CL-02 (Measurement)

Figure 6.1-11 Comparison of RCS Pressure between US-APWR 1-ft^2 CLB (Calculation) and ROSA/LSTF IB-CL-02 (Measurement)

Figure 6.1-12 Comparison of Mass Flow rate at Break between US-APWR 1-ft^2 CLB (Calculation) and ROSA/LSTF IB-CL-02 (Measurement)

Figure 6.1-13 Comparison of Core Void Fractions between US-APWR 1-ft^2 CLB and ROSA/LSTF IB-CL-02 (Calculations)

Figure 6.1-14 Comparison of Upper Plenum Void Fractions between US-APWR 1-ft^2 CLB and ROSA/LSTF IB-CL-02 (Calculations)

Figure 6.1-15 Comparison of Hot Leg Void Fractions between US-APWR 1-ft^2 CLB and ROSA/LSTF IB-CL-02 (Calculations)

Figure 6.1-16 Comparison of SG (Inlet Plenum to U-Tube Uphill Side) Void Fractions between US-APWR 1-ft^2 CLB and ROSA/LSTF IB-CL-02 (Calculations)

6.1.2.2 Governing Conservation Equations

In evaluating the global transient behavior of interest, the method developed by S. Banerjee et al. for the AP600 SBLOCA[6-5] is employed for the basis of the present top-down scaling analysis. The same equations are applied to both break sizes. The reference conditions used to evaluate the dimensionless groups are selected as appropriate for each break size.

It is assumed that the reactor system is running at rated power and at a pressure of approximately 15.5 MPa before the transient starts. During steady state operation, the system pressure is regulated by the pressurizer control system to maintain the pressurizer fluid at saturation condition, while the rest of the primary coolant system contains subcooled fluid. When a small break is postulated to occur in the cold leg, the system pressure will immediately start decreasing in response to the mass and energy loss out the break, inducing liquid flashing in the pressurizer. During the initial portion of the blowdown phase, the break flow is subcooled and the majority of the RCS remains subcooled. In the US-APWR 7.5-in and larger CLBs and in the corresponding ROSA/LSTF tests, however, the break size is large enough that the RCS fluid reaches the saturation condition and starts flashing as discussed in the preceding section.

The fluid behavior during the blowdown phase in the primary system can be simply modeled with two fields consisting of a two-phase mixture and subcooled liquid as shown in Figure 6.1-17. Liquid from the pressurizer is added to the primary system, where some of it flashes and some is vaporized in the core region. The generated steam remains in the system or is condensed at the steam generators. A mass balance between the incoming and outgoing fluids determines the system mass inventory. Similarly, a balance between the energy added to the fluid and the energy removed with the break flow determines the system pressure. Therefore, from the global response point of view, the transient of interest is sufficiently represented with the mass and energy conservation equations in the primary system.

During the blowdown phase, the fluid in the primary system can be approximated as two fields of two-phase mixture and subcooled liquid in evaluating the global mass and energy conservations. The mass balance is related to the incoming and outgoing flow rates as follows:

Mass conservation equation:

$$\frac{d\left(\rho_\ell V_\ell + \rho_{\ell m} V_{\ell m} + \rho_v V_v\right)}{dt} = \frac{d\left(\rho_\ell V_\ell + \rho_m V_m\right)}{dt} = -\dot{m}_{break} \tag{6.1-1}$$

$$\rho_m = \frac{\rho_{\ell m} V_{\ell m} + \rho_v V_v}{V_m} \tag{6.1-2}$$

where ρ_m, V and m_{break} are the mixture density, volume and break flow rate, respectively.

Similar to the mass conservation, the energy conservation equation is obtained.

Energy conservation equation:

$$\frac{d\left(\rho_\ell V_\ell \varepsilon_\ell + \rho_{\ell m} V_{\ell m} \varepsilon_{\ell m} + \rho_v V_v \varepsilon_v\right)}{dt} = \frac{d\left(\rho_\ell V_\ell \varepsilon_\ell + \rho_m V_m \varepsilon_m\right)}{dt} = \dot{q}_{core} + \dot{q}_{SG} - \dot{m}_{break}\varepsilon_{break} \quad (6.1\text{-}3)$$

$$\varepsilon_m = \frac{\rho_{\ell m} V_{\ell m} \varepsilon_{\ell m} + \rho_v V_v \varepsilon_v}{\rho_m V_m} = \frac{\rho_{\ell m} V_{\ell m} \varepsilon_{\ell m} + \rho_v V_v \varepsilon_v}{\rho_{\ell m} V_{\ell m} + \rho_v V_v} \quad (6.1\text{-}4)$$

where ε_m, ε_{break}, q_{core} and q_{SG} are the mixture fluid energy (enthalpy), break flow enthalpy and heat transfer from the core and SG, respectively. In the above equation, the fluid energy is represented as follows, by neglecting the kinetic and potential energy:

$$\varepsilon = h = u + Pv \quad (6.1\text{-}5)$$

where u, P, and v are the internal energy, pressure, and specific volume, respectively. By using the equation (6.1-5), the energy conservation is converted into a derivative equation to represent the pressure change as follow:

Pressure equation:

$$\frac{dP}{dt} = \left(\frac{\rho_\ell V_\ell}{\partial P / \partial v_\ell \big|_{u_\ell}} + \frac{\rho_m V_m}{\partial P / \partial v_m \big|_{u_m}} \right)^{-1} \cdot \left\{ \frac{\partial P / \partial u_\ell \big|_{v_\ell}}{\partial P / \partial v_\ell \big|_{u_\ell}} \left[-\dot{m}_{break} \left(h_{break} - u_\ell \right) \right] + \frac{\partial P / \partial u_m \big|_{v_m}}{\partial P / \partial v_m \big|_{u_m}} \dot{q}_{net} + v_\ell \dot{m}_{break} \right\} \quad (6.1\text{-}6)$$

$$\dot{q}_{net} = \dot{q}_{core} + \dot{q}_{SG} \quad (6.1\text{-}7)$$

Details in deriving the pressure equation are presented in Appendix C of Reference 6-5.

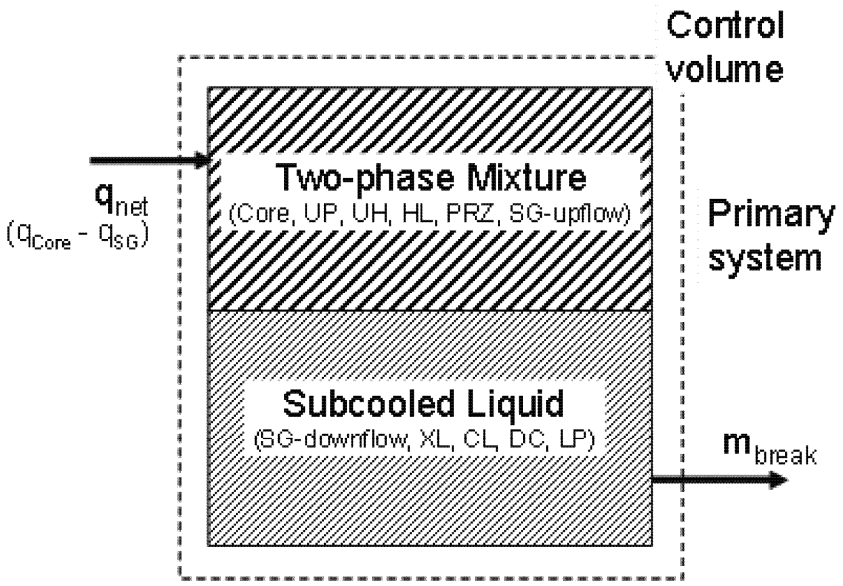

Figure 6.1-17 Schematic of Control Volume and Related Variables for Blowdown

6.1.2.3 Nondimensional Equations and Groups

Each of the physical parameters in the governing conservation equations is nondimensionalized by dividing by the reference quantity of the parameter, e.g. the initial value. Then, the equations are mathematically solved to obtain the temporal derivatives of the pressurizer pressure and liquid level. The resulting nondimensionalized equations that include all the relevant terms for this phase are as follows.

Nondimensionalized mass equation:

$$\frac{dM^*}{dt^*} = \Psi_{13}\left(-\dot{m}^*_{break}\right) \tag{6.1-8}$$

Equations Nondimensionalized pressure equation:

$$\frac{dP^*}{dt^*} = \Psi_2 C^*_{1,\ell} I^*_{b,\ell} + \Psi_6 C^*_{1,m} I^*_{c,m} + \Psi_{10} C^*_2 II^*_\ell \tag{6.1-9}$$

where

$$I^*_{b,\ell} = \frac{I_{b,\ell}}{\dot{m}_{break,0}\left(h_{break} - u_\ell\right)_0} \tag{6.1-10}$$

$$I^*_{c,m} = \frac{I_{c,m}}{\dot{q}_{net0}} \tag{6.1-11}$$

$$II^*_\ell = \frac{II_\ell}{v_{\ell,0}\left(-\dot{m}_{break0}\right)} \tag{6.1-12}$$

$$I_{b,\ell} = \dot{m}_{break}\left(h_{break} - u_\ell\right) \tag{6.1-13}$$

$$I_{c,m} = \dot{q}_{net} \tag{6.1-14}$$

$$II_\ell = v_\ell\left(-\dot{m}_{break}\right) \tag{6.1-15}$$

The quantities with an asterisk represent normalized variables, and subscript of zero denotes the reference value for the variable. The nondimensional time *t** indicates the time normalized to the temporal period of interest. The coefficients $C^*_{1,k}$ and C^*_2 are defined as follows:

$$C^*_{1,k} = \frac{C_{1,k}}{C_{1,k,0}} \tag{6.1-16}$$

$$C^*_2 = \frac{C_2}{C_{2,0}} \tag{6.1-17}$$

$$C_{1,k} = \frac{\partial P/\partial u_k\big|_{v_k} \Big/ \partial P/\partial v_k\big|_{u_k}}{\sum_k \left(\rho_k V_k \Big/ \partial P/\partial v_k\big|_{u_k}\right)} \tag{6.1-18}$$

$$C_2 = \frac{1}{\rho_\ell V_\ell \Big/ \partial P/\partial v_\ell\big|_{u_\ell}} \tag{6.1-19}$$

The nondimensional groups defined for the above equations are Ψ_2, Ψ_6, Ψ_{10} and Ψ_{13},

which are defined as follows:

$$\Psi_2 = \frac{C_{1,\ell,0}(h_{break} - u_\ell)_0 \dot{m}_0 t_0}{P_0} \quad (6.1\text{-}20)$$

$$\Psi_6 = \frac{C_{1,m,0}\dot{q}_{net0} t_0}{P_0} \quad (6.1\text{-}21)$$

$$\Psi_{10} = \frac{C_{2,0} v_{\ell,0} \dot{m}_0 t_0}{P_0} \quad (6.1\text{-}22)$$

$$\Psi_{13} = \frac{\dot{m}_{break,0} t_0}{M_0} \quad (6.1\text{-}23)$$

Ψ_2 is the ratio of pressure change, due to change in specific energy of the subcooled field from mass outflows, to the reference pressure. Ψ_6 is the ratio of pressure change, due to change in specific energy of the saturated field from heat transfer, to the reference pressure. Ψ_{10} is the ratio of pressure change, due to change in specific volume of the subcooled field from volumetric flow, to reference pressure. And finally, Ψ_{13} is defined as the ratio of break mass flow to the reference system mass. The reference mass is the RCS mass at the beginning of the phase. This selection makes Ψ_{13} the fraction of RCS mass lost during the phase.

The specific volume and internal energy of the mixture, v_m and u_m in the equations represent the averaged values over RCS-two-phase flow region, which are determined by the saturated fluid properties as follows:

$$v_m = x v_g + (1-x) v_f \quad (6.1\text{-}24)$$

$$u_m = x u_v + (1-x) u_f \quad (6.1\text{-}25)$$

6.1.2.4 Scaling Analysis Results

In the top-down approach, the scalability between the test facility and plant in terms of the transient behaviors of interest can be evaluated by quantifying and comparing the nondimensional groups for each test facility and plant.

Physical parameters used to quantify the nondimensional groups and the resultant nondimensional groups Ψ are summarized in Table 6.1-1 for the 7.5-in break. The order of magnitude analysis is performed by comparing the numerically evaluated nondimensional groups. The analysis shows that the most significant nondimensional group for the pressure behavior is Ψ_{10} relating to the break volumetric outflow both for the US-APWR and ROSA/LSTF. The relative magnitude of Ψ_2 and Ψ_6 to Ψ_{10} is almost the same between the two systems which indicates the relative importance of each mechanism is the same in the systems.

The reference values were estimated at the end of this phase. When the middle timing was selected, Ψ_2 for the ROSA/LSTF became much smaller than that for the US-APWR. This different tendency was caused by the different characteristics for the break flow rate as indicated in Figure 6.1-4.

The ratio of nondimensional groups between the US-APWR and ROSA/LSTF are compared in Table 6.1-2. The ratios are in the range of 0.85 to 1.5.

Figure 6.1-18 and Figure 6.1-19 compare the normalized pressure and mass of the reduced models between the US-APWR 7.5-in CLB and ROSA/LSTF SB-CL-18. The decreasing rate of pressure and mass is slightly higher until about **[ ]** for the US-APWR but the overall behavior is similar for the two systems. The higher decreasing rate is related to the different characteristics of break flow rate.

For the 1-ft^2 break case, Table 6.1-3 summarizes the physical parameters to quantify the nondimensional groups and the resultant nondimensional groups, Ψ. The order of magnitude analysis is also performed and the analysis shows that the most significant nondimensional group for the pressure behavior is Ψ_{10} for both systems and the relative magnitude of Ψ_2 and Ψ_6 to Ψ_{10} is almost the same between the two systems. The order of magnitude ranking of the ψ groups is the same in both systems which indicates the relative importance of each mechanism is the same in ROSA and the US-APWR.

The ratios of nondimensional groups between the US-APWR and ROSA/LSTF are compared in Table 6.1-4. All the ratios are also within the range of 0.65 to 1.2.

Figure 6.1-20 and Figure 6.1-21 compare the normalized pressure and mass of the reduced models between the US-APWR 1-ft^2 CLB and ROSA/LSTF IB-CL-02. For this break size, no significant deviation and distortion are recognized from these temporal changes.

Table 6.1-1 Comparison of Physical Values and Nondimensional Groups between US-APWR 7.5-in CLB and ROSA/LSTF SB-CL-18 for Blowdown Phase

Reference Parameters	US-APWR 7.5-in CLB	ROSA/LSTF SB-CL-18	Notes
t_0 (sec)	[ ]		Time period
M_0 (kg)			Initial RCS mass
P_0 (MPa)			Initial RCS pressure
$\dot{q}_{net0}$ (MW)			Net heat source at the end
$\dot{m}_{break,0}$ (kg/s)			Break flow rate at the end
$h_{break,0}$ (kJ/kg)			Break enthalpy at the end
$u_{m,0}$ (kJ/kg)			Reactor internal energy at the end
$v_{m,0}$ (m^3/kg)			Reactor specific volume at the end
$C_{1m,0}$ (Pa/J)			
$C_{1l,0}$ (Pa/J)			
$C_{2m,0}$ (Pa/m^3)			
Nondimensional Group			
Ψ_2	[ ]		
Ψ_6			
Ψ_{10}			
Ψ_{13}			
Ranking groups in the depressurization equation			
Ψ_2 / Ψ_{10}	[ ]		
Ψ_6 / Ψ_{10}			

Table 6.1-2 Scaling Criteria between US-APWR 7.5-in CLB and ROSA/LSTF SB-CL-18 for Blowdown Phase

Scaling Parameters	$\frac{\Psi_{i,ROSA}}{\Psi_{i,US-APWR}}$	Definitions
$\frac{\Psi_{2,ROSA}}{\Psi_{2,US-APWR}}$	[ ]	Ratio of pressure change, due to change in specific energy of the subcooled field from mass outflows, to reference pressure
$\frac{\Psi_{6,ROSA}}{\Psi_{6,US-APWR}}$		Ratio of pressure change, due to change in specific energy of the saturated field from heat transfer, to reference pressure
$\frac{\Psi_{10,ROSA}}{\Psi_{10,US-APWR}}$		Ratio of pressure change, due to change in specific volume of the subcooled field from volumetric flow, to reference pressure
$\frac{\Psi_{13,ROSA}}{\Psi_{13,US-APWR}}$		Ratio of integrated mass flow to reference mass

Table 6.1-3 Comparison of Physical Values and Nondimensional Groups between US-APWR 1-ft^2 CLB and ROSA/LSTF IB-CL-02 for Blowdown Phase

Reference Parameters	US-APWR 1-ft^2 CLB	ROSA/LSTF IB-CL-02	Notes
t_0 (sec)	[redacted]		Time period
M_0 (kg)			Initial RCS mass
P_0 (MPa)			Initial RCS pressure
$\dot{q}_{net0}$ (MW)			Net heat source at middle period
$\dot{m}_{break,0}$ (kg/s)			Break flow rate at middle period
$h_{break,0}$ (kJ/kg)			Break enthalpy at middle period
$u_{m,0}$ (kJ/kg)			Reactor internal energy at middle period
$v_{m,0}$ (m^3/kg)			Reactor specific volume at middle period
$C_{1m,0}$ (Pa/J)			
$C_{1l,0}$ (Pa/J)			
$C_{2m,0}$ (Pa/m^3)			
Nondimensional Group			
Ψ_2			
Ψ_6			
Ψ_{10}			
Ψ_{13}			
Ranking groups in the depressurization equation			
Ψ_2 / Ψ_{10}			
Ψ_6 / Ψ_{10}			

Table 6.1-4 Scaling Criteria between US-APWR 1-ft^2 CLB and ROSA/LSTF IB-CL-02 for Blowdown Phase

Scaling Parameters	$\frac{\Psi_{i,ROSA}}{\Psi_{i,US-APWR}}$	Definitions
$\frac{\Psi_{2,ROSA}}{\Psi_{2,US-APWR}}$	[ ]	Ratio of pressure change, due to change in specific energy of the subcooled field from mass outflows, to reference pressure
$\frac{\Psi_{6,ROSA}}{\Psi_{6,US-APWR}}$		Ratio of pressure change, due to change in specific energy of the saturated field from heat transfer, to reference pressure
$\frac{\Psi_{10,ROSA}}{\Psi_{10,US-APWR}}$		Ratio of pressure change, due to change in specific volume of the subcooled field from volumetric flow, to reference pressure
$\frac{\Psi_{13,ROSA}}{\Psi_{13,US-APWR}}$		Ratio of integrated mass flow to reference mass

Figure 6.1-18 Comparison of Normalized RCS Pressure between US-APWR 7.5-in CLB and ROSA/LSTF SB-CL-18 for Blowdown Phase

Figure 6.1-19 Comparison of Normalized RCS Mass between US-APWR 7.5-in CLB and ROSA/LSTF SB-CL-18 for Blowdown Phase

Figure 6.1-20 Comparison of Normalized RCS Pressure between US-APWR 1-ft^2 CLB and ROSA/LSTF IB-CL-02 for Blowdown Phase

Figure 6.1-21 Comparison of Normalized RCS Mass between US-APWR 1-ft^2 CLB and ROSA/LSTF IB-CL-02 for Blowdown Phase

6.1.2.5 Validation of Scaling Results

In the process of the present top-down scaling analysis, accuracy of the developed reduced model must be verified to ensure the reliability of the results evaluated in the preceded section. In order to accomplish this purpose, the normalized pressure and mass responses reproduced by the reduced model are compared with results from the M-RELAP5 calculations and experimental measurements (ROSA/LSTF SB-CL-18 and IB-CL-02).

Prior to discussing validity of the obtained results, status of the variables used to determine the nondimensional parameters P^* and M^* for the ROSA/LSTF tests is described. The outgoing flow rate is based on the measured break flow rate. On the other hand, the SG and hot wall heat transfer were extracted from the M-RELAP5 calculation because there are no available measured data. It is noted that an agreement for the nondimensional RCS mass inventory M^* between the measurement and the reduced model was quite good, because the measured break flow rate was commonly used to derive M^* from the measurements and to evaluate M^* in the reduced model using Equation (6.1-8). Similarly, a good agreement can be found in M^* for the US-APWR SBLOCAs.

The reduced model is able to provide the temporal changes for the normalized RCS pressure and mass by numerically solving the reduced equations, (6.1-8) and (6.1-9). The results are compared with those calculated by M-RELAP5 in Figure 6.1-22 and Figure 6.1-23 for the US-APWR 7.5-in CLB case. The same comparisons are depicted in Figure 6.1-24 and Figure 6.1-25 for the 1-ft^2 CLB case. The comparisons with ROSA/LSTF measurements are shown in Figure 6.1-26 through Figure 6.1-29. These comparisons demonstrate that the reduced model almost reproduces the code-calculated blowdown responses. And however, there are some discrepancies on the pressure decreasing rate in the initial period for the comparisons with measurements. The decreasing rate is slightly underestimated for both CLB cases. As mentioned in Section 6.1.2.1, an uncertainty and an underestimation can be considered for the measurement of break flow rate just after the break initiation in ROSA/LSTF. Since the discrepancy on the pressure decreasing rate becomes smaller by taking into account the uncertainty, it can be concluded that the evaluated scaling results are reliable although the initial discrepancy should be carefully addressed.

Figure 6.1-22 Comparison of Normalized RCS Pressure between M-RELAP5 and Reduced Model for US-APWR 7.5-in CLB Blowdown Phase

Reduced Model for US-APWR 7.5-in CLB Blowdown Phase

Figure 6.1-24 Comparison of Normalized RCS Pressure between M-RELAP5 and Reduced Model for US-APWR 1-ft^2 CLB Blowdown Phase

Figure 6.1-25 Comparison of Normalized RCS Mass between M-RELAP5 and Reduced Model for US-APWR 1-ft^2 CLB Blowdown Phase

Figure 6.1-26 Comparison of Normalized RCS Pressure between Measurement and Reduced Model for ROSA/LSTF SB-CL-18 Blowdown Phase

Figure 6.1-27 Comparison of Normalized RCS Mass between Measurement and Reduced Model for ROSA/LSTF SB-CL-18 Blowdown Phase

Figure 6.1-28 Comparison of Normalized RCS Pressure between Measurement and Reduced Model for ROSA/LSTF IB-CL-02 Blowdown Phase

Figure 6.1-29 Comparison of Normalized RCS Mass between Measurement and Reduced Model for ROSA/LSTF IB-CL-02 Blowdown Phase

6.1.2.6 Evaluation of Scaling Distortions

As discussed in Section 6.1.2.4, no significant distortion is found in the ROSA/LSTF scalability to the US-APWR during the blowdown phase. However, a different characteristic of break flow rate in the initial period is indicated between the ROSA/LSTF and the US-APWR as shown in Figure 6.1-4 and Figure 6.1-12. A sharp change of break flow rate is realized for the US-APWR just after the break initiation, while the transients for the ROSA/LSTF vary with more gradual manner. This different trend resulted in a distortion of the top-down scaling as in Section 6.1.2.4 and the impact on depressurization behavior is discussed here.

As shown in Figure 6.1-18, the depressurization of US-APWR is faster until about **[ ]** for 7.5-in CLB case and gives the deviation of P* of about **[ ]**. This deviation results in about **[ ]** faster initiation of scram signal. The time period of **[ ]** is within the assumed time delay (**[ ]**) of reactor trip and is considered to be an acceptable distortion. Furthermore, the reduced equation for the ROSA/LSTF tends to give a higher pressure against the measurement as shown in Figure 6.1-26 because of the uncertainty of break flow rate and then the pressure transient for the ROSA/LSTF in Figure 6.1-18 is possible to be close to that for the US-APWR if the tendency is taking into account.

On the other hand, no significant deviation is recognized for the US-APWR 1-ft^2 CLB and the ROSA/LSTF IB-CL-02 as shown in Figure 6.1-20. However, the reduced equation for the ROSA/LSTF might give a faster depressurization if the deviation against the measurement shown in Figure 6.1-28 is taking into account. The deviation results in about **[ ]** faster initiation of scram signal for the ROSA/LSTF. This distortion is considered to affect the dryout (DNB) characteristics and however the distortion does not provoke any safety concerns because the DNB did not occurred during the blowdown phase of this break size for both systems.

6.1.3 Bottom-up Scaling Analysis

From the viewpoint of the bottom-up approach, the discharge flow characteristic out the break is important in determining the initial plant response. Since the US-APWR SBLOCA methodology employs a break flow model approved in Appendix K to 10 CFR 50 for its application to the licensing safety analysis, the break flow model in M-RELAP5 was not explicitly assessed using SET data. However, the model has been assessed using several IET data, although occurrence of dryout (DNB) is not expected during the blowdown phase which was confirmed in the spectrum analyses of US-APWR SBLOCAs.[6-1] Therefore, there is no need to evaluate the break flow model and relevant experimental data by using the bottom-up scaling approach. However, as discussed in Section 6.1.2 Top-Down Scaling Analysis, the initial deviation of break flow rate between the US-APWR and the ROSA/LSTF gives a scaling distortion. As discussed in the previous Section 6.1.2.6, the distortion does not provoke any significant problems but as the scalability point of view for the break flow model it is needed to evaluate the applicability of the M-RELAP5 break flow model to the ROSA/LSTF.

Figure 6.1-30 and Figure 6.1-31 compare the break flow rate and the integrated one for the ROSA/LSTF SB-CL-18, respectively. Figure 6.1-32 and Figure 6.1-33 compare the same values for the ROSA/LSTF IB-CL-02. As for the SB-CL-02, the total amount of break flow in Figure 6.1-31 is well predicted although the initial single phase discharge until **[ ]** in Figure 6.1-30 shows a different transient where an overestimation is realized just after the break initiation and an underestimation is followed after **[ ]**. Although the best estimate characteristics differ to the Appendix K treatment, the validity is verified through the spectrum analyses for the break area.

For the IB-CL-02 test, the total amount of break flow in Figure 6.1-33 is overestimated by the M-RELAP5 model and the overestimation is mainly attained in the first **[ ]** as shown in Figure 6.1-32. The overestimation of break flow in the 1-ft^2 CLB case corresponds to the Appendix K treatment. The faster depressurization gives an early activation of accumulator and the code applicability including the prediction of PCT should be verified in the assessment section for IB-CL-02. Reference 6-1 demonstrates that M-RELAP5 is capable of predicting PCTs appropriately or conservatively against the measurements.

The heat transfer between the primary and secondary sides of the SG can also be an important phenomenon during the blowdown phase. In the top-down scaling analysis, the results from the M-RELAP5 analyses were used for the steam generator heat transfer and no significant distortion relating to the SG heat transfer was recognized. In this report, the verification for the SG heat transfer will be performed in Section 7.2.7 in the code scale-up capability and the M-RELAP5 model predicts the ROSA/LSTF SG transients well as discussed in that section.

Figure 6.1-30 Comparison of Break Flow rate between MRELAP5 calculation and ROSA/LSTF SB-CL-18 (Measurement)

Figure 6.1-31 Comparison of Integral of Break Mass Flow rate between MRELAP5 calculation and ROSA/LSTF SB-CL-18 (Measurement)

Figure 6.1-32 Comparison of Break Flow rate between MRELAP5 calculation and ROSA/LSTF IB-CL-02 (Measurement)

Figure 6.1-33 Comparison of Integral of Break Mass Flow rate between MRELAP5 calculation and ROSA/LSTF IB-CL-02 (Measurement)

6.1.4 Summary

The depressurization characteristic during blowdown is important because that determines the signal timing for the scram and the safety injection and the timing of the transition to the natural circulation phase. The ROSA/LSTF facility is a major IET providing integral system responses including the blowdown phase, for which it is necessary to evaluate the scalability to the US-APWR.

This section mainly investigated the depressurization behavior in the US-APWR SBLOCA 7.5-in and 1-ft^2 CLBs and in the ROSA/LSTF SB-CL-18 and IB-CL-02 tests, and characterized the behavior using nondimensional equations to examine the scalability quantitatively. The study revealed that the controlling mechanism for the depressurization is almost identical for the US-APWR and the ROSA/LSTF. The similitude between the two systems was examined comparing the order of magnitude of the nondimensional parameters and the similitude was confirmed except for the different characteristics of the break flow rate. The difference from the break flow rate was evaluated and it was concluded that no significant impacts on the depressurization behavior and on the safety issue exist.

In the bottom-up scaling, the applicability of the break flow model of the M-RELAP5 was examined using the measured data from the ROSA/LSTF SB-CL-18 and IB-CL-02. The break flow model indicates a best-estimate prediction for the SB-CL-18 although a different transient is recognized in the initial period. And the break flow model indicates an overestimation for the IB-CL-02. On the safety analysis point of view, spectrum analyses for the break size and orientation cover the best-estimate tendency and the overestimation tendency corresponds to the Appendix-K treatment.

6.2 Natural Circulation

6.2.1 Phenomena and Applied Test Facility

For the US-APWR, in a postulated SBLOCA, the natural circulation phase starts when the pumps have coasted down and the steam generator is acting as a heat sink for the primary system. For the 7.5-in CLB, the primary conditions necessary to identify the natural circulation phase are as follows: the primary system pressure is greater than that of secondary system pressure, and most importantly, the RCP has fully coasted down. The natural circulation phase ends when there is no substantial net liquid flow at the top of steam generators' (SG) U-tubes. From mass and energy balances point of view, when the steam quality is high enough, the liquid flow rate at the top of SG U-tubes decreases to zero. The decay heat is removed by heat transfer (condensation and convection) to the SG secondary side. The emergency feedwater system is initiated to maintain the secondary side inventory. Vapor generated in the core is trapped within the RCS by the loop seal. As more low quality coolant flow exits the break, the vapor accumulates in the downhill side of the SG U-tubes and the crossover leg. The natural circulation will continue until the driving-head on the cold leg side of the loops is no longer sufficient to maintain the liquid flow rate through the top of SG U-tubes, due to the accumulation of steam in loops between the top of the SG U-tubes and the loop seals. Hence, the end of the natural circulation phase is defined by the time when the liquid mass flow rate at the top of SG U-tubes approaches zero.

The natural circulation phase in a postulated 7.5-in cold leg break in the US-APWR is characterized by a nearly constant RCS pressure. In general, there are no complex phenomena occurring during the natural circulation phase, except for the outflow from the continuous discharge from the break location. There is no mass and energy inflow to the system because the ECCS is not in operation during natural circulation. The RCS pressure is still above the actuation set point of the advanced accumulator, while the safety injection pumps have not injected any coolant due to the loss-of-offsite power (LOOP) assumption. Core power is at a decay heat level of ~4% of the rated thermal power. The steam generators' secondary side serves as the heat sink. Break flow is initially subcooled then reaches saturation. Based on the M-RELAP5 analysis, the RCS pressure is assumed constant at ~1300 psia. The steam quality in the RCS is growing monotonically due to the break flow that decreases the system mass inventory. Steam quality is considered only in the hot region, consisting of core, upper plenum, hot legs, SG inlet plenums, and up flow-side of SG U-tubes.

This section studies the US-APWR response to a 7.5-in CLB where the limiting PCT occurs during the loop seal period. This section addresses the scalability of the ROSA/LSTF SB-CL-18 test.

The US-APWR SBLOCA PIRT identifies heat transfer in the steam generators and void distribution in the downcomer and lower plenum as the important phenomena and processes during this phase. In the present study, the natural circulation phase is investigated first from the global mass and energy balances in the system, since the flow out the break and the net heat transfer to coolant (heat generation from the core and heat removal to the SG secondary side) increases steam quality in the system, affecting both the natural circulation behavior and the duration of the natural circulation phase. Scalability of the system response with respect to the mass inventory is quantified in this

evaluation. This approach allows implicit scalability evaluation of the steam quality behavior during the natural circulation phase. Second, the scalability between the US-APWR and ROSA/LSTF will be addressed based on the integral momentum balance through the reactor system.

6.2.2 Top-Down Scaling Analysis

6.2.2.1 Transient Behavior of Interest

For the natural circulation phase, the transient behaviors of interest are the depressurization rate and the mass inventory of the RCS from the beginning to the end of the phase. The decay power at the end of natural circulation affects fuel cladding heat-up behavior during the subsequent loop seal clearing phase.

In order to determine the various reference parameters required to perform the top-down scaling analysis for the natural circulation phase, the start and end times of natural circulation phase shall be first defined. The start of the natural circulation phase can be defined as the time when the RCP has been fully coasted down and its head pressure has been sufficiently low, as not to affect the natural circulation. Figure 6.2-1 shows the time dependent variation of primary and secondary pressures for US-APWR. The figure shows that following the blowdown depressurization the RCS pressure stabilizes a little bit higher than the steam generator secondary pressure. Figure 6.2-2 represents the transient liquid mass flow rate at the top of the U-tubes and the RCP head plotted as a function of time. This figure confirms that the RCPs head is too low to have any effect on the natural circulation flow. Based on the RCP coast down time it can be defined that the natural circulation phase begins at **[ ]**.

The end of the natural circulation phase is defined as the time when the liquid mass flow rate at the top of the SG U-tubes becomes very small or approaches zero, or no net liquid flow at the top of U-tubes. Figure 6.2-3 illustrates that the liquid mass flow rate at the top of U-tubes reaches the lowest value, almost zero, at **[ ]**. The figure also shows the transient behavior of the static steam quality at the same location. The steam quality is low at the start of the natural circulation phase, and gradually increases as the natural circulation phase progresses.

In the ROSA/LSTF test, the pressure has an inflection point at about 25 seconds and then the depressurization rate becomes much lower, although not as low as in the US-APWR. The ROSA/LSTF primary and secondary side pressures are shown in Figure 6.2-4. The primary pressure remains above the secondary pressure until 180 seconds. In Figure 6.2-5**,** the primary system pressure in ROSA/LSTF is compared with the primary system pressure in the US-APWR. Following the inflection point, the pressures agree reasonably well, with the pressure in ROSA having a gradual decrease. In Figure 6.2-6, the RCP head is overlaid with the liquid flow at the top of the steam generator U-tubes. The liquid flow rate becomes decoupled from the pump head at about **[ ]**. The start of the natural circulation phase in ROSA/LSTF is defined at **[ ]** judged from the decoupling time. In Figure 6.2-7 the liquid mass flow rate and static quality at the top of the U-tubes are overlaid. The plot shows that the liquid flow approaches zero at **[ ]** which corresponds to the time when the quality approaches 1.0. Both of these events are consistent with the termination of the natural circulation flow. The end of the natural circulation phase in ROSA/LSTF is defined at **[ ]**.

Figure 6.2-8 shows the time dependent variation of primary and secondary pressures for US-APWR 1-ft^2 CLB case. The figure shows that following the blowdown depressurization the RCS pressure stabilizes a little bit higher than the steam generator secondary pressure until **[ ]**. Figure 6.2-9 represents the transient liquid mass flow rate at the top of the U-tubes and the RCP head plotted as a function of time. This figure confirms that the RCPs head is too low to have any effect on the natural circulation flow. Based on the RCP coast down time it can be defined that the natural circulation phase begins at **[ ]** although a slight head is still recognized. The end of the natural circulation phase is defined as the time when the liquid mass flow rate at the top of the SG U-tubes becomes very small or approaches zero under the higher primary pressure than secondary pressure. Thus the end time can be defined at **[ ]**.

For the ROSA/LSTF IB-CL-02 test, the primary and secondary side pressures are shown in Figure 6.2-10. The primary pressure remains above the secondary pressure until **[ ]**. Figure 6.2-11 represents the transient liquid mass flow rate at the top of the U-tubes and the RCP head plotted as a function of time. Although the start of natural circulation is considered to be **[ ]** from the pressure transients and the RCP head, the liquid mass flow rate at the U-tube top is almost zero from the time and suddenly increases from **[ ]**. This peculiar transient implies that an idealized natural circulation is not maintained in the ROSA/LSTF IB-CL-02. Because of this different characteristic for the existence of natural circulation between the US-APWR and the ROSA/LSTF, MHI judged that this period after blowdown phase will be analyzed as a part of boil-off phase in this report.

Figure 6.2-1 Primary and Secondary Pressures for US-APWR 7.5-in CLB (Calculation)

Figure 6.2-2 Liquid Mass Flow rate at U-Tube Top and RCP Pressure Head for US-APWR 7.5-in CLB (Calculation)

Figure 6.2-3 Liquid Mass Flow rate and Static Quality at U-Tube Top for US-APWR 7.5-in CLB (Calculation)

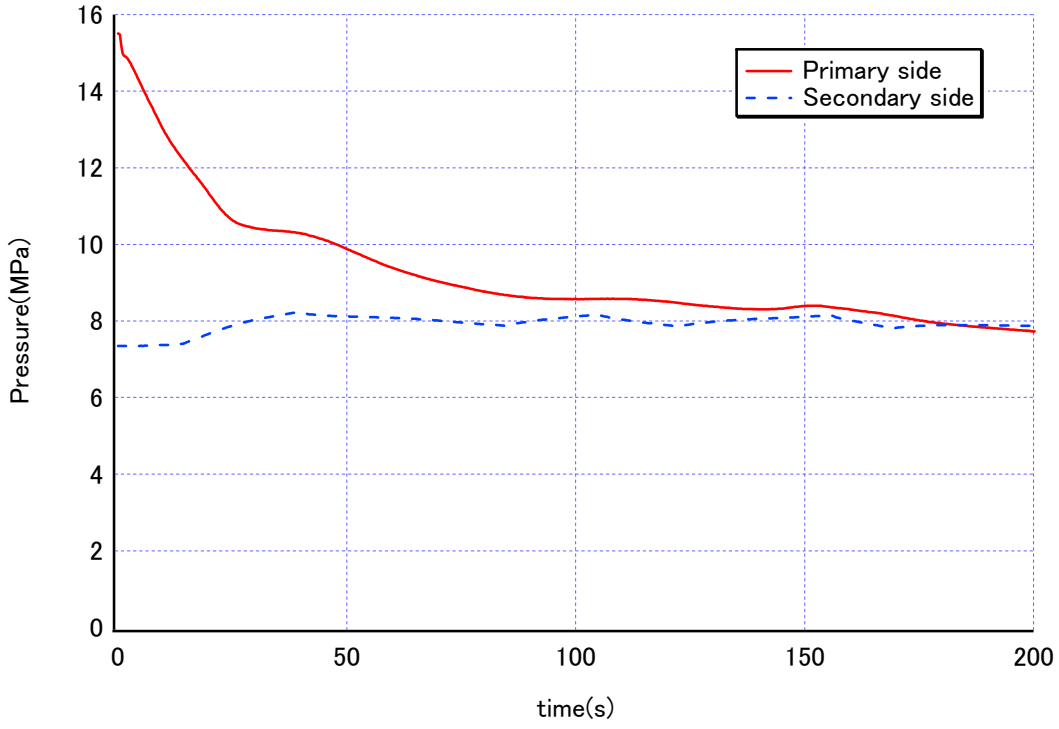

Figure 6.2-4 Primary and Secondary Pressures in ROSA/LSTF SB-CL-18 (Measurement)

Figure 6.2-5 Comparison of Primary Pressure between US-APWR 7.5-in CLB (Calculation) and ROSA/LSTF SB-CL-18 (Measurement)

Figure 6.2-6 Liquid Mass Flow rate at U-Tube Top and RCP Head for ROSA/LSTF SB-CL-18 (Calculation)

Figure 6.2-7 Liquid Mass Flow rate and Static Quality at U-Tube Top for ROSA/LSTF SB-CL-18 (Calculation)

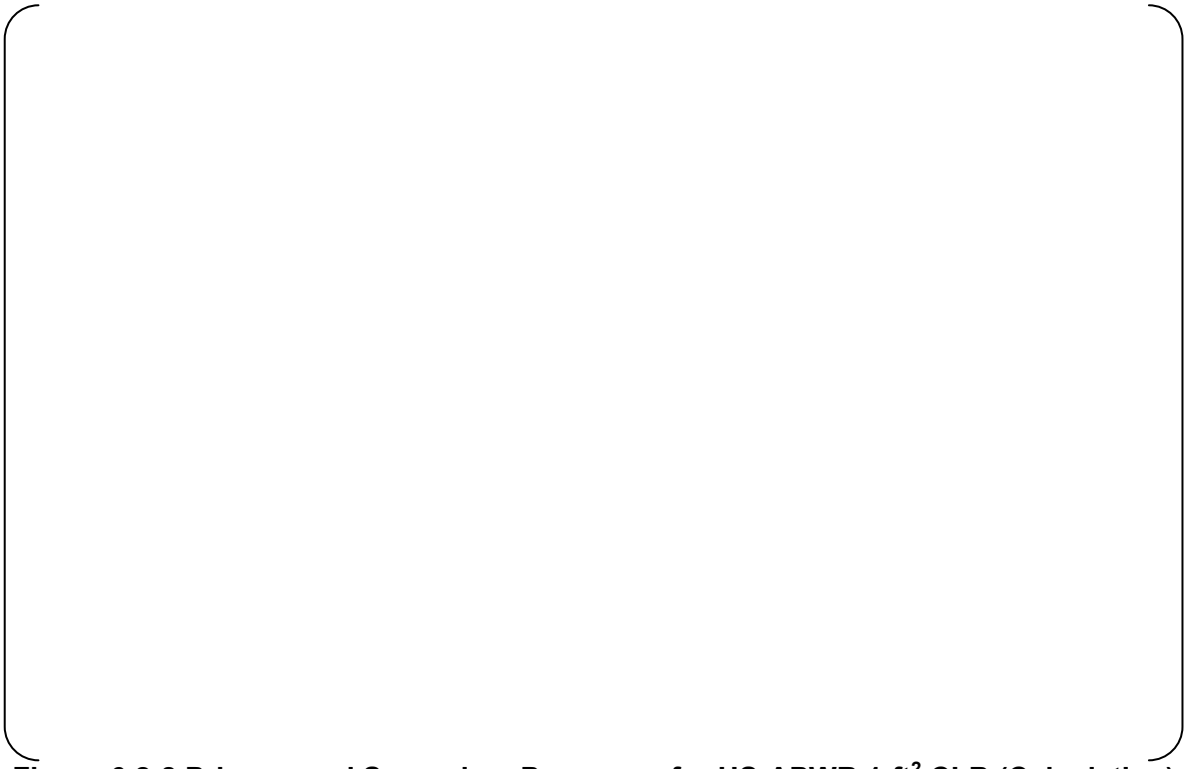

Figure 6.2-8 Primary and Secondary Pressures for US-APWR 1-ft^2 CLB (Calculation)

Figure 6.2-9 Liquid Mass Flow rate at U-Tube Top and RCP Pressure Head for US-APWR 1-ft^2 CLB (Calculation)

Figure 6.2-10 Primary and Secondary Pressures in ROSA/LSTF IB-CL-02 (Measurement)

Figure 6.2-11 Liquid Mass Flow rate at U-Tube Top and RCP Pressure Head for ROSA/LSTF IB-CL-02 (Calculation)

6.2.2.2 Mass and Energy Balances

6.2.2.2.1 Governing Conservation Equations

As the initial approach, the natural circulation phase is evaluated from the viewpoint of mass and energy balances. Given a certain depressurization rate during the phase, the rate of natural circulation, represented by the mass flow rate at the top of SG U-tube can be directly correlated to the RCS mass inventory. It will be shown that the rate of natural circulation will gradually decrease with the continued mass and energy discharges from the break and the impact of continued vapor generation in the core. The following figure is the system flow diagram for the general representation of the natural-circulation phase:

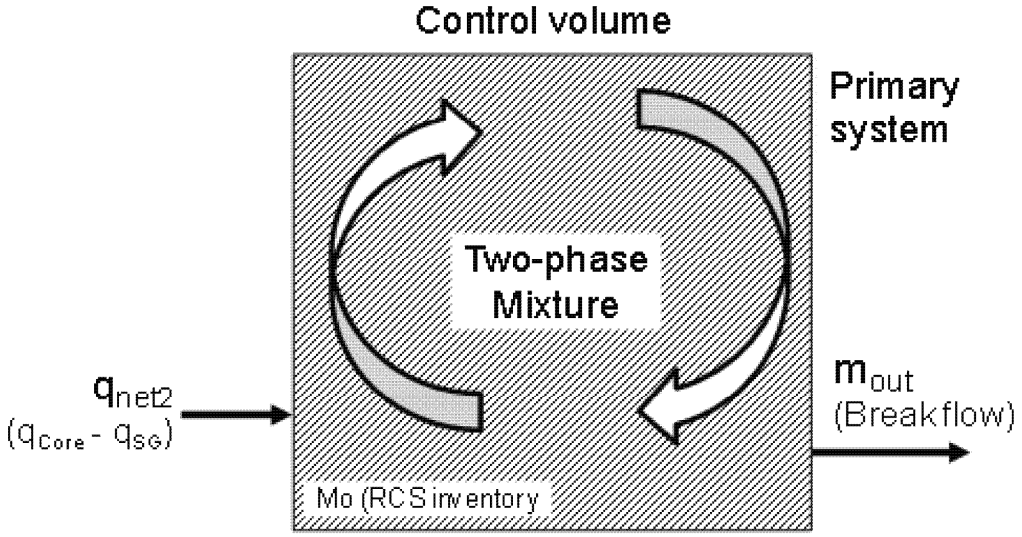

Figure 6.2-12 Schematic of Control Volume and Related Variables for Natural Circulation (Mass and Energy Balances)

The purpose of the analysis is to evaluate the scalability of ROSA/LSTF test data to the natural circulation during an SBLOCA in the US-APWR, as compared to the US-APWR plant analysis performed using M-RELAP5. The objective of this analysis is to identify the dominating nondimensional groups applicable for both the US-APWR and ROSA/LSTF. Then the ordering of the magnitude of these nondimensional groups will be evaluated to judge the scalability and/or applicability of the ROSA/LSTF to represent the US-APWR natural circulation.

The governing mass and energy equations for the two-phase system are given as follows;

Mass conservation equation:

$$\frac{d\left(\rho_\ell V_\ell + \rho_v V_v\right)}{dt} = \frac{d\rho_m V}{dt} = -\dot{m}_{break} \tag{6.2-1}$$

$$\rho_m = \frac{\rho_\ell V_\ell + \rho_v V_v}{V} \tag{6.2-2}$$

where ρ_m, V, and m_{break} are the mixture density, volume and break flow rates, respectively.

For the natural-circulation phase, the one-field two-phase saturated mixture approach is employed. The advantage of employing the saturated mixture equation is the elimination of complicated vaporization and condensation terms in the conservation equation. Since the liquid and vapor in the RCS remain in saturated condition, this simplification is applicable to represent the fluid behavior. It is noted, however, that a small amount of superheat and subcooling appear in the SG outlet vapor and in the core inlet liquid, respectively.

Figure 6.2-13 and Figure 6.2-14 are presented as the basis of the applicability of two-phase mixture approach from the viewpoint of void-fraction transient behavior in the representative parts of the RCS (both in the US-APWR and ROSA) throughout the duration of the natural circulation phase. Figure 6.2-13 shows the comparison of void fraction at the broken loop SG entrance between the two systems. For both systems, the phase starts out with a void fraction value of about **[ ]** and terminates with that of about **[ ]**. These magnitudes of void fraction in the SG entrance provide a strong basis for using the two-phase mixture approach.

Figure 6.2-14 compares the transient behavior of void fraction at the top of SG U-tubes in the broken-loop, between US-APWR and ROSA/LSTF. The US-APWR starts out at a void fraction of **[ ]** at the top of SG U-tubes, while for the ROSA/LSTF SB-CL-18, that of about **[ ]**. However, due to the scaled volume, the void fraction in ROSA/LSTF increases at a faster rate and the natural circulation terminates at a void fraction of **[ ]** for both systems. **[ ]**, the fluid conditions in the two systems clearly require the application of the saturated two-phase mixture approach.

Similar to the mass conservation, the mixture energy conservation equation is obtained.

Energy conservation equation:

$$\frac{d\left(\rho_\ell V_\ell \varepsilon_\ell + \rho_v V_v \varepsilon_v\right)}{dt} = \frac{d\rho_m V \varepsilon_m}{dt} = \dot{q}_{core} + \dot{q}_{SG} - \dot{m}_{break}\varepsilon_{break} \tag{6.2-3}$$

$$\varepsilon_m = \frac{\rho_\ell V_\ell \varepsilon_\ell + \rho_v V_v \varepsilon_v}{\rho_m V} = \frac{\rho_\ell V_\ell \varepsilon_\ell + \rho_v V_v \varepsilon_v}{\rho_\ell V_\ell + \rho_v V_v} \tag{6.2-4}$$

where ε_m, ε_{break}, q_{core}, and q_{SG} are the mixture fluid energy (enthalpy), break flow enthalpy, heat transfer from the core, SG, and reactor hot wall, respectively. In the above equation, the fluid energy is represented as follows, by neglecting the kinetic and potential energy:

$$\varepsilon = h = u + Pv \tag{6.2-5}$$

where u, P, and v are the internal energy, pressure, and specific volume, respectively. By using equation (6.2-5), the energy conservation is converted into a differential equation to represent the pressure change as follows:

Pressure equation:

$$\frac{dP}{dt} = \frac{\partial P / \partial v_m \big|_{u_m}}{\rho_m V} \left\{ \frac{\partial P / \partial \mu_m \big|_{v_m}}{\partial P / \partial v_m \big|_{u_m}} \left[-\dot{m}_{break} \left(h_{break} - u_m \right) + \dot{q}_{net} \right] - v_m \left(-\dot{m}_{break} \right) \right\} \quad (6.2\text{-}6)$$

$$\dot{q}_{net} = \dot{q}_{core} + \dot{q}_{SG} \quad (6.2\text{-}7)$$

As shown in the above set of equations, during the natural circulation phase, the conservation equations only contain the storage rate and outflow rate terms. There is no associated inflow mass and energy into the system, as the safety injection and the accumulator have not been initiated during this phase for the postulated break size of 7.5-inch.

Details of deriving the pressure equation are presented in Appendix C of Reference 6-5.

Figure 6.2-13 Comparison of Void Fraction at the Broken-Loop SG Entrance between US-APWR 7.5-in CLB and ROSA/LSTF SB-CL-18 during Natural Circulation Phase

Figure 6.2-14 Comparison of Void Fraction at the Broken-Loop SG U-tube top between US-APWR 7.5-in CLB and ROSA/LSTF SB-CL-18 during Natural Circulation Phase

6.2.2.2.2 Nondimensional Equations and Groups

The mass equation (6.2-1) and the pressure equation (6.2-6) are nondimensionalized by normalizing each variable to the reference value. Details in deriving the nondimensional equations are also given in Appendix C of Reference 6-5. The resulting equations are as follows:

Nondimensionalized mass equation:

$$\frac{dM^*}{dt^*} = \Psi_{13}\left(-\dot{m}^*_{break}\right) \tag{6.2-8}$$

Nondimensionalized pressure equation:

$$\frac{dP^*}{dt^*} = \Psi_5 C^*_{1,m} I^*_{b,m} + \Psi_6 C^*_{1,m} I^*_{c,m} + \Psi_{11} C^*_2 II^*_m \tag{6.2-9}$$

where

$$I^*_{b,m} = \frac{I_{b,m}}{\dot{m}_{break,0}\left(h_{break} - u_m\right)_0} \tag{6.2-10}$$

$$I^*_{c,m} = \frac{I_{c,m}}{\dot{q}_{net0}} \tag{6.2-11}$$

$$II^*_m = \frac{II_m}{v_{m,0}\left(-\dot{m}_{break0}\right)} \tag{6.2-12}$$

$$I_{b,m} = \dot{m}_{break}\left(h_{break} - u_m\right) \tag{6.2-13}$$

$$I_{c,m} = \dot{q}_{net} \tag{6.2-14}$$

$$II_m = v_m\left(-\dot{m}_{break}\right) \tag{6.2-15}$$

The quantities with an asterisk represent normalized variables, and subscript of zero denotes the reference value for the variable. The nondimensional time t^* indicates the time normalized to the temporal period of interest. The coefficients $C^*_{1,m}$ and C^*_2 are defined as follows:

$$C^*_{1,m} = \frac{C_{1,m}}{C_{1,m,0}} \tag{6.2-16}$$

$$C^*_{2,m} = \frac{C_2}{C_{2,m,0}} \tag{6.2-17}$$

$$C_{1,m} = \frac{\partial P / \partial u_m\big|_{v_m}}{\rho_m V} \tag{6.2-18}$$

$$C_{2,m} = \frac{\partial P / \partial v_m\big|_{\mu_m}}{\rho_m V} \tag{6.2-19}$$

The nondimensional groups defined for the above equations are Ψ_5, Ψ_6, Ψ_{11}, and Ψ_{13},

which are defined as follows:

$$\Psi_5 = \frac{C_{1,m,0}(h_{break} - u_m)_0 \dot{m}_0 t_0}{P_0} \quad (6.2\text{-}20)$$

$$\Psi_6 = \frac{C_{1,m,0}\dot{q}_{net0} t_0}{P_0} \quad (6.2\text{-}21)$$

$$\Psi_{11} = \frac{C_{2,0} v_{m,0} \dot{m}_0 t_0}{P_0} \quad (6.2\text{-}22)$$

$$\Psi_{13} = \frac{\dot{m}_0 t_0}{M_0} \quad (6.2\text{-}23)$$

Ψ_5 is the ratio of pressure change, due to change in specific energy of the saturated field from mass outflows, to the reference pressure. Ψ_6 is the ratio of pressure change, due to change in specific energy of the saturated field from heat transfer, to the reference pressure. Ψ_{11} is the ratio of pressure change, due to change in specific volume of the saturated field from volumetric flow, to reference pressure. And finally, Ψ_{13} is defined as the ratio of net mass flow to the reference system mass.

The specific volume and internal energy of the mixture, v_m and u_m in the equations represent the RCS-averaged values, which are determined by the saturated fluid properties as follows:

$$v_m = x v_g + (1-x) v_f \quad (6.2\text{-}24)$$

$$u_m = x u_v + (1-x) u_f \quad (6.2\text{-}25)$$

6.2.2.2.3 Scaling Analysis Results

To evaluate the reduced nondimensional equations, (6.2-8) and (6.2-9), a spreadsheet was developed to calculate the nondimensional groups of Ψ_5, Ψ_6, Ψ_{11} and Ψ_{13} for both US-APWR and ROSA/LSTF. Table 6.2-1 shows the spreadsheet with embedded formula to determine the dominating nondimensional groups. In the table, reference parameters are listed that comprise the break's liquid flow rate, liquid enthalpy and specific energy, the difference between core power from decay heat as heat input and the heat removal by SGs, RCS mass inventory at a specified time, reference pressure, and fluid property. The purpose of evaluating Ψ_{13} is to address the mass balance consideration. Initial RCS mass is used as the reference value for M_0. By doing this, Ψ_{13} represents the fraction of system mass lost out the break during the natural circulation phase.

In order to investigate the similitude of both systems, the order of magnitude analysis is performed by comparing the numerically evaluated nondimensional groups. The analysis shows that the most significant nondimensional group for the pressure behavior is Ψ_6 and Ψ_{11} for the US-APWR but only Ψ_{11} for the ROSA/LSTF as well as Ψ_{13}. The relative magnitude of Ψ_5 to Ψ_{11} is almost the same between the two systems.

The ratio of nondimensional groups between the US-APWR and ROSA/LSTF are compared in Table 6.2-2. From the viewpoint of the characterized scaling criteria both for

the P^* and M^*, the ratios of dominating scaling parameters of Ψ_5, Ψ_{11} and Ψ_{13} between the ROSA/LSTF and the US-APWR fall in the range of **[ ].**

The ratio of Ψ_6 group is an exception with a value of **[ ]**. The physical process represented by the Ψ_6 group is the effect of net heat transfer to the two-phase fluid on pressure. The net heat transfer is defined as the heat removed by the steam generators subtracted from the decay heat added by the core, over the duration of the phase. Looking at the individual heat flow terms, the steam generator heat transfer in ROSA/LSTF is disproportionally larger than in the US-APWR. This may be due to the larger difference between primary and secondary pressures in ROSA/LSTF as seen in Figure 6.2-1 and Figure 6.2-4. **[**

] The above explains why the pressure is slowly decreasing in ROSA/LSTF while it is nearly constant in the US-APWR.

Finally, the table shows that throughout the natural circulation phase both the US-APWR and ROSA/LSTF lose **[ ]** of the initial mass inventory. Because the natural circulation phase does not give a strong effect on PCT, the roughly equal value of Ψ_{13} shows that the RCS mass inventory response of the ROSA/LSTF should be representative of the US-APWR RCS mass inventory response.

Figure 6.2-15 compares nondimensional mass inventory reduction rate (dM*/dt*) for the US-APWR and ROSA/LSTF to demonstrate the scalability of the ROSA/LSTF. The figure demonstrates that from the mass and energy balances standpoint, the loss of inventory during the natural circulation phase in both the US-APWR and ROSA/LSTF are in good agreement. Both of the systems lose **[ ]** of their initial inventory at the end of natural circulation phase.

The comparison of nondimensional depressurization rate (dP*/dt*) between US-APWR and ROSA/LSTF is shown in Figure 6.2-16. The figure shows that for the US-APWR, the natural circulation phase occurs at virtually constant pressure, while a gradual decrease in RCS pressure takes place during the natural circulation phase in the ROSA/LSTF. However, the magnitude of the pressure difference at the end of natural circulation is not significant.

Table 6.2-1 Comparison of Physical Values and Nondimensional Groups between US-APWR 7.5-in CLB and ROSA/LSTF SB-CL-18 for Natural Circulation Phase (Mass and Energy Balances)

Reference Parameters	US-APWR 7.5-in CLB	ROSA/LSTF SB-CL-18	Notes
t_0 (sec)			Time period
M_0 (kg)			Initial RCS mass
P_0 (MPa)			Initial RCS pressure
$\dot{q}_{net0}$ (MW)			Net heat source averaged in this phase
$\dot{m}_{break,0}$ (kg/s)			Break flow rate averaged in this phase
$h_{break,0}$ (kJ/kg)			Break enthalpy averaged in this phase
$u_{m,0}$ (kJ/kg)			Reactor internal energy averaged in this phase
$v_{m,0}$ (m^3/kg)			Reactor specific volume averaged in this phase
$C_{1m,0}$ (Pa/J)			
$C_{2m,0}$ (Pa/m^3)			
Nondimensional Group			
Ψ_5			
Ψ_6			
Ψ_{11}			
Ψ_{13}			
Ranking groups in the depressurization equation			
ψ_5/ψ_{11}			
ψ_6/ψ_{11}			

Table 6.2-2 Scaling Criteria between US-APWR 7.5-in CLB and ROSA/LSTF SB-CL-18 for Natural Circulation Phase (Mass and Energy Balances)

Scaling Parameters	$\frac{\Psi_{i,ROSA}}{\Psi_{i,US-APWR}}$	Definitions
$\frac{\Psi_{5,ROSA}}{\Psi_{5,US-APWR}}$	[ ]	Ratio of pressure change, due to change in specific energy of the saturated field from mass outflows, to reference pressure
$\frac{\Psi_{6,ROSA}}{\Psi_{6,US-APWR}}$		Ratio of pressure change, due to change in specific energy of the saturated field from heat transfer, to reference pressure
$\frac{\Psi_{11,ROSA}}{\Psi_{11,US-APWR}}$		Ratio of pressure change, due to change in specific volume of the saturated field from volumetric flow, to reference pressure
$\frac{\Psi_{13,ROSA}}{\Psi_{13,US-APWR}}$		Ratio of integrated mass flow to reference mass

Figure 6.2-15 Comparison of Normalized RCS Mass between US-APWR 7.5-in CLB and ROSA/LSTF SB-CL-18 for Natural Circulation Phase (Mass and Energy Balances)

Figure 6.2-16 Comparison of Normalized RCS Pressure between US-APWR 7.5-in CLB and ROSA/LSTF SB-CL-18 for Natural Circulation Phase (Mass and Energy Balances)

6.2.2.2.4 Validation of Scaling Results

Status of the variables used to derive the nondimensional parameters *M** and *P** for the ROSA/LSTF SB-CL-18 test is described below. The measured break flow rate was used for the reduced model, while the break flow enthalpy and the SG heat transfer were extracted from the M-RELAP5 calculation because there are no available measurements.

Figure 6.2-17 shows the consistency between the M-RELAP5 calculation and the applied reduced model in calculating the nondimensional mass inventory reduction rate (dM*/dt*) for the US-APWR 7.5-in cold-leg break during the natural circulation phase. The results demonstrate the validity of the reduced model to verify the M-RELAP5 calculation showing that the US-APWR losses **[ ]** of its total system mass inventory at the end of natural circulation phase.

Similarly, Figure 6.2-18 depicts the consistency of the M-RELAP5 calculation and the applied reduced model in calculating the nondimensional depressurization rate (dP*/dt*) for the US-APWR 7.5 in cold-leg break. The calculation and the application of the reduced model both demonstrate that for the US-APWR, the natural circulation phase in a SBLOCA takes place at virtually constant pressure.

Figure 6.2-19 shows the comparison of normalized RCS mass based on experiment measurements and the reduced model for ROSA/LSTF SB-CL-18 during the natural circulation phase. The figure is intended to show that the reduced equation for mass and energy balances is capable of predicting the inventory, consistent with the measured data. The result calculated using the reduced equation is in good agreement with the measured data. This agreement is reasonable and natural, because the measured break flow rate was used to derive *M** for the measurement and to evaluate *M** by the reduced model as shown in Equation (6.2-8).

Similarly, Figure 6.2-20 is intended to show the capability of the reduced equation to predict the measured depressurization rate in ROSA/LSTF SB-CL-18 during the natural circulation phase. Although ROSA/LSTF SB-CL-18 experienced a gradual decrease in RCS pressure during the natural circulation phase, the reduced equation shows a smaller decrease in pressure, the difference in pressure response is not significant. Because no cladding heat up occurs during the natural circulation phase, this minor distortion is not a concern for the PCT calculation.

Figure 6.2-21 shows the US-APWR and ROSA/LSTF natural circulation mass flow rates at the top of the SG U-tubes plotted as a function of RCS mass inventory. As read from right-to-left, the figure clearly demonstrates that the natural circulation rate gradually decreases with the continual decrease in RCS mass inventory. In both the US-APWR and ROSA/LSTF, the natural circulation phase terminates when the RCS has lost **[ ]** of its initial inventory.

Finally, Figure 6.2-22 shows the comparison of static quality at the top of SG U-tubes between US-APWR and ROSA/LSTF. Due to the difference in system volume, the characteristic of change in various parameters between the two systems is also different. For US-APWR, the natural circulation phase starts at a higher static quality than that of ROSA/LSTF. However the quality in ROSA/LSTF becomes higher after about **[ ]** and rapidly increases after about **[ ].** The rapid increase was caused by the pressure

relief valve set point in the secondary cooling system. Once the relief valve is actuated, the decrease in secondary system pressure is subsequently followed by the decrease in the primary system pressure that increases the voiding. With the simulated core power in the ROSA/LSTF being higher than the US-APWR, the increase in static quality occurs at a higher rate and gives the higher quality after about **[ ]**. However, this does not cause any concern to the PCT.

Figure 6.2-17 Comparison of Normalized RCS Mass between M-RELAP5 and Reduced Model for US-APWR 7.5-in CLB Natural Circulation Phase (Mass and Energy Balances)

Figure 6.2-18 Comparison of Normalized RCS Pressure between M-RELAP5 and Reduced Model for US-APWR 7.5-in CLB Natural Circulation Phase (Mass and Energy Balances)

Figure 6.2-19 Comparison of Normalized RCS Mass between Measurement and Reduced Model for ROSA/LSTF SB-CL-18 Natural Circulation Phase (Mass and Energy Balances)

Figure 6.2-20 Comparison of Normalized RCS Pressure between Measurement and Reduced Model for ROSA/LSTF SB-CL-18 Natural Circulation Phase (Mass and Energy Balances)

Figure 6.2-21 Comparison between US-APWR 7.5-in CLB and ROSA/LSTF SB-CL-18 on Relationship between RCS Mass Inventory and Natural Circulation Flow (Mass Flow rate at SG U-Tubes Top)

Figure 6.2-22 Comparison of Static Quality Transient at SG U-Tubes Top between US-APWR 7.5-in CLB and ROSA/LSTF SB-CL-18

6.2.2.3 Momentum Balance

6.2.2.3.1 Governing Conservation Equations

The top-down scaling of the system momentum balance is based on the methodology developed by M. Ishii and I. Kataoka for the two-phase natural circulation system[6-7], and further on the methodology applied to the AP600 scaling analysis by J. N. Reyes, Jr. and L. Hochreiter[6-8].

In the present scaling analysis, the momentum conservation is considered independently from the mass and energy conservations. This follows the approach of Reyes and Hochreiter. The two-phase flow effects are directly modeled by including two-phase multipliers in the loss terms based on the actual system quality in the US-APWR and ROSA/LSTF. This approach is reasonable because the preceding analysis demonstrated that the mass inventory behavior and resulting global steam quality in the system are scalable between the plant and test facility.

During the US-APWR natural circulation phase, approximately saturated water enters the core heated section, and then some fraction of it is evaporated by the decay heat. All the vapor bubbles will be condensed back to saturated water after passing through the steam generator. Thus, steady state natural circulation is established, driven by density difference between the saturated liquid in the SG downwards flow side, cold leg and downcomer with two-phase fluid in the core, upper plenum, hot leg and the SG upper flow side. Here, the reactor coolant system is represented as a closed loop system as shown in Figure 6.2-23, and the mass flow rate through the system is mathematically expressed with the momentum conservation integrated over the closed loop as follow:

Momentum conservation equation:

$$\frac{1}{2}\rho_{m,0}^2 v_{m,0}^2 \cdot \sum_i \left[\left(f\frac{l}{d} + K \right)_i \left(\frac{A_0}{A_i} \right)^2 \frac{1}{\rho_{m,i}} \right] = \sum_i \left[\left(\rho_{\ell,sat} - \rho_m \right) \cdot g \cdot \Delta H_i \right] \qquad (6.2\text{-}26)$$

The subscripts 0 and *i* represent the reference component (core section) and *i*-th component in the system, respectively. In deriving the above equation, the dynamic effect on the momentum balance is ignored since the mass flow rate gradually decreases during the natural circulation phase. In addition, core inlet subcooling is also neglected to simplify the equation, which is a valid assumption for the US-APWR SBLOCA natural circulation phase.

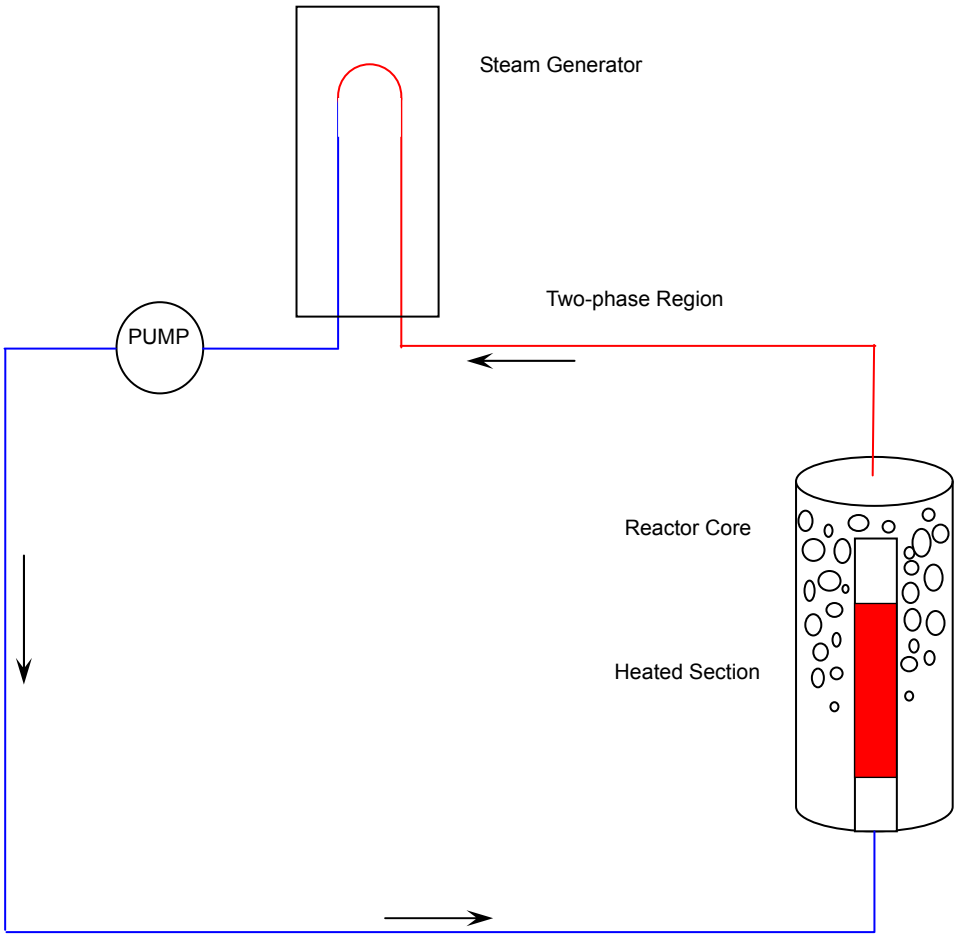

Figure 6.2-23 Schematic of Closed Loop System for Natural Circulation

6.2.2.3.2 Nondimensional Parameters

In evaluating the two-phase flow system, the integrated momentum equation (6.2-26) is represented by a combination of the single-phase and two-phase components. Ishii and Kataoka provided the following expression to account the two-phase multiplication effect on the frictional and local pressure drops[6-7]:

$$\frac{1}{2}\rho_{m,0}^2 v_{m,0}^2 \sum_i \left(N_{f,i} + N_{o,i}\right)\frac{1}{\rho_{m,i}} = \sum_i \left(\rho_{\ell,sat} - \rho_{m,i}\right) g \cdot \Delta H_i \qquad (6.2\text{-}27)$$

The $N_{f,i}$ and $N_{o,i}$ are the friction number and orifice number, respectively, the nondimensional parameters accounting for the two-phase effect in the friction and local losses are as follows:

$$N_{f,i} = \left(f\frac{l}{d}\right)_i \left(\frac{1 + x\,\Delta\rho/\rho_g}{\left(1 + x\Delta\nu/\nu_g\right)^{0.25}}\right)_i \left(\frac{A_0}{A_i}\right)^2 \qquad (6.2\text{-}28)$$

$$N_{o,i} = K_i \left(1 + x^{1.5}\Delta\rho/\rho_g\right)\left(\frac{A_0}{A_i}\right)^2 \qquad (6.2\text{-}29)$$

In evaluating the momentum effect from the top-down approach, sums of $N_{f,i}$ and $N_{o,i}$ for each of the single-phase and two-phase regions in the system are compared between US-APWR and ROSA/LSTF, as well as sums of the gravity head component (right hand side of equation (6.2-27).

6.2.2.3.3 Scaling Analysis Results

Table 6.2-3 shows a comparison of the reference parameters and the nondimensional coefficient between US-APWR and ROSA/LSTF. In determining the parameter values, the core, upper plenum, hot leg and uphill side of SG are accounted as the two-phase region, while the downhill side of SG, crossover leg, cold leg, downcomer and lower plenum as the single-phase saturated liquid region. Details of the facility parameters are given in Appendix A to the present document.

In computing the friction number ($N_{f,i}$), orifice number ($N_{o,i}$), and the gravity head for each component, the reference density and steam quality are required. The reference density is determined based on the reference time, which is consistent with the preceding scaling analysis for the mass and energy balances. The steam quality at the core exit is and the core decay power averaged for the natural circulation period accompany with the core flow rate obtained by solving the integral momentum equation (6.2-27). Since the integral momentum equation is a function of the core flow rate and steam quality, several iterations are necessary to determine the flow rate and steam quality.

Each of the scaling ratios listed in Table 6.2-3 indicates that the ROSA/LSTF natural circulation is reasonably scalable from the momentum point of view. For the single-phase region, there appear slight scaling distortions in the friction and orifice numbers, which are reversely deviated from the unity. However, integral of the friction and orifice numbers provide a good scaling ratio to the US-APWR. Similarly, the scaling ratios for the

two-phase region agree between US-APWR and ROSA/LSTF.

To this end, the ROSA/LSTF is scalable to the US-APWR from the viewpoint of the momentum balance through the closed system as well as from the mass and energy balances.

Table 6.2-3 Comparison of Nondimensional Parameters between US-APWR and ROSA/LSTF for Natural Circulation Phase (Momentum Balance)

Nondimensional Number	US-APWR	ROSA/LSTF	ROSA/US-APWR
$\sum_i N_{f,i}$ in single-phase region			
$\sum_i N_{o,i}$ in single-phase region			
$\sum_i N_{f,i}$ in two-phase region			
$\sum_i N_{o,i}$ in two-phase region			
Nondimensional driving head $\dfrac{\sum_i \left(\rho_{\ell,sat} - \rho_{m,i}\right) \cdot g \cdot \Delta H_i}{\rho_{\ell,sat} \cdot g \cdot L_{th}}$			

L_{th}: Height difference between the middle of core and the middle of average height of SG U-tubes

6.2.2.4 Evaluation for Scaling Distortions

As discussed in Sections 6.2.2.2 and 6.2.2.3, the measurement and analysis results of the ROSA/LSTF show good scalability to the US-APWR on the mass and energy point of view as well as the momentum point of view during the natural circulation phase. However, a slight difference was apparent in the depressurization behavior during the phase. Natural circulation phase occurs under virtually constant pressure in the US-APWR while in the ROSA/LSTF, the phase occurs under a moderate depressurization throughout the transient, as shown in Figure 6.2-18 and Figure 6.2-20. The reason for the moderate depressurization in the ROSA/LSTF during the natural circulation phase is discussed below.

The difference in depressurization rate between the ROSA/LSTF and the US-APWR is caused by the physical mechanism invoked by the pressure relief valve setpoint in the secondary side of the ROSA/LSTF. Once the relief valve is actuated, the pressure reduction in the secondary side induces subsequent decrease in the primary system pressure at a slightly faster rate. This condition causes the steam generator heat transfer in the ROSA/LSTF to be disproportionally larger than in the US-APWR. However, the magnitude of the pressure difference at the end of natural circulation is not significant. The fact that the value of dP*/dt* is not as close to zero in ROSA/LSTF as it is in US-APWR is not a concern. For the analysis purpose, it is not specifically required that the dP/dt should be close to zero. The data given Table 6.2-1 show that for US-APWR where dP*/dt* nears zero, the Ψ_6 and Ψ_{11} groups are nearly cancel out. Whereas for ROSA/LSTF, where dP*/dt* has a non-zero value, the sum of the Ψ_6 and Ψ_{11} groups do not cancel out.

6.2.3 Bottom-up Scaling Analysis

ROSA/LSTF SB-CI-18 test was examined from the top-down approach in Section 6.2.2, showing its sufficient scalability to the representative US-APWR SBLOCA natural circulation even though a slight distortion appears in temporal change of pressure in ROSA/LSTF. This section supplements the top-down scaling analysis with investigations from the bottom-up approach for some local portions of the facility.

6.2.3.1 Steam Generation in Core

Effect of the net heat generation, which integrally consists of heat generation in core and heat removal in SGs, is accounted for in the global mass and energy balances in Section 6.2.2.2. The present section investigates local scalability for the steam generation in core.

Ishii and Kataoka proposed the phase change number, which is a nondimensional parameter defined by a ratio of the flux for phase change to the inlet flux as follows:

$$N_{pch} = \frac{q''_0 \xi L_0 \Delta\rho}{A_0 v_{f,in0} \Delta i_{fg} \rho_\ell \rho_g} \tag{6.2-30}$$

In the above equation, a zero subscript indicates the core component as in Section 6.2.2.3. N_{pch} represents the steam generation in the core, and are determined by using the data used in Section 6.2.2.3, heat flux, mass flow rate, fluid properties, and geometrical data. The resultant N_{pch} which is the average value during natural circulation phase is compared between US-APWR and ROSA/LSTF in Table 6.2-4. And the temporal change of N_{pch} during natural circulation phase is compared in Figure 6.2-24. Since the power density of the US-APWR core is slightly reduced relative to the existing 4-loop PWR and/or ROSA/LSTF, the phase change number of US-APWR becomes lower than that of ROSA/LSTF. N_{pch} connects to the steam quality which relates to the driving force for the two-phase flow natural circulation. The higher value for ROSA corresponds to the higher nondimensional parameters in Table 6.2-3 in Momentum Balance Section 6.2.2.3. The higher steam quality results in the higher friction and orifice numbers under two-phase flow region and gives also the higher nondimensional driving head. For about half the duration of the natural circulation phase the value of N_{pch} for ROSA is in the range of N_{pch} values for the US-APWR. This indicates that the conditions in ROSA include most of the phenomena expected in the US-APWR. The similitude between the US-APWR and the ROSA is considered to be high because the qualitative and the quantitative tendencies among N_{pch} and the nondimensional parameters in Table 6.2-3 are the same between the US-APWR and ROSA Thus the ROSA data are suitable to validate the capability of M-RELAP5 to model the phenomena expected in the US-APWR.

6.2.3.2 Two-Phase Flow in Piping

Two-phase transition from bubbly to stratification in the hot leg piping is one of the phenomena of interest during the natural circulation phase. When the flow regime differs significantly between the plant and test facility, pressure drop in the piping also becomes different, affecting the flow rate under the natural circulation. Zuber[6-9] provided that similarity of the flow transition can be represented by using the Froude number defined as follow:

$$N_{Fr} = \frac{j_g \sqrt{\rho_g}}{\sqrt{g \Delta \rho D}} \tag{6.2-31}$$

Under the natural circulation condition, core inlet fluid is approximately saturated, therefore steam generated in core is assumed to be proportional to the core power. And, when fluid properties are identical between plant and test facility like between US-APWR and ROSA/LSTF, a scaling ratio of the Froude number between plant and test facility can be obtained by the following relation:

$$\frac{N_{Fr}^{test}}{N_{Fr}^{plant}} = \left(\frac{Q}{N_{Loop} D^{2.5}} \right)^{test} \Bigg/ \left(\frac{Q}{N_{Loop} D^{2.5}} \right)^{plant} \tag{6.2-32}$$

Scale ratio of the Froude number between the US-APWR and ROSA/LSTF hot legs which is the average value during natural circulation is listed in Table 6.2-4. And the temporal change of N_{Fr} during natural circulation phase is compared in Figure 6.2-25. For about half the duration of the natural circulation phase the value of N_{Fr} for ROSA is in the range of N_{Fr} values for the US-APWR. This indicates that the conditions in ROSA include most of the phenomena expected in the US-APWR. Thus the ROSA data are suitable to validate the capability of M-RELAP5 to model the phenomena expected in the US-APWR. Therefore, it is judged that ROSA/LSTF is reasonably acceptable from the scaling for the two-phase flow regime in the hot leg piping.

6.2.3.3 Time Scale in Piping

It is known that when the Froude number scaling is used in conjunction with the power-to-volume scaling, one cannot satisfy simultaneously, geometric similarity and equality of the Froude numbers for plant and test facility. This also has an effect on the time scale. **[**

]

$$\left(\qquad \right) \tag{6.2-33}$$

Table 6.2-4 shows the **[ ]**, showing the acceptable similarity as well as the Froude number. Therefore, it is concluded that the ROSA/LSTF is scalable to US-APWR from the viewpoint of time scale through the primary system piping.

Table 6.2-4 Comparison of Nondimensional Parameters between US-APWR and ROSA/LSTF for Natural Circulation Phase (Bottom-up Scaling)

Nondimensional Number	US-APWR	ROSA/LSTF	ROSA/ US-APWR	Notes
N*pch*	[ ]	[ ]	[ ]	N_{pch} by Eq. (6.2-30)
$N_{Fr,\mathrm{HotLeg}}$	[ ]	[ ]	[ ]	Froude No. ratio by Eq. (6.2-32)
Δ_{TS}	[ ]	[ ]	[ ]	Time scale ratio by Eq. (6.2-33)

Figure 6.2-24 Comparison of N_{pch} between US-APWR 7.5-in CLB and ROSA/LSTF SB-CL-18 during natural circulation phase

Figure 6.2-25 Comparison of N_{Fr} between US-APWR 7.5-in CLB and ROSA/LSTF SB-CL-18 during natural circulation phase

6.2.4 Summary

Similarity of the natural circulation behaviors between the representative US-APWR SBLOCA and ROSA/LSTF SB-CL-18 test has been investigated using top-down and bottom-up approaches. In the top-down approach, the global behaviors in terms of the system pressure and mass are represented by using the reduced nondimensional equations, and the significant nondimensional groups are identified and quantified. The depressurization is dominated by break volumetric flow in both facilities. The fraction of system mass inventory lost during the phase was about one third in both facilities. Based on these comparisons the ROSA/LSTF results are judged to be representative of the US-APWR. Similarly, the integral momentum balance through the system is quantified both for the US-APWR and ROSA/LSTF, which results in that the similarity is acceptable.

The bottom-up approach is simultaneously employed for the present scaling analysis, since the local thermal-hydraulic phenomena strongly affect the natural circulation behavior. Here, the steam generation, two-phase flow regime and time scale in piping are characterized by quantifying the applicable nondimensional parameter both for the US-APWR and ROSA/LSTF. The bottom-up scaling shows that there are no significant scaling distortions between the plant and test facility. This is a reasonable conclusion, because the ROSA/LSTF was designed so that the test facility is scalable to the reference plant (Westinghouse-designed 4-loop PWR) which is similar to the US-APWR.

Therefore it was determined that the ROSA/LSTF is reasonably scalable to the US-APWR for the natural circulation behavior.

6.3 Loop Seal Clearance

6.3.1 Phenomena and Applied Test Facility

After the natural circulation phase terminates, the RCS water inventory continues to decrease while the steam volume increases. The pressure in the RCS remains almost constant because the SG secondary side acts as an effective heat sink for removal of core decay heat, while the energy outflow from the break is restricted because of the low quality break flow. As mentioned in Section 4.2.3, the core liquid level is considered a significant parameter of interest for the loop seal period because of its potential impact on the core dryout. The core liquid level is closely related to the fluid distribution throughout the RCS.

Figure 6.3-1 schematically represents a typical water distribution throughout the primary system after the natural circulation terminates. The amount of water refers to the M-RELAP5 calculation for the US-APWR 7.5-in CLB. The liquid level in the core and in the upper plenum is decreasing during this period while the liquid level in the SG outlet plena and the downhill side of the loop seal is decreasing due to a manometer-like mechanism. Furthermore, the water holdup in the uphill side of SG U-tubes and in the SG inlet plena also contributes to the depression of the core and the upper plenum liquid levels. This holdup is governed by the CCFL in the SG U-tubes and at the inlet of the SG inlet plena.

In the M-RELAP5 code assessment, the ROSA/LSTF test facility[6-2] provides the IET data (SB-CL-18 test[6-3]) for the loop seal period. For 1-ft^2 CLB case, no clear recovery of core liquid level after loop seal clearance was observed for US-APWR and also for ROSA/LSTF IB-CL-02[6-4]. The observed transients are shown in the next Section 6.3.2.1. MHI judged that the a well defined loop seal clearance phase did not occur in the 1-ft^2 CLB case and the top-down scaling analyses focuses on the 7.5-in CLB case.

The scalability of the data will be evaluated by comparing the system behaviors between the ROSA/LSTF and US-APWR, using the top-down approach. ROSA/LSTF is an integral test facility which is a volumetrically 1/48-scaled and full height model of the Westinghouse-type 3423 MWt 4-loop PWR. The test facility was designed to reproduce thermal-hydraulic phenomena representative of SBLOCAs and operational transients in the reference plant. The ROSA/LSTF is reasonably applicable for investigation of the loop seal behavior occurring in the US-APWR, since the US-APWR design is very similar to the Westinghouse 4-loop PWR as mentioned in Section 3.1. However, as described below, relative elevation differences between ROSA/LSTF and the US-APWR will result in differences in the fluid distribution between the two systems.

Figure 6.3-2 compares several elevations measured from the hot leg centerline. The elevation from the top of core to the hot leg centerline is almost the same for the two systems but the bottom of the core for the US-APWR is deeper due to the 14-ft core length. On the other hand, the loop seal bottom centerline is deeper for ROSA/LSTF than that for US-APWR. Since the lowest core liquid level depends on the depth of loop seal, the core liquid level for ROSA/LSTF is likely to be lower than that for the US-APWR. The effect of this geometrical difference will be discussed in more detail in the top-down scaling section.

Local phenomena and processes of interest, which affect the above global responses, will be addressed using the bottom-up approach.

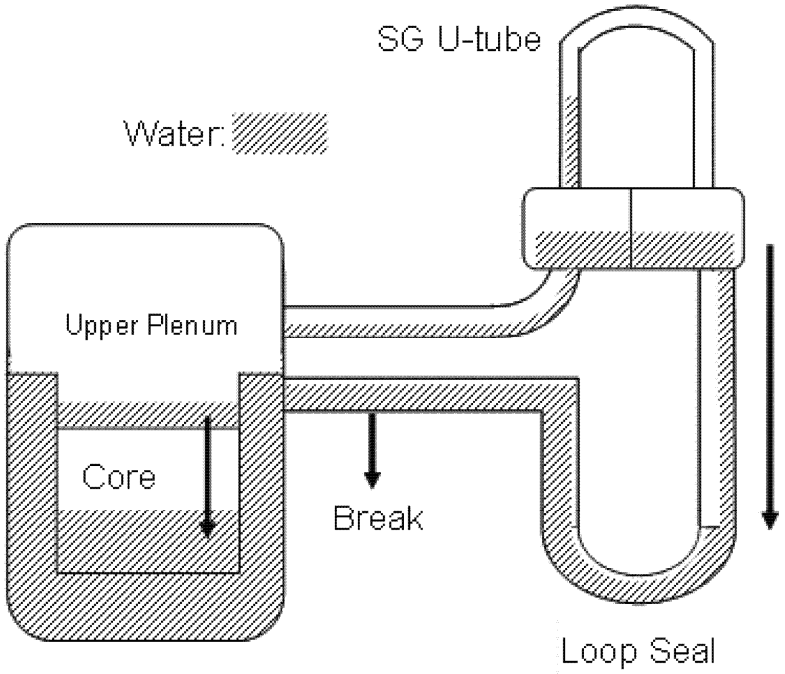

Figure 6.3-1 Schematic of Typical RCS State during the Loop Seal Clearing Phase

Figure 6.3-2 Schematic of primary system with important elevations

6.3.2 Top-Down Scaling Analysis

6.3.2.1 Transient Behavior of Interest

First of all, the time period should be defined for the loop seal phase. The start of the loop seal phase is considered to be the termination of natural circulation and the end is to be the loop seal clearing time. The termination of natural circulation was defined in the Section 6.2.2.1 as follows: **[ ]** for the US-APWR 7.5-in CLB and **[ ]** for the ROSA/LSTF SB-CL-18. The end timing was defined as the initiation of rapid decrease of liquid head along the uphill side of crossover leg. And the time was as follows: **[ ]** for the US-APWR 7.5-in CLB and **[ ]** for the ROSA/LSTF SB-CL-18.

Figure 6.3-3 and Figure 6.3-4 show the transient behavior of the measured liquid heads in both the uphill and downhill sides of the loop seal in the ROSA/LSTF SB-CL-18 broken loop and intact loop, respectively. The liquid head along the downhill side decreases monotonically with time and becomes lower than that along the uphill side in between the start time (t_1) of this phase and the end time (t_2). After t_2, the head along the uphill side rapidly decreases.

Figure 6.3-5 and Figure 6.3-6 compare the uphill and downhill liquid head transient responses from the US-APWR 7.5-in CLB calculation for the broken and intact loop, respectively. Overall behavior is similar to the ROSA/LSTF although a fluctuation of liquid head along the uphill side is recognized.

Figure 6.3-7 shows the sum of collapsed liquid levels in the core and in the upper plenum for the US-APWR calculation comparing with that for the ROSA/LSTF measurement & M-RELAP5 calculation. The timings of initiation of loop seal (t_1) and the loop seal clearance (t_2) are also indicated in the figure. The liquid level is almost the same between the two systems at t_1 although a slightly higher level is observed in the US-APWR. After the start of the loop seal clearing period (t_1), the two systems show an increase in the rate at which the liquid levels decrease, but the duration is longer for ROSA/LSTF. The longer duration results in a deeper depression in the ROSA/LSTF core liquid level. The longer duration is considered to be related to the deeper loop seal in ROSA/LSTF. After the loop seal clearance, the liquid level in each system increases but the recovery rate seems to be somewhat faster for ROSA/LSTF.

The pressure is almost constant during the loop seal clearing period as shown in Figure 6.3-8, the liquid levels in the core and in the upper plenum are governed by the characteristics of water accumulation along the loop seal and the SG U-tubes. As shown in Figure 6.3-3 through Figure 6.3-6, sometime prior to t_2 the liquid head in the uphill side of the loop seal exceeds that in the downhill side of the SG and loop seal. This head difference contributes to the reduction of liquid levels in the core and in the upper plenum.

Figure 6.3-9 and Figure 6.3-10 show the comparison of liquid heads along SG inlet plenum and uphill side of SG U-tubes between the two systems for the broken loop and for the intact loop, respectively. These values are related to the CCFL phenomena. The liquid head during the loop seal clearing period is almost the same for the two systems.

From the comparisons up to here, the depression of the core liquid level is larger in

ROSA/LSTF than that in the US-APWR and the difference is attributed to the difference in the loop seal elevations and differences in liquid distribution around the loops. A more detailed quantitative investigation will be performed in the next section.

For the 1-ft^2 CLB case, the liquid head in the crossover leg gradually decreased with time and the uphill side was almost depleted around **[ ]** for the US-APWR and also for the ROSA/LSTF IB-CL-02. Figure 6.3-11 compares the sum of liquid levels in core and in upper plenum for this break case. No recovery of liquid levels is observed after around **[ ]** and MHI judged that the loop seal clearance phase did not exist for this break size.

Figure 6.3-3 Comparison of Head between the Uphill side of Loop Seal and the Downhill side of SG and Loop Seal for ROSA/LSTF SB-CL-18 Broken Loop (Measurement)

Figure 6.3-4 Comparison of Head between the Uphill side of Loop Seal and the Downhill side of SG and Loop Seal for ROSA/LSTF SB-CL-18 Intact Loop (Measurement)

Figure 6.3-5 Comparison of Head between the Uphill side of Loop Seal and the Downhill side of SG and Loop Seal for US-APWR Broken Loop (Calculation)

Figure 6.3-6 Comparison of Head between the Uphill side of Loop Seal and the Downhill side of SG and Loop Seal for US-APWR Intact Loop (Calculation)

Figure 6.3-7 Comparison of Sum of Collapsed Liquid Levels in Core and in Upper Plenum between US-APWR (Calculation) and ROSA/LSTF SB-CL-18 (Measurement & M-RELAP5 Calculation)

Figure 6.3-8 Comparison of Upper Plenum Pressure between US-APWR (Calculation) and ROSA/LSTF SB-CL-18 (Measurement)

Figure 6.3-9 Comparison of Head in SG inlet plenum and Uphill side of U-tubes of Broken Loop between US-APWR (Calculation) and ROSA/LSTF SB-CL-18 (Measurement)

Figure 6.3-10 Comparison of Head in SG inlet plenum and Uphill side of U-tubes of Intact Loop between US-APWR (Calculation) and ROSA/LSTF SB-CL-18 (Measurement)

Figure 6.3-11 Comparison of Sum of Collapsed Liquid Levels in Core and in Upper Plenum between US-APWR (Calculation) and ROSA/LSTF IB-CL-02 (Measurement & M-RELAP5 Calculation)

6.3.2.2 Governing Conservation Equations

In evaluating the core liquid level transient behavior of interest, a static pressure balance is considered through the RCS. The pressure locations and levels are shown in the Figure 6.3-12.

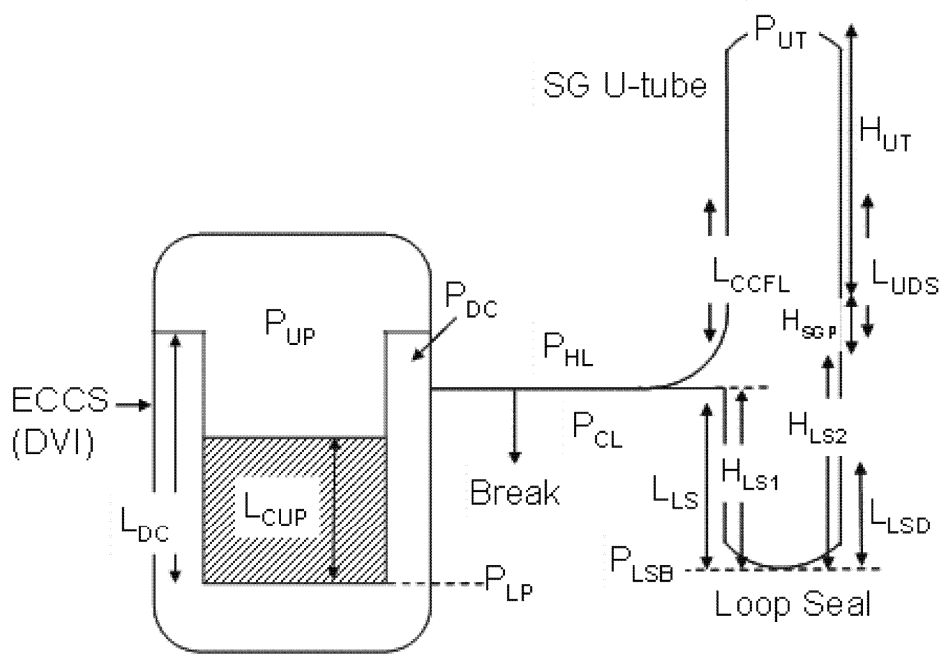

Figure 6.3-12 Schematic of Related Variables for Loop Seal

The relationships are derived in the following equations.

$$P_{LSB} = P_{UT} + \rho_g g\left(H_{UT} + H_{SGP} - L_{UDS}\right) + \rho_g g\left(H_{LS2} - L_{LSD}\right) + \rho_\ell g L_{LSD} + \rho_\ell g L_{UDS} \quad (6.3\text{-}1)$$

$$P_{DC} = P_{CL} = P_{LSB} - \rho_\ell g L_{LS} - \rho_g g\left(H_{LS1} - L_{LS}\right) \quad (6.3\text{-}2)$$

$$P_{UP} = P_{HL} = P_{UT} + \rho_g g\left(H_{UT} + H_{SGP} - L_{CCFL}\right) + \rho_\ell g L_{CCFL} \quad (6.3\text{-}3)$$

$$P_{LP} = P_{DC} + \rho_\ell g L_{DC} = P_{UP} + \rho_{CUP} g L_{CUP} \quad (6.3\text{-}4)$$

where
P_{LSB} = pressure at the bottom of the loop seal
P_{UT} = pressure at the top of the U-tubes
P_{DC} = pressure at the top of the downcomer
P_{CL} = pressure in the cold leg
P_{UP} = pressure in the upper plenum
P_{LP} = pressure in the lower plenum (bottom of core barrel)
P_{HL} = pressure in the hot leg
H_{UT} = height of the U-tubes
H_{SGP} = height of the steam generator plena
H_{LS1} = depth of the loop seal below the reactor coolant pump
H_{LS2} = distance from the bottom of the loop seal to the bottom of the SG outlet plenum

L_{LS} = height of liquid in uphill side of loop seal
L_{LSD} = height of liquid in downhill side of loop seal
L_{CCFL} = height of liquid held up by CCFL in the uphill side of U-tubes and SG inlet plena
L_{UDS} = height of liquid held up in downhill side of U-tubes and the outlet plenum
L_{DC} = depth of liquid in downcomer
L_{CUP} = depth of collapsed liquid level in core and upper plenum
ρ_g = density of vapor
ρ_ℓ = density of liquid
ρ_{CUP} = density of liquid in core and upper plenum

The expressions for lower plenum pressure in equation (6.3-4) can be rearranged to show the relationship between the liquid level in the downcomer and the core/upper plenum region.

$$L_{DC} - \rho_{CUP} L_{CUP} / \rho_\ell = \left(P_{UP} - P_{DC}\right) / \rho_\ell g \tag{6.3-5}$$

Then substituting equations (6.3-1), (6.3-2) and (6.3-3) gives

$$\begin{aligned} L_{DC} - \rho_{CUP} L_{CUP} / \rho_\ell = (&P_{UT} + \rho_g g\left(H_{UT} + H_{SGP} - L_{CCFL}\right) + \rho_\ell g L_{CCFL} - P_{UT} - \\ &\rho_g g\left(H_{UT} + H_{SGP} - L_{UDS}\right) - \rho_g g\left(H_{LS2} - L_{LSD}\right) - \rho_\ell g L_{LSD} - \rho_\ell g L_{UDS} + \\ &\rho_\ell g L_{LS} + \rho_g g\left(H_{LS1} - L_{LS}\right)) / \rho_\ell g \end{aligned} \tag{6.3-6}$$

Removing terms that cancel out and collecting terms gives

$$L_{DC} - \rho_{CUP} L_{CUP} / \rho_\ell = \left(\left(\rho_\ell - \rho_g\right)\left(L_{CCFL} + L_{LS} - L_{UDS} - L_{LSD}\right) + \rho_g\left(H_{LS1} - H_{LS2}\right)\right) / \rho_\ell \tag{6.3-7}$$

For the liquid density in the core and lower plenum, downcomer, and loop seal at saturation, ρ_ℓ, the equation reduces to

$$L_{DC} - L_{CUP} = \left(\left(\rho_\ell - \rho_g\right)\left(L_{CCFL} + L_{LS} - L_{UDS} - L_{LSD}\right) + \rho_g\left(H_{LS1} - H_{LS2}\right)\right) / \rho_\ell \tag{6.3-8}$$

This is the liquid level difference just prior to loop seal clearing. Equations (6.3-7) and (6.3-8) describe the difference in liquid level between the downcomer and the core and upper plenum. In the 7.5-in break the downcomer remains full during the loop seal clearing phase so equation (6.3-8) can be rearranged to define the liquid level in the core and upper plenum.

$$L_{CUP} = L_{DC} - \frac{\rho_\ell - \rho_g}{\rho_\ell}\left(L_{CCFL} + L_{LS} - L_{UDS} - L_{LSD}\right) - \frac{\rho_g}{\rho_\ell}\left(H_{LS1} - H_{LS2}\right) \tag{6.3-9}$$

The overall mass balance for the RCS is given by

$$\frac{dM_{RCS}}{dt} = \sum \dot{m}_{in} - \sum \dot{m}_{out} \tag{6.3-10}$$

During the loop seal clearing phase the only flows in and out of the RCS are the break flow and the ECCS flow. The pumped SI flow starts right at the end of the loop seal clearing phase in the US-APWR 7.5-in break so it does not affect any processes during the phase. In the ROSA SB-CL-18 test the pumped ECC was intentionally not functioning, and the accumulator began injecting at about 455 seconds. The ECCS flow will therefore not be included in the system mass balance or depressurization equations for the loop seal clearing phase. This makes the mass balance

$$\frac{dM_{RCS}}{dt} = -\dot{m}_{break} \tag{6.3-11}$$

The primary system depressurization equation can be modeled using the same equation used for the natural circulation phase.

$$\frac{dP}{dt} = \frac{\partial P/\partial v_m\big|_{u_m}}{\rho_m V}\left\{\frac{\partial P/\partial \mu_m\big|_{v_m}}{\partial P/\partial v_m\big|_{u_m}}\left[-\dot{m}_{break}\left(h_{break}-u_m\right)+\dot{q}_{net}\right]-v_m\left(-\dot{m}_{break}\right)\right\}$$

$$\dot{q}_{net} = \dot{q}_{core} + \dot{q}_{SG}$$

6.3.2.3 Nondimensional Equations and Groups

Each of the physical parameters in the governing conservation equations is nondimensionalized by dividing by a reference quantity of the parameter, e.g. the initial value. The resulting nondimensionalized equations that include all the relevant terms for this phase are as follows.

Nondimensionalized core and upper plenum liquid level equation:

$$L^*_{CUP} = \psi_1 L^*_{DC} - \psi_2 \frac{(\rho_\ell-\rho_g)^*}{\rho^*_\ell} L^*_{CCFL} - \psi_3 \frac{(\rho_\ell-\rho_g)^*}{\rho^*_\ell} L^*_{LS} + \psi_4 \frac{(\rho_\ell-\rho_g)^*}{\rho^*_\ell} L^*_{UDS} + \psi_5 \frac{(\rho_\ell-\rho_g)^*}{\rho^*_\ell} L^*_{LSD}$$
$$-\psi_6 \frac{\rho^*_g (H_{LS1}-H_{LS2})^*}{\rho^*_\ell} \tag{6.3-12}$$

where

$$L^*_{CUP} = \frac{L_{CUP}}{L_{CUP0}}, L^*_{DC} = \frac{L_{DC}}{L_{DC0}}, L^*_{CCFL} = \frac{L_{CCFL}}{L_{CCFL0}}, L^*_{LS} = \frac{L_{LS}}{L_{LS0}}, L^*_{UDS} = \frac{L_{UDS}}{L_{UDS0}}, L^*_{LSD} = \frac{L_{LSD}}{L_{LSD0}},$$
$$(H_{LS1}-H_{LS2})^* = \frac{(H_{LS1}-H_{LS2})}{(H_{LS1}-H_{LS2})_0}, (\rho_\ell-\rho_g)^* = \frac{(\rho_\ell-\rho_g)}{(\rho_\ell-\rho_g)_0}, \rho^*_g = \frac{\rho_g}{\rho_{g0}}, \rho^*_\ell = \frac{\rho_\ell}{\rho_{\ell 0}}$$

The dimensionless groups are defined as

$$\psi_1 = \frac{L_{DC0}}{L_{CUP0}}$$

$$\psi_2 = \frac{(\rho_\ell - \rho_g)_0}{\rho_{\ell 0}} \frac{L_{CCFL0}}{L_{CUP0}}$$
$$\psi_3 = \frac{(\rho_\ell - \rho_g)_0}{\rho_{\ell 0}} \frac{L_{LS0}}{L_{CUP0}}$$
$$\psi_4 = \frac{(\rho_\ell - \rho_g)_0}{\rho_{\ell 0}} \frac{L_{USD0}}{L_{CUP0}}$$
$$\psi_5 = \frac{(\rho_\ell - \rho_g)_0}{\rho_{\ell 0}} \frac{L_{LSD0}}{L_{CUP0}}$$
$$\psi_6 = \frac{\rho_{g0}(H_{LS1} - H_{LS2})_0}{\rho_{\ell 0} L_{CUP0}}$$

The first five Ψ groups represent the ratios of liquid heights multiplied by the ratio of the difference in saturated liquid and vapor densities to the saturated liquid density. The sixth Ψ group is the distance from the cold leg centerline to the bottom of the steam generator outlet plenum multiplied by the ratio of saturated vapor density to saturated liquid density. When the loop seal clears the down side of the U-tubes and loop seal are filled with vapor so the L_{USD0} and L_{LSD0} terms are equal to zero. This makes the Ψ_4 and Ψ_5 terms zero.

The mass balance can be nondimensionalized as

$$\frac{dM^*_{RCS}}{dt^*} = -\psi_7 \dot{m}^*_{break} \tag{6.3-13}$$

The dimensionless group $\psi_7 = \frac{-\dot{m}_{break0} t_0}{M_0}$ represents the ratio of the break mass flow during the reference time to the initial core and upper plenum liquid mass.

The depressurization equation is non-dimensionalized as

$$\frac{dP^*}{dt^*} = \Psi_8 C^*_{1,m} I^*_{b,m} + \Psi_9 C^*_{1,m} I^*_{c,m} + \Psi_{10} C^*_2 II^*_m \tag{6.3-14}$$

where

$$I^*_{b,m} = \frac{I_{b,m}}{\dot{m}_{break,0}(h_{break} - u_m)_0} \tag{6.3-15}$$
$$I^*_{c,m} = \frac{I_{c,m}}{\dot{q}_{net0}} \tag{6.3-16}$$
$$II^*_m = \frac{II_m}{v_{m,0}(-\dot{m}_{break0})} \tag{6.3-17}$$
$$I_{b,m} = \dot{m}_{break}(h_{break} - u_m) \tag{6.3-18}$$
$$I_{c,m} = \dot{q}_{net} \tag{6.3-19}$$
$$II_m = v_m(-\dot{m}_{break}) \tag{6.3-20}$$

The quantities with an asterisk represent normalized variables, and subscript of zero denotes the reference value for the variable. The nondimensional time *t** indicates the

time normalized to the temporal period of interest. The coefficients $C^*_{1,m}$ and C^*_2 are defined as follows:

$$C^*_{1,m} = \frac{C_{1,m}}{C_{1,m,0}} \tag{6.3-21}$$

$$C^*_{2,m} = \frac{C_2}{C_{2,m,0}} \tag{6.3-22}$$

$$C_{1,m} = \frac{\partial P / \partial u_m \big|_{v_m}}{\rho_m V} \tag{6.3-23}$$

$$C_{2,m} = \frac{\partial P / \partial v_m \big|_{\mu_m}}{\rho_m V} \tag{6.3-24}$$

The nondimensional groups defined for the above equations are Ψ_8, Ψ_9, and Ψ_{10}, which are defined as follows:

$$\Psi_8 = \frac{C_{1,m,0}(h_{break} - u_m)_0 \dot{m}_0 t_0}{P_0} \tag{6.3-25}$$

$$\Psi_9 = \frac{C_{1,m,0}\dot{q}_{net0} t_0}{P_0} \tag{6.3-26}$$

$$\Psi_{10} = \frac{C_{2,0} v_{m,0} \dot{m}_0 t_0}{P_0} \tag{6.3-27}$$

Ψ_8 is the ratio of pressure change, due to change in specific energy of the saturated field from mass outflows, to the reference pressure. Ψ_9 is the ratio of pressure change, due to change in specific energy of the saturated field from heat transfer, to the reference pressure. Ψ_{10} is the ratio of pressure change, due to change in specific volume of the saturated field from volumetric flow, to reference pressure.

The specific volume and internal energy of the mixture, v_m and u_m in the equations represent the RCS-averaged values, which are determined by the saturated fluid properties as follows:

$$v_m = x v_g + (1 - x) v_f \tag{6.3-28}$$

$$u_m = x u_v + (1 - x) u_f \tag{6.3-29}$$

6.3.2.4 Scaling Analysis Results

In the top-down approach, the scalability between the test facility and plant in terms of the transient behaviors of interest can be evaluated by quantifying and comparing the nondimensional groups or parameters for the test facility and plant. For the loop seal clearance phase, the nondimensional liquid level at the loop seal clearing is first examined using Equation (6.3-12) and then the mass inventory and the depressurization characteristics are investigated using Equations (6.3-13) and (6.3-14).

Physical parameters used to evaluate the resultant nondimensional groups Ψ are summarized in Table 6.3-1. First of all, the reference time t_0 is compared in the top of Table 6.3-1 and is almost the same for both systems. In order to investigate the similitude of both systems, the order of magnitude analysis is performed by comparing the numerically evaluated nondimensional groups. The analysis shows that the most significant nondimensional group for the liquid level is Ψ_1 for the US-APWR and also for the ROSA/LSTF. The relative magnitude of Ψ_2, Ψ_3, Ψ_6 to Ψ_1 is almost the same between the two systems but the contribution of liquid level along the uphill side of loop seal Ψ_3 is about 50% lower for the US-APWR. This difference corresponds to the relative depth difference of loop seal between the US-APWR and the ROSA/LSTF. And the contribution due to the CCFL Ψ_2 is about 40% higher for the US-APWR. Then the resultant L^*_{CUP} is about 10% lower for the ROSA/LSTF compared to the US-APWR. This means the ROSA/LSTF tends to give a conservative PCT due to the lower liquid level during the loop seal clearance phase.

As for the mass and the pressure transients, the similitude is maintained and the significant nondimensional group for the depressurization is Ψ_{10} for both systems relating to the volumetric outflow.

Figure 6.3-13 compares nondimensional mass inventory reduction rate (dM*/dt*) for the US-APWR and ROSA/LSTF to demonstrate the scalability of the ROSA/LSTF. The figure demonstrates that from the mass and energy balances standpoint, the loss of inventory during the loop seal clearance phase in both the US-APWR and ROSA/LSTF is in good agreement.

The comparison of nondimensional depressurization rate (dP*/dt*) between US-APWR and ROSA/LSTF is shown in Figure 6.3-14. The figure shows that the loop seal phase occurs at virtually constant pressure for both systems and no significant scale distortion is recognized.

Table 6.3-1 Comparison of Physical Values and Nondimensional Groups for core and upper plenum liquid level between US-APWR 7.5-in CLB and ROSA/LSTF SB-CL-18 (Measured) for Loop Seal Clearance Phase

Parameter	US-APWR	ROSA	ROSA /US-APWR	Comments
$t_0 = t_2 - t_1$ (sec)	[redacted]			Time period of this phase
t_1 (sec)				End of natural circulation
t_2 (sec)				Timing of rapid decrease of L_{LSU}
M_0 (kg)				Initial of this phase
P_0 (MPa)				Initial of this phase
$\dot{q}_{net0}$ (MW)				Initial net heat source
$\dot{m}_{break0}$ (kg/s)				Initial of this phase
X_0				RCS average quality
$h_{break,0}$ (kJ/kg)				Initial of this phase
$u_{m,0}$ (kJ/kg)				Initial of this phase
$v_{m,0}$ (m^3/kg)				Initial of this phase
$C_{1m,0}$ (Pa/J)				
$C_{2m,0}$ (Pa/m^3)				
L_{DC0} (m)				Initial of this phase
L_{CUP0} (m)				Initial of this phase
L_{CCFL0} (m)				End of this phase
L_{LS0} (m)				Initial of this phase
$(H_{LS1} - H_{LS2})_0$ (m)				Initial of this phase
Nondimensional Group				
ψ_1	[redacted]			
ψ_2				
ψ_3				
ψ_6				
Ranking groups in the liquid level equation				
ψ_2/ψ_1	[redacted]			
ψ_3/ψ_1				
ψ_6/ψ_1				
L^*_{CUP}				
ψ_7				
ψ_8				
ψ_9				
ψ_{10}				
Ranking groups in the depressurization equation				
ψ_8/ψ_{10}	[redacted]			
ψ_9/ψ_{10}				

Figure 6.3-13 Comparison of Normalized RCS Mass between US-APWR 7.5-in CLB and ROSA/LSTF SB-CL-18 for Loop Seal Phase (Mass and Energy Balances)

Figure 6.3-14 Comparison of Normalized RCS Pressure between US-APWR 7.5-in CLB and ROSA/LSTF SB-CL-18 for Loop Seal Phase (Mass and Energy Balances)

two systems. The break volumetric flow was the most important mechanism, followed by net heat transfer, and break energy flow. The validity of the reduced model is shown in Figure 6.3-17 and Figure 6.3-19. The temporal variation corresponds well to the M-RELAP transient and the ROSA/LSTF measurement.

6.3.2.6 Evaluation for Scaling Distortion

In the core level response the deeper loop seal in ROSA resulted in a slightly lower core liquid level in ROSA. As noted above this lower core level makes the ROSA response conservative relative to the US-APWR.

In the mass and pressure equations, no significant scale distortion was observed during the loop seal clearance phase.

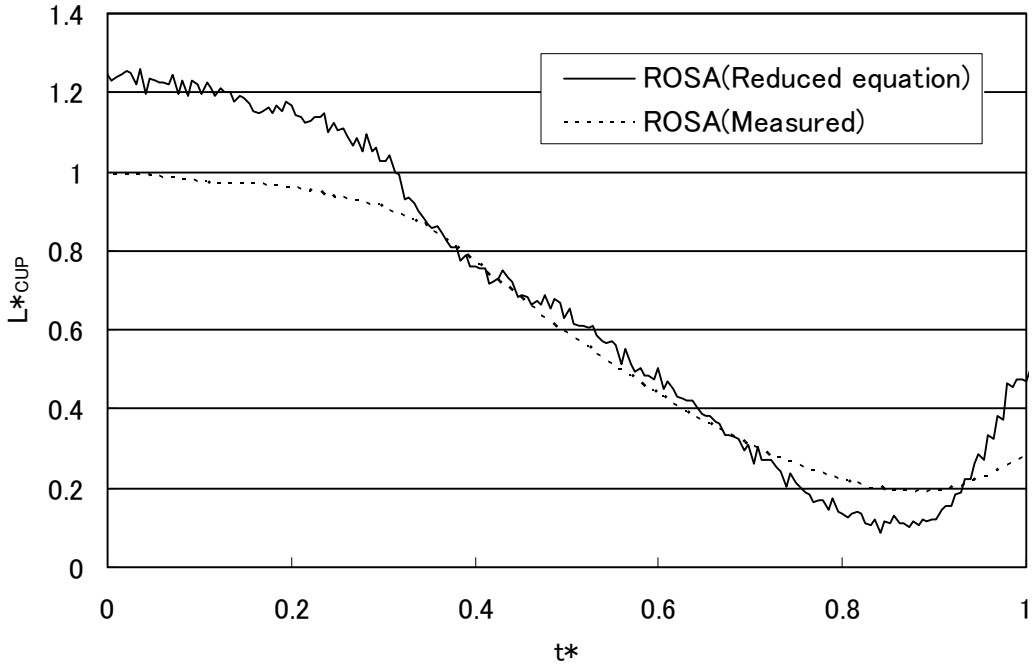

Figure 6.3-15 Comparison of Normalized Liquid Level Measurement and Reduced Model for ROSA/LSTF SB-CL-18 Loop Seal Phase (Liquid Level Balance)

Figure 6.3-16 Comparison of Normalized RCS Mass between M-RELAP5 and Reduced Model for US-APWR 7.5-in CLB Loop Seal Phase (Mass and Energy Balances)

Figure 6.3-17 Comparison of Normalized RCS Pressure between M-RELAP5 and Reduced Model for US-APWR 7.5-in CLB Loop Seal Phase (Mass and Energy Balances)

Figure 6.3-18 Comparison of Normalized RCS Mass between Measurement and Reduced Model for ROSA/LSTF SB-CL-18 Loop Seal Phase (Mass and Energy Balances)

Figure 6.3-19 Comparison of Normalized RCS Pressure between Measurement and Reduced Model for ROSA/LSTF SB-CL-18 Loop Seal Phase (Mass and Energy Balances)

6.3.3 Bottom-up Scaling Analysis

The ROSA/LSTF SB-CL-18 test was examined from the top-down approach in Section 6.3.2, showing a scaling distortion appears in the temporal change of core liquid level and the distortion was confirmed to be caused by the geometrical difference of loop seal section. The distortion caused the ROSA response to be conservative relative to the expected US-APWR response. This section supplements the scaling analysis with investigations from the bottom-up approach for some local portions of the facility. The other important phenomena and processes related to the fuel cladding heat-up are to be addressed in Sections 6.4.3 and 6.5.3.

6.3.3.1 CCFL in Hot Leg

The following Kutateladze correlation is applied to Hot Leg at the CCFL condition for the US-APWR.

$$\left[\qquad\qquad\right] \tag{6.3-30}$$

This correlation was derived from the UPTF CCFL test data[6-1]. Differences in configuration and the fluid combination between the UPTF CCFL test and the US-APWR are summarized in Table 6.3-2. The flow area is about 10% larger for US-APWR and the pressure is higher.

Since the Kutateladze number (Ku) for zero penetration of water approaches a constant value with increasing inner diameter for vertical flow configuration, the empirical Ku correlation derived from UPTF data was considered to be applicable to the US-APWR because the diameter of 0.75m is large enough. On the other hand for the ROSA analysis, the CCFL parameter (m = 0.65 and c=1.78) by Tien model[6-10] was applied. The parameter set is different from the UPTF (m = 0.87 and c=2.68) because the water accumulation in ROSA SG inlet plenum was better predicted by the Tien model. The c value for UPTF is larger and the scale effect might be existed for the hot leg geometry. The c value turns to be a little larger if the scale effect keeps the trend where the c value increases with scale. The correlation with a larger c gives more water penetration at the same steam velocity and using the UPTF correlation for the US-APWR turns to be a conservative treatment because the amount of water accumulation due to the CCFL is increased and the driving head suppressing the core liquid level is increased. Then the use of UPTF correlation is considered to be adequate from the conservativeness point of view.

The effect of pressure was recently reported in NURETH-13 by Dresden group[6-11]. The hot leg geometry is simulated using a rectangular duct of 5cm in width and 25cm in height and high pressure steam-water experiments were conducted under 15bar, 30bar and 50bar. The CCFL data under different pressures were almost correlated with Ku and however it is recognized that the Ku for water down-flow rate at a steam flow rate tends to be larger with pressure. This tendency means that the UPTF correlation derived below 15bar gives conservative results under higher pressure because more water accumulates around the SG inlet plenum when using the UPTF correlation than would be expected under higher pressure. The more water accumulation gives the lower liquid level in the core during the loop seal period which is likely to result in core dryout.

Since the CCFL correlation strongly depends on flow-path geometry, the Ku relationship by Dresden group using the rectangular geometry can not apply directly to the US-APWR but the qualitative tendency on the pressure is considered to be a relevant finding when the uncertainty on the pressure is discussed. Therefore, the use of the CCFL correlation derived from the UPTF data is considered to be adequate on the M-RELAP5 conservative treatment for SBLOCA analyses.

As for the scalability point of view for the ROSA, the c value which is suitable to the ROSA is smaller than the UPTF as mentioned above. This means more water accumulation due to the CCFL is likely to be occurred in ROSA compared with the US-APWR. Figure 6.3-20 compare the Ku* relationship among the calculated results for US-APWR and ROSA and the CCFL correlations during the loop seal phase. The range of Ku_G* for the ROSA almost corresponds to that for the US-APWR but the Ku_L* is smaller although some portion of ROSA downflow rate is in the range of the US-APWR.

6.3.3.2 CCFL in SG U-Tubes

The following Wallis correlation is applied to SG U-tubes under CCFL condition for US-APWR and ROSA/LSTF.

$$J_g^{*0.5} + J_f^{*0.5} = 0.88 \tag{6.3-31}$$

The applicability was assessed by the Dukler air-water flooding test[6-1]. The scaling comparison between the Dukler air-water flooding test and the US-APWR was provided in Table 6.3-3 for the configuration and the fluid combination. The ROSA/LSTF is also included.

As for the tube diameter, the J* scaling is considered to have a high applicability for a small-scale pipe. As shown in Figure 6.3-21 Ku giving zero penetration of water increases with D*:$(D \cdot (g(\rho_L - \rho_G)/\sigma)^{1/2})$ and approaches a constant value which is about 3.2 for D* greater than about 60[6-12]. The value of D at D*=60 was derived as a function of pressure as shown in Table 6.3-4. From this table, we applied the Ku correlation to the hot leg and the J* to the SG U-tubes. Equation (6.3-31) can predict the Dukler data (2" diameter) as shown in Figure 8.1.5-4 of the topical report[6-1] and correlates well the data irrespective of the tube diameter 3/4" or 5/4" shown in Reference 6-13. The tube diameter 3/4" is near the US-APWR and the adaptability of the correlation is considered to be high.

As for the tube length, the phenomena restricting the downward liquid flow rate in the SG U-tubes is considered to be governed by those near the bottom of the tubes where the steam and condensed liquid flows are maximized. The effect of tube length is unlikely to be important under the situation. Figure 5.2.1.6-5 in Reference 6-13 shows several experimental data but the effect of length is not reported to be an affecting parameter.

Figure 6.3-22 shows the typical evidence where Eq. (6.3-31) compares the measured steam flow rate giving zero water penetration at the bottom of SG U-tubes for ROSA/LSTF[6-14] The steam flow rates agree well with Eq. (6.3-31). The results in this section support the adequacy for the quantitative evaluation for L^*_{CCFL} in Section 6.3.2.4.

Figure 6.3-23 compares the relationship of J* between the US-APWR and ROSA analyses during the loop seal phase. The variation range of US-APWR has a large overlap with that of ROSA. There is a general trend for the J* values to be lower in the US-APWR. These lower J* values make CCFL less probable in the US-APWR relative to ROSA.

6.3.3.3 Water Retention in Crossover Leg

The scaling analysis is summarized in Table 6.3-5 for the UPTF crossover leg, the US-APWR and ROSA/LSTF. The scale distortion on the geometry is small between the UPTF and the US-APWR and however the diameter of ROSA/LSTF is small. Since the characteristics of differential pressure transient along the crossover leg are important, MHI investigated the applicability of M-RELAP5 to the UPTF Test 5 which examined residual amount of water in the crossover leg[6-15]. And the temporal variation of differential pressure along the crossover leg was compared between the US-APWR and the ROSA/LSTF to investigate the scalability point of view.

Figure 6.3-24 compares the results for the UPTF Test 5. M-RELAP5 predicts the qualitative relationship between the residual amount of water in the loop seal and the steam flow rate, and also predicts the amount quantitatively. The temporal variation of differential pressure along the upflow-side of loop seal is compared in Figure 6.3-25 between the US-APWR and the ROSA/LSTF. The differential pressure is normalized by the initial value when the differential pressure starts to decrease. The time is also normalized by the period during the differential pressure decreasing. The temporal variation is similar between the two systems regardless of the difference of diameter. The results in this section support the scalability of ROSA/LSTF and the adequacy of the quantitative evaluation for L^{*}_{LS} in Section 6.3.2.4.

Table 6.3-2 Comparison of UPTF CCFL Test and US-APWR, ROSA/LSTF Hot Leg Conditions

	UPTF CCFL	US-APWR	ROSA/LSTF
Hot leg diameter (m)	0.75	0.787 (31in.)	0.207
Fluid combination	Steam/Water	Steam/Water	Steam/Water
System pressure	0.3MPa 1.5MPa	about 9MPa at loop seal	about 9MPa at loop seal

Table 6.3-3 Comparison of Dukler Test and US-APWR, ROSA/LSTF SG-U tubes Conditions

	Dukler	US-APWR	ROSA/LSTF
Tube inner diameter (in.)	2	0.664	0.772
Tube length (ft)	13.3	[ ]	
Tube wall material	Plexiglas	Inconel	SUS
Fluid combination	Air/Water	Steam/Water	Steam/Water
System pressure	atmospheric pressure	about 9MPa at loop seal	about 9MPa at loop seal

Table 6.3-4 Value of D at D*=60 under Different Pressure

Pressure (bar)	3	15	70	150
D (in.)	5.5	5.1	3.9	2.4

Table 6.3-5 Comparison of UPTF Test 5 and US-APWR, ROSA/LSTF Loop Seal Conditions

	UPTF Test5	US-APWR	ROSA/LSTF
Crossover leg diameter (m)	0.75	0.787 (31in.)	0.168
Crossover leg height (m)	2.565	[ ]	
Fluid combination	Steam/Water	Steam/Water	Steam/Water
System pressure	0.3MPa 1.5MPa	about 9MPa at loop seal	about 9MPa at loop seal

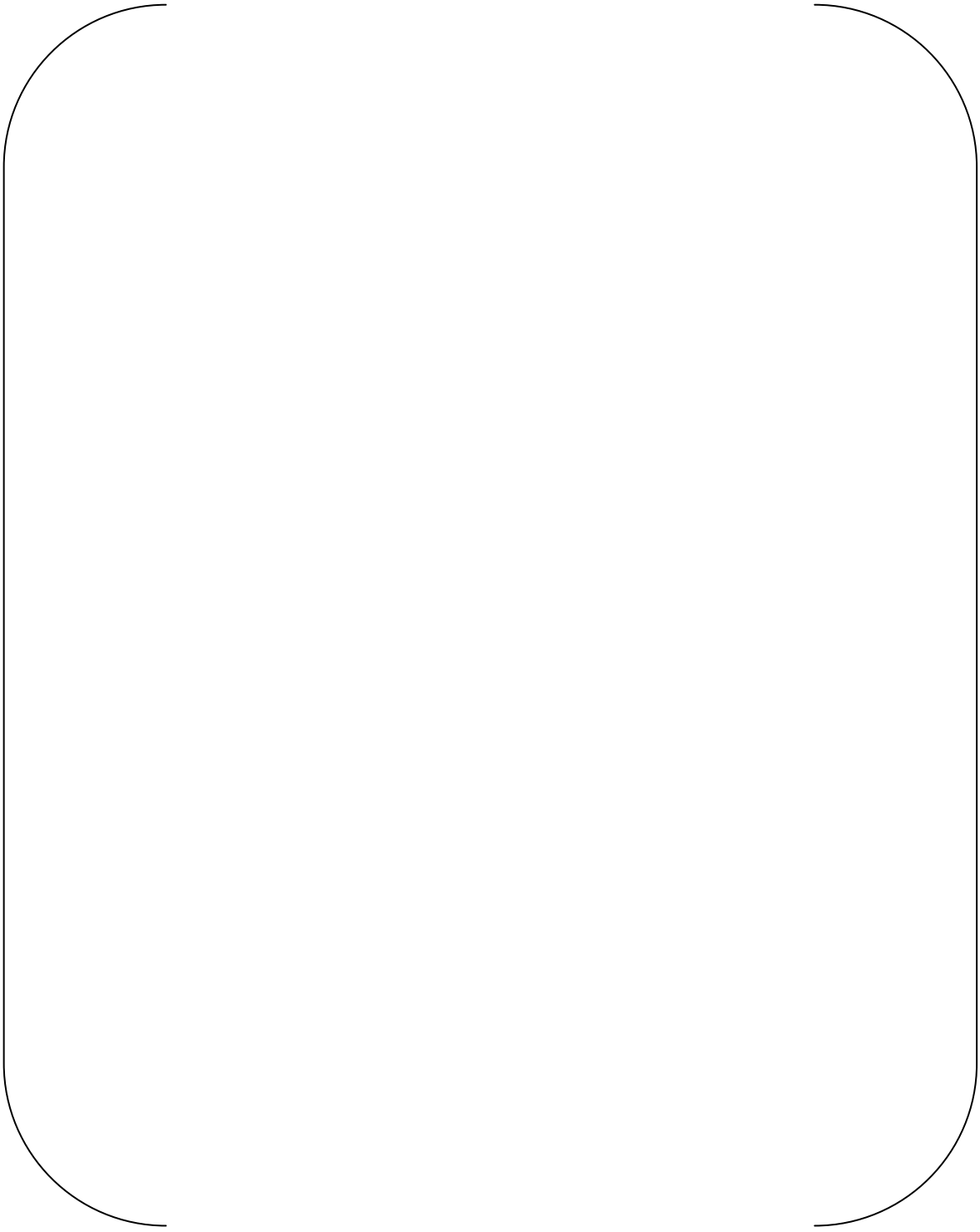

Figure 6.3-20 Comparison of Ku* between US-APWR and ROSA analyses during the loop seal phase

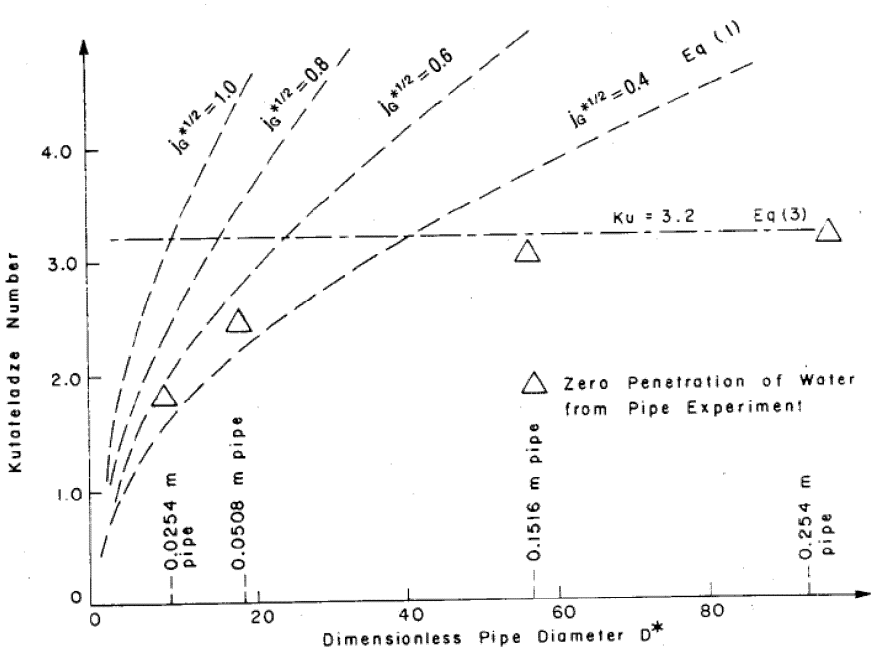

Figure 6.3-21 Kutateladze Number vs. Nondimensional Geometric Parameter and Experimental Results for Zero Penetration of Liquid[6-12]

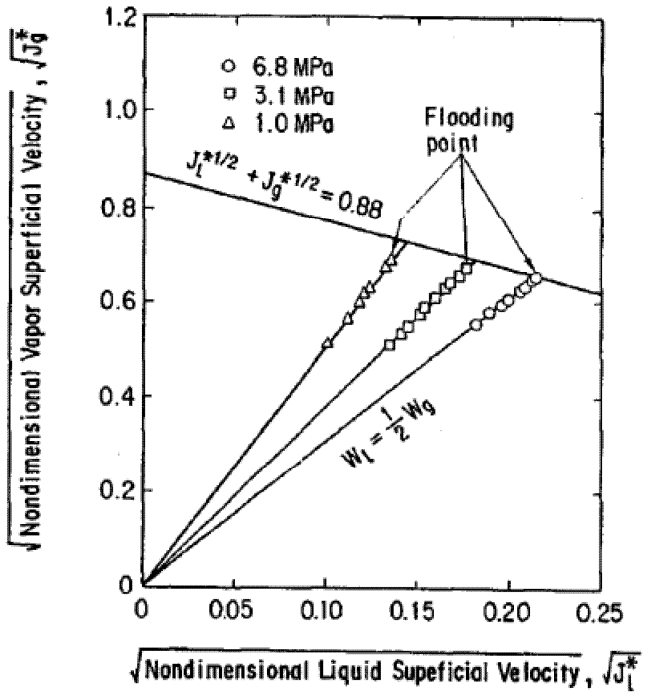

Figure 6.3-22 SG U-tube CCFL Characteristics in ROSA-/LSTF[6-14]

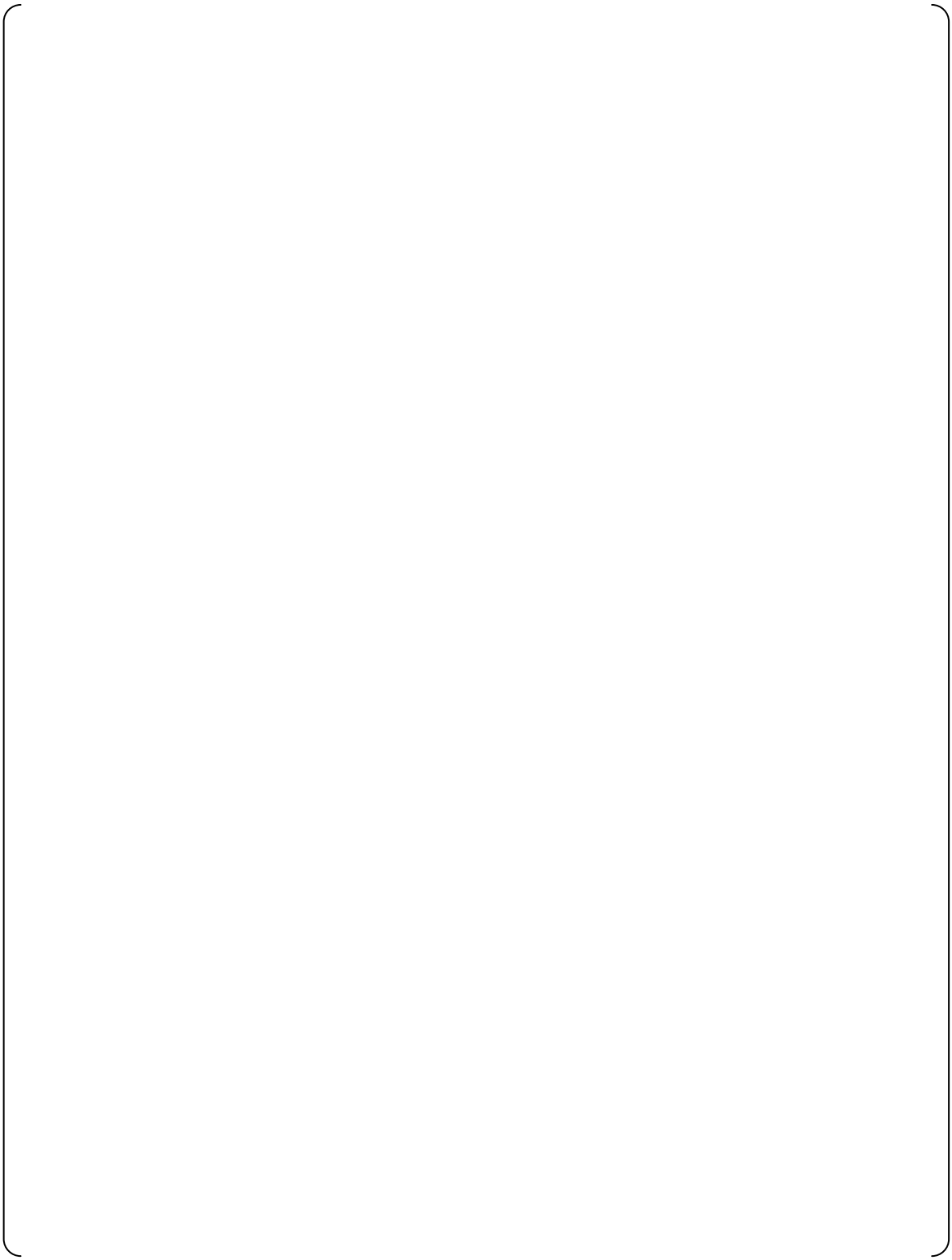

Figure 6.3-23 Comparison of J* between US-APWR and ROSA analyses during the loop seal phase

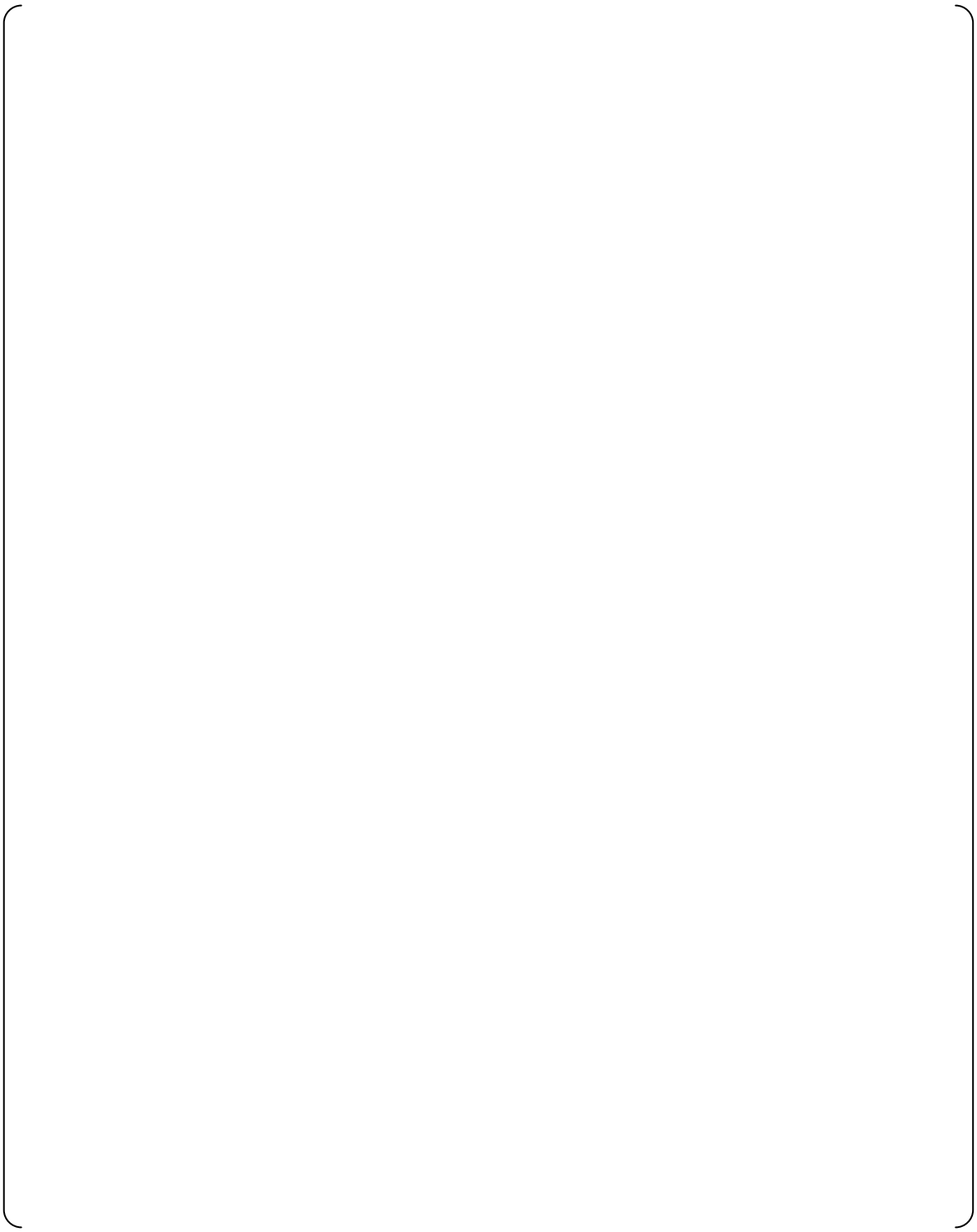

Figure 6.3-24 Assessment Results for Residual Water Amount in UPTF Test 5 ((a) 3 bar case and (b) 15 bar case)

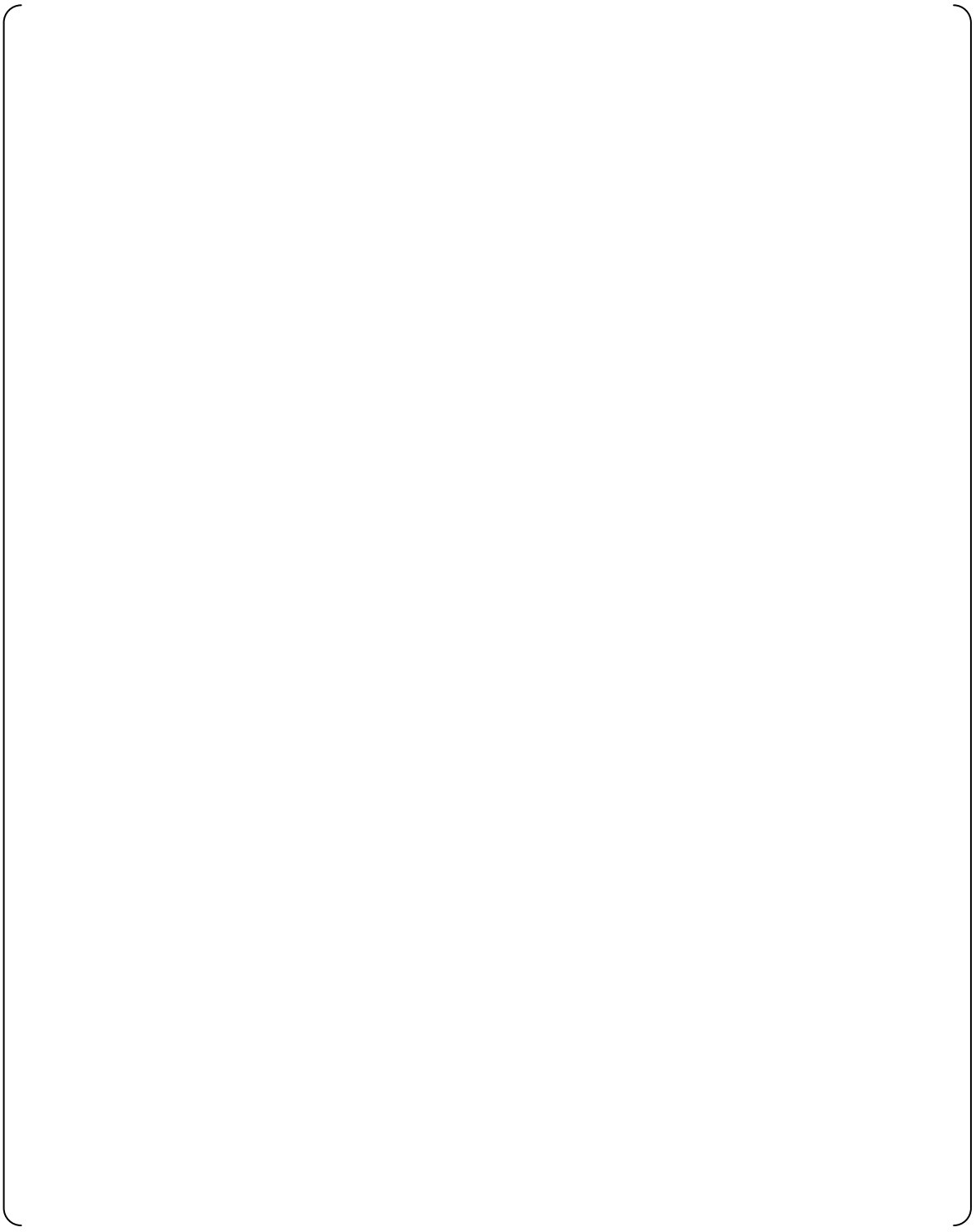

Figure 6.3-25 Comparison of Nondimensional Differential Pressure of Upflow side of Loop Seal between US-APWR and ROSA

6.3.4 Summary

The core liquid level behavior during the loop seal period is important because the liquid level contributes to the potential for core dryout. The ROSA/LSTF facility is a major IET providing integral system data on core liquid level behavior, which must be evaluated to determine its scalability to the US-APWR.

This section compared the liquid level behavior in the US-APWR SBLOCA 7.5-in CLB with that in the ROSA/LSTF SB-CL-18 test using nondimensional equations to quantitatively examine the scalability between the two systems. The study revealed that the core liquid level is primarily controlled by the CCFL induced liquid head in the uphill side of SG U-tubes and inlet plena, and by the head balance caused by the distribution of liquid along the loop seal. The same mechanisms are dominant for both the US-APWR and ROSA/LSTF test, but the core liquid level is likely to be more depressed in ROSA/LSTF compared to the US-APWR. This different characteristic is mainly caused by the larger loop seal depth in ROSA. The scalability of the CCFL in the uphill side of SG U-tubes was confirmed through the bottom-up scaling evaluation although more water accumulation in the SG inlet plena is likely to occur in ROSA because of the CCFL scale distortion for the hot leg geometry. The adequacy of loop seal behavior predicted for the US-APWR was also confirmed by the assessment for the residual water prediction in UPTF tests.

The scalability for the pressure and the mass transients is also examined using the reduced models and no significant scale distortions were revealed during the loop seal clearance phase.

6.4 Boil-Off

6.4.1 Phenomena and Applied Test Facility

The boil-off phase commences at the end of the loop seal clearance phase and continues until the RCS mass inventory starts recovering. After the coolant seals in the crossover legs clear, the RCS primary-side pressure gradually falls below the secondary-side pressure, because of the large volume of steam vapor discharging out the break. Core power remains at decay heat levels, vaporizing the coolant during this phase. Therefore, the core liquid level is gradually decreasing, leading to the potential for core uncovery and a fuel cladding temperature excursion (heat-up) if the SI flow rate is insufficient to maintain the liquid inventory in the core.

Table 4.3.2-2 of the US-APWR SBLOCA topical report[6-1] and Table 5.1-1 of the present report list important phenomena and processes during the boil-off phase, 1) CHF/dryout, 2) uncovered core heat transfer, and 3) mixture level in the core and reactor vessel. These localized phenomena and processes are important in addressing the impact on the PCT in SBLOCAs. The break flow and ECCS flow rates, on the other hand, play important roles in determining the global response, the RCS mass inventory and system depressurization behaviors. The break flow is essentially saturated vapor. During the boil-off phase, the liquid coolant remains nearly stagnant in the lower portion of the RCS, and the core inlet flow rate approaches zero. The core is in a pool boiling state. The coolant is vaporized due to the core decay heat, and the core may experience uncovery if insufficient safety coolant is injected into the RCS. In the typical SBLOCA scenario for the US-APWR, the HHIS, pumped safety injection (SI), starts delivering the safety coolant to the RCS. When the break flow rate is smaller than the HHIS flow rate, the core uncovery can be prevented. In the case of larger break sizes, the HHIS is not able to compensate for the coolant vaporized and lost from the RCS, and thus core uncovery and heat-up occur. In this case, the heat-up behavior is terminated by a large amount of safety coolant injected from the accumulator, which is actuated when the RCS pressure falls below its operating level.

The boil-off phase appears over a wide range of the break size spectrum, which is discussed in the sensitivity analysis report for US-APWR SBLOCA[6-16]. For the top-down scaling analysis of the boil-off phase, the 7.5-in cold leg break (CLB) case is selected as a typical US-APWR SBLOCA transient, as was done for the other phases. However, since the most severe heat-up occurs for larger break sizes, the 1-ft^2 CLB, which provides the limiting PCT, is also evaluated. The integral effects test (IET) examined in the top-down approach are the ROSA/LSTF SB-CL-18 and IB-CL-02 tests. The SB-CL-18 test was originally performed to simulate a 5% cold leg break in the 4-loop PWR. This IET corresponds most closely to the US-APWR **[ ]** CLB. The IB-CL-02 test was performed specifically to simulate the 1-ft^2 break in the US-APWR.

The locally important phenomena and processes, such as the CHF/dryout, uncovered core heat transfer, and two-phase mixture level are addressed by the bottom-up scaling approach. Specifically, the separate effects test (SET) facility, ORNL/THTF, used for the M-RELAP5 assessment is examined to determine whether the test facility and the experimental conditions are scaled to the US-APWR SBLOCAs.

6.4.2 Top-Down Scaling Analysis

6.4.2.1 Transient Behavior of Interest

From the viewpoint of the global plant responses, the RCS mass inventory and depressurization are of interest. In particular, scalability with respect to the pressure response needs to be examined between the plant and the test facility, because the safety coolant injection, the HHIS flow rate and accumulator actuation, are strongly dependent on the system depressurization rate.

Transient evolutions of RCS mass inventory and pressure are compared between the US-APWR 7.5-in CLB and the ROSA/LSTF SB-CL-18 test in Figure 6.4-1 and Figure 6.4-2. The RCS mass inventory and pressure responses are primarily dominated by the break flow, ECCS flow, and core power, which are compared in Figure 6.4-3 to Figure 6.4-5, respectively. Similar comparisons between the US-APWR 1-ft^2 CLB and ROSA/LSTF IB-CL-02 test are made in Figure 6.4-6 through Figure 6.4-10. During the boil-off phase, the core coolant is vaporized, and the steam primarily flows into the SGs through the hot legs. The steam is heated in the SGs, since the secondary-side behaves as a heat source during the boil-off phase. Fluid entering the SGs changes from a two-phase mixture to single-phase vapor. The degree of superheat at the SG exit is not significant as confirmed in Figure 6.4-11 and Figure 6.4-12 for the US-APWR SBLOCAs, and in Figure 6.4-13 and Figure 6.4-14 for the ROSA tests, respectively.

The steam flowing in the broken loop tends to discharge out the break. The steam remaining in the RCS is partially condensed by the safety coolant. The liquid in the RCS stays at the saturated temperature as shown in Figure 6.4-15 and Figure 6.4-16 for the US-APWR SBLOCAs, and in Figure 6.4-17 and Figure 6.4-18 for the ROSA tests, respectively. For the US-APWR 1-ft^2 CLB, there appears to be slightly larger vapor superheat at the SG exit and liquid subcooling at the core inlet, because the boil-off phase starts with higher core power and the larger amount of safety coolant is quickly injected by the advanced accumulator[6-17].

For the US-APWR 7.5-in CLB, the coolant sealing the crossover leg clears around **[ ]** after the break initiation. Similarly, the loop seal cleared around **[ ]** in the ROSA test. From the definition for the boil-off phase, the times described above correspond to the beginning of the boil-off phase. After the seal clearing, reduction in the RCS mass inventory is mitigated both for the US-APWR and ROSA, because the break flow transitions from single-phase liquid to a two-phase mixture or single-phase vapor. The vapor break flow contributes to discharging the energy accumulated in the system, resulting in an increase in the RCS depressurization. The core liquid level reduction continues until around **[ ]** in the US-APWR and about **[ ]** in ROSA, which is defined as the end of the boil-off phase.

It is noted that there is a difference between the US-APWR 7.5-in CLB and the ROSA test. The pumped SI system, HHIS, supplies the safety coolant during the boil-off phase of the US-APWR 7.5-in CLB, whereas the pumped SI system was intentionally removed from the safety system during the SB-CL-18 test so as to obtain higher PCT in the experiment. This may introduce scaling distortion between the plant and test facility, which will be quantitatively evaluated in Section 6.4.2.4.

For the US-APWR 1-ft^2 CLB, on the other hand, there appears to be no obvious natural

circulation and loop seal clearance phases following the blowdown, since the larger break flow invokes a very rapid depressurization below the secondary-side pressure level. The accumulator starts injecting safety coolant prior to the HHIS, when the RCS pressure falls below the accumulator actuation level. The accumulator flow rate exceeds the break flow rate, and thus the RCS mass inventory recovery starts. Since there was not a well defined natural circulation phase, it is judged that the boil-off time-period for the 1-ft^2 CLB can be defined from the end of the subcooled discharge (around **[ ]**), to the time when the core liquid level becomes minimum (around **[ ]**) which is the end of boil-off phase in this study. The accumulator starts delivering the safety coolant at about 90 seconds and the core mass inventory begins a sustained increase around **[ ]**.

It must be noticed, however, there remains a potential concern on the definition of the boil-off time-period for the 1-ft^2 CLB. The figures in the US-APWR DCD[6-18] show that the liquid break flow obviously continues during the period from 40 to 120 seconds in the 1-ft^2 CLB. This indicates the core liquid level is dominated not only by the core boil-off behavior, but also by the break flow rate. In addition, the core reflooding starts slightly later around **[ ]**, although the downcomer liquid level starts increasing when the RCS mass starts recovering around **[ ]**. This is caused by the significant hot wall boiling in the downcomer and lower plenum regions due to the rapid depressurization under the 1-ft^2 CLB, which retains the coolant entering the core even after the safety coolant is delivered to the reactor vessel. These behaviors were not clearly observed in the ROSA/LSTF IB-CL-02 test. In spite of the differences in the transient behaviors described above, the present study attempts to examine the quantitative scalability of the ROSA/LSTF IB-CL-02 test to the US-APWR 1-ft^2 CLB with respect to the RCS mass and pressure transients.

For the ROSA/LSTF IB-CL-02 test, the boil-off phase is defined by the time-period from **[ ]**, which is determined in the same manner as for the US-APWR 1-ft^2 CLB.

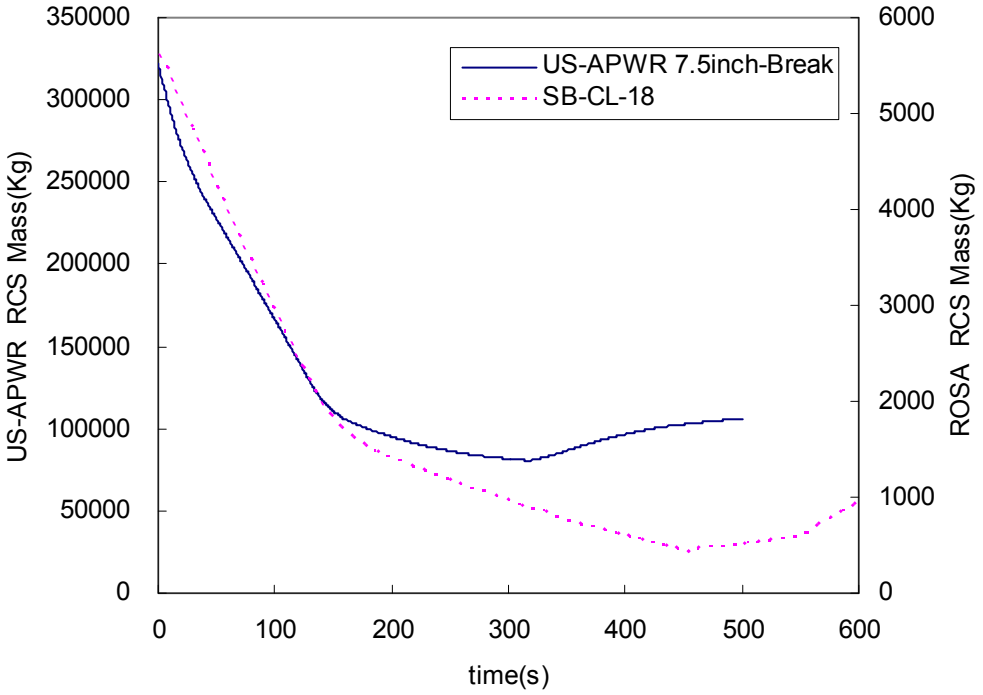

Figure 6.4-1 Comparison of RCS Mass Inventory between US-APWR 7.5-in CLB and ROSA/LSTF SB-CL-18

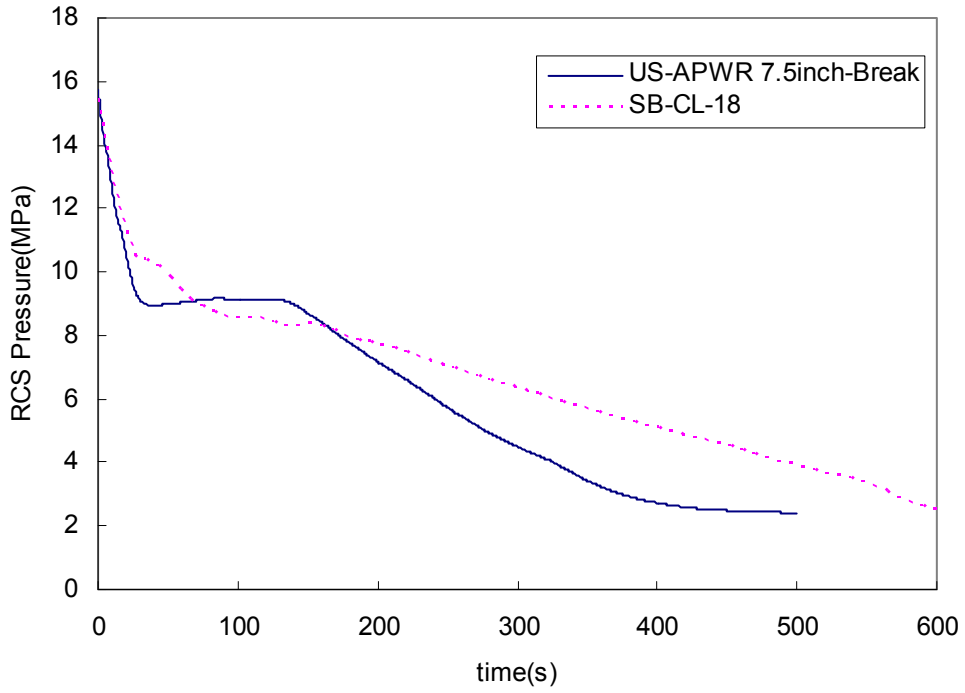

Figure 6.4-2 Comparison of RCS Pressure between US-APWR 7.5-in CLB and ROSA/LSTF SB-CL-18

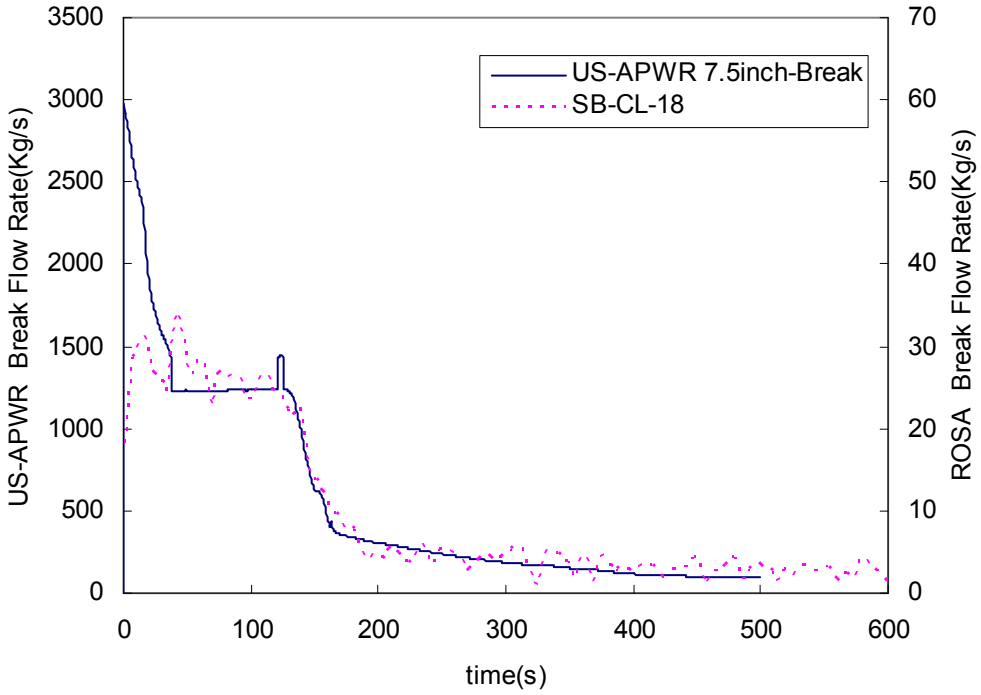

Figure 6.4-3 Comparison of Break Flow rate between US-APWR 7.5-in CLB and ROSA/LSTF SB-CL-18

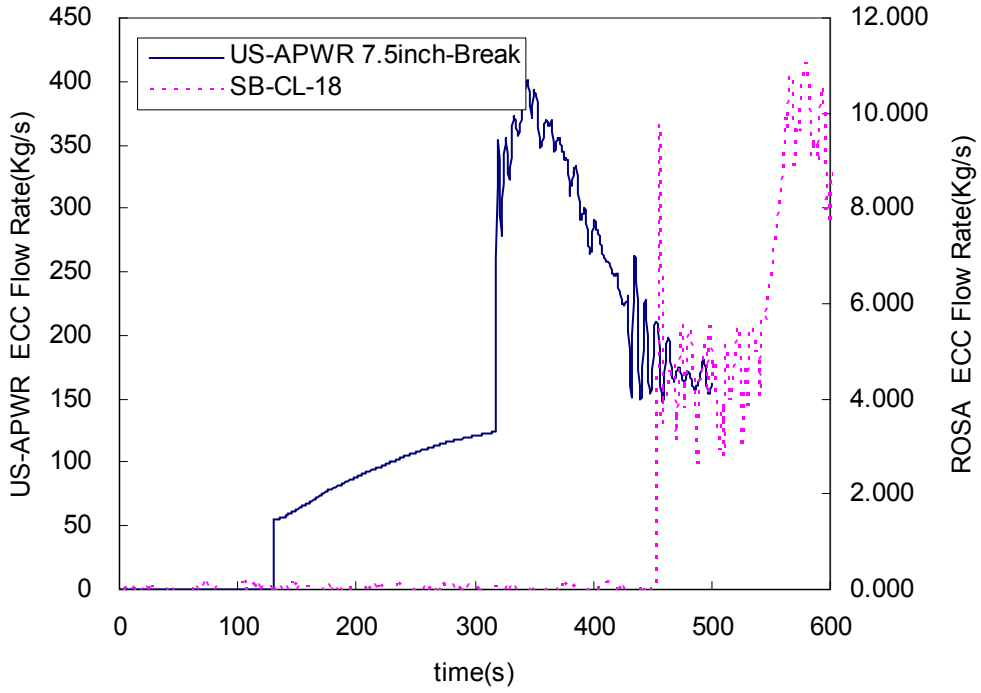

Figure 6.4-4 Comparison of ECCS Flow rate between US-APWR 7.5-in CLB and ROSA/LSTF SB-CL-18

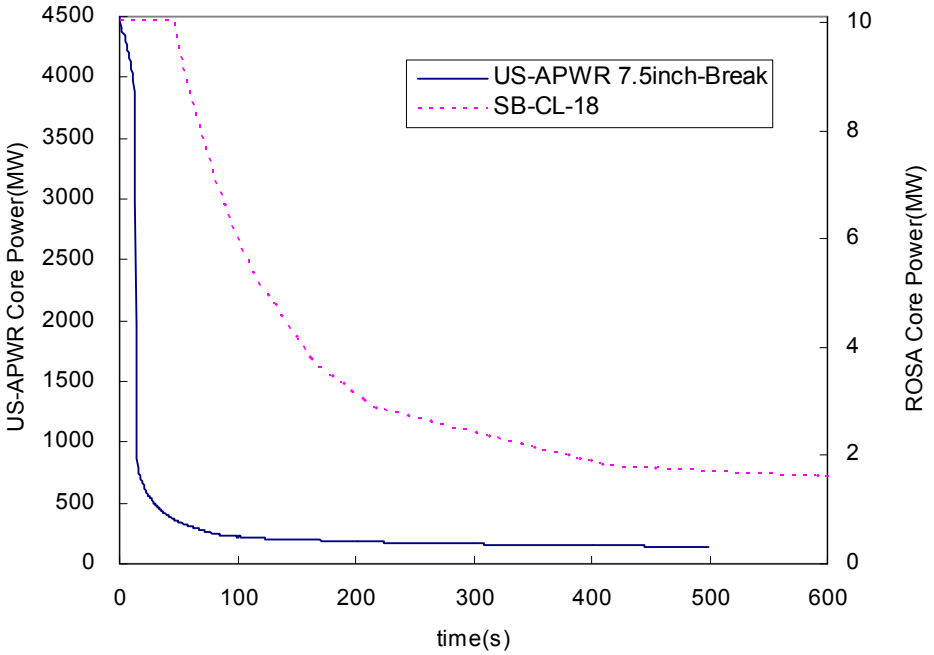

Figure 6.4-5 Comparison of Core Power between US-APWR 7.5-in CLB and ROSA/LSTF SB-CL-18

Figure 6.4-6 Comparison of RCS Mass Inventory between US-APWR 1-ft^2 CLB and ROSA/LSTF IB-CL-02

Figure 6.4-7 Comparison of RCS Pressure between US-APWR 1-ft^2 CLB and ROSA/LSTF IB-CL-02

Figure 6.4-8 Comparison of Break Flow rate between US-APWR 1-ft^2 CLB and ROSA/LSTF IB-CL-02

Figure 6.4-9 Comparison of ECCS Flow rate between US-APWR 1-ft^2 CLB and ROSA/LSTF IB-CL-02

Figure 6.4-10 Comparison of Core Power between US-APWR 1-ft^2 CLB and ROSA/LSTF IB-CL-02

Figure 6.4-11 Vapor Enthalpy at SG Exit for US-APWR 7.5-in CLB

Figure 6.4-12 Vapor Enthalpy at SG Exit for US-APWR 1-ft^2 CLB

Figure 6.4-13 Vapor Enthalpy at SG Exit for ROSA/LSTF SB-CL-18

Figure 6.4-14 Liquid Enthalpy a at SG Exit for ROSA/LSTF IB-CL-02

Figure 6.4-15 Liquid Enthalpy at Core Inlet for US-APWR 7.5-in CLB

Figure 6.4-16 Liquid Enthalpy at Core Inlet for US-APWR 1-ft^2 CLB

Figure 6.4-17 Liquid Enthalpy at Core Inlet for ROSA/LSTF SB-CL-18

Figure 6.4-18 Liquid Enthalpy at Core Inlet for ROSA/LSTF IB-CL-02

6.4.2.2 Governing Conservation Equations

The fluid behavior during the boil-off phase can be simply modeled by the two-phase mixture flow in a boiler tank as shown in Figure 6.4-19. Liquid is added to the system by the safety injection, and is vaporized in the core region. A part of the generated steam discharges out the break, while the rest of the steam remains in the system or is condensed by the liquid. A mass balance between the incoming and outgoing fluids determines the system mass inventory. Similarly, a balance between the energy added to the fluid and the energy removed with the break flow determines the system pressure. Therefore, from the global response point of view, the transient of interest is sufficiently represented with the mass and energy conservation equations for the tank.

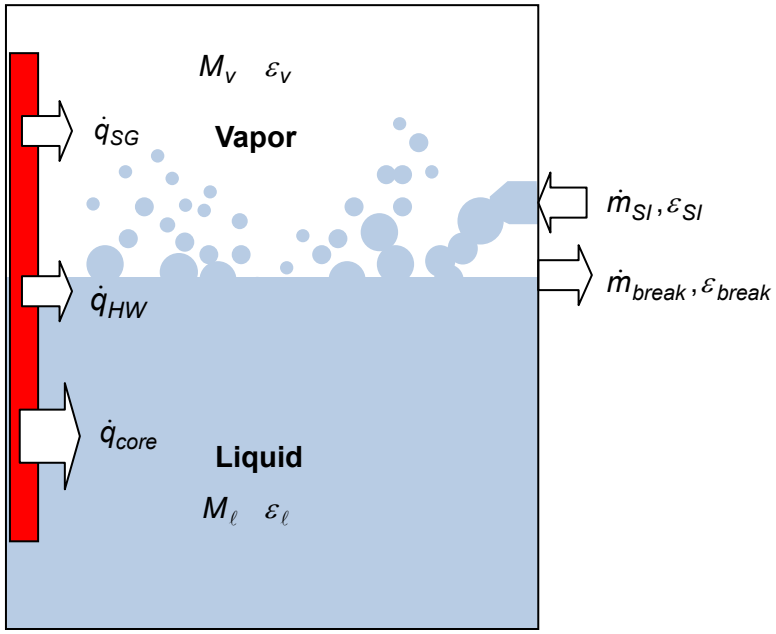

Figure 6.4-19 Schematic of Control Volume and Related Variables for Boil-off Phase

During the boil-off phase, the fluid can be approximated as a two-phase mixture in evaluating the global mass and energy conservations. The method developed for the natural circulation top-down scaling analysis is applicable to the present phase with some minor modifications in terms of the parameters addressed in the governing equations. The mass balance is related to the incoming and outgoing flow rates as follow:

Mass conservation equation:

$$\frac{d\left(\rho_\ell V_\ell + \rho_v V_v\right)}{dt} = \frac{d\rho_m V}{dt} = \dot{m}_{SI} + \dot{m}_{ACC} - \dot{m}_{break} \tag{6.4-1}$$

$$\rho_m = \frac{\rho_\ell V_\ell + \rho_v V_v}{V} \tag{6.4-2}$$

where ρ_m, V, m_{SI}, and m_{break} are the mixture density, volume, SI and break flow rates,

respectively.

An advantage of employing the saturated mixture fluid equation is the elimination of the complicated vaporization and condensation terms in the conservation equation. Since the liquid and vapor stay in the RCS under the mostly saturated condition as discussed in the preceding section, this simplification is sufficiently applicable to represent the fluid behavior. It is noted, however, that a small amount superheat and subcooling appears in the SG outlet vapor and in the core inlet liquid, respectively. Therefore, the applicability to the US-APWR 1-ft^2 CLB shall be carefully examined in the validation of scaling analysis results.

Similar to the mass conservation, the mixture energy conservation equation is obtained.

Energy conservation equation:

$$\frac{d\left(\rho_\ell V_\ell \varepsilon_\ell + \rho_v V_v \varepsilon_v\right)}{dt} = \frac{d\rho_m V \varepsilon_m}{dt} = \dot{q}_{core} + \dot{q}_{SG} + \dot{q}_{HW} + \dot{m}_{SI}\varepsilon_{SI} - \dot{m}_{break}\varepsilon_{break} \quad (6.4\text{-}3)$$

$$\varepsilon_m = \frac{\rho_\ell V_\ell \varepsilon_\ell + \rho_v V_v \varepsilon_v}{\rho_m V} = \frac{\rho_\ell V_\ell \varepsilon_\ell + \rho_v V_v \varepsilon_v}{\rho_\ell V_\ell + \rho_v V_v} \quad (6.4\text{-}4)$$

where ε_m, ε_{SI} , ε_{break}, q_{core}, q_{SG}, and q_{HW} are the mixture fluid energy (enthalpy), safety injection energy, break flow enthalpy, heat transfer from the core, SG, and reactor hot wall, respectively. In the above equation, the fluid energy is represented as follows, by neglecting the kinetic and potential energy:

$$\varepsilon = h = u + Pv \quad (6.4\text{-}5)$$

where u, P, and v are the internal energy, pressure, and specific volume, respectively. By using the equation (6.4-5), the energy conservation is converted into a derivative equation to represent the pressure change as follow:

Pressure equation:

$$\frac{dP}{dt} = \frac{\partial P / \partial v_m\big|_{u_m}}{\rho_m V} \left\{ \frac{\partial P / \partial \mu_m\big|_{v_m}}{\partial P / \partial v_m\big|_{u_m}} \left[\dot{m}_{ECC}\left(h_{ECC} - u_m\right) - \dot{m}_{break}\left(h_{break} - u_m\right) + \dot{q}_{net}\right] - v_m\left(\dot{m}_{ECC} - \dot{m}_{break}\right) \right\} \quad (6.4\text{-}6)$$

$$\dot{q}_{net} = \dot{q}_{core} + \dot{q}_{SG} + \dot{q}_{HW} \quad (6.4\text{-}7)$$

Details in deriving the pressure equation are referred to Appendix C of Reference 6-5. The terms with the ECC subscripts in equation (6.4-6) include the SI and accumulator flows.

6.4.2.3 Nondimensional Equations and Groups

As done for the natural circulation model, the mass equation (6.4-1) and the pressure equation (6.4-6) are nondimensionalized by normalizing each variable to the reference value. The resultant equations are as follows:

Nondimensionalized mass equation:

$$\frac{dM^*}{dt^*} = \Psi_{13}\left(\dot{m}^*_{SI} + \dot{m}_{ACC} - \dot{m}^*_{break}\right) \tag{6.4-8}$$

Nondimensionalized pressure equation:

$$\frac{dP^*}{dt^*} = \Psi_4 C^*_{1,m} I^*_{a,m} + \Psi_5 C^*_{1,m} I^*_{b,m} + \Psi_6 C^*_{1,m} I^*_{c,m} + \Psi_{11} C^*_2 II^*_m \tag{6.4-9}$$

where

$$I^*_{a,m} = \frac{I_{a,m}}{\dot{m}_{ECC,0}\left(h_{ECC} - u_m\right)_0} \tag{6.4-10}$$

$$I^*_{b,m} = \frac{I_{b,m}}{\dot{m}_{break,0}\left(h_{break} - u_m\right)_0} \tag{6.4-11}$$

$$I^*_{c,m} = \frac{I_{c,m}}{\dot{q}_{net0}} \tag{6.4-12}$$

$$II^*_m = \frac{II_m}{v_{m,0}\left(\dot{m}_{SI0} + \dot{m}_{ACC} - \dot{m}_{break0}\right)} \tag{6.4-13}$$

$$I_{a,m} = \dot{m}_{ECC}\left(h_{ECC} - u_m\right) \tag{6.4-14}$$

$$I_{b,m} = \dot{m}_{break}\left(h_{break} - u_m\right) \tag{6.4-15}$$

$$I_{c,m} = \dot{q}_{net} \tag{6.4-16}$$

$$II_m = v_m\left(\dot{m}_{SI} + \dot{m}_{ACC} - \dot{m}_{break}\right) \tag{6.4-17}$$

The quantities with an asterisk represent normalized variables, and subscript of zero denotes the reference value for the variable. The nondimensional time t^* indicates the time normalized to the temporal period of interest. The coefficients $C^*_{1,m}$ and C^*_2 are defined as follows:

$$C^*_{1,m} = \frac{C_{1,m}}{C_{1,m,0}} \tag{6.4-18}$$

$$C^*_{2,m} = \frac{C_2}{C_{2,m,0}} \tag{6.4-19}$$

$$C_{1,m} = \frac{\partial P / \partial u_m\big|_{v_m}}{\rho_m V} \tag{6.4-20}$$

$$C_{2,m} = \frac{\partial P / \partial v_m\big|_{\mu_m}}{\rho_m V} \tag{6.4-21}$$

The nondimensional groups defined for the above equations are Ψ_4, Ψ_5, Ψ_6, Ψ_{11}, and Ψ_{13}, which are defined as follows:

$$\Psi_4 = \frac{C_{1,m,0}(h_{ECC} - u_m)_0 \dot{m}_{ECC} t_0}{P_0} \quad (6.4\text{-}22)$$

$$\Psi_5 = \frac{C_{1,m,0}(h_{break} - u_m)_0 \dot{m}_{break0} t_0}{P_0} \quad (6.4\text{-}23)$$

$$\Psi_6 = \frac{C_{1,m,0} \dot{q}_{net0} t_0}{P_0} \quad (6.4\text{-}24)$$

$$\Psi_{11} = \frac{C_{2,0} v_{m,0} \dot{m}_0 t_0}{P_0} \quad (6.4\text{-}25)$$

$$\Psi_{13} = \frac{\dot{m}_0 t_0}{M_0} \quad (6.4\text{-}26)$$

Ψ_4 is the ratio of pressure change, due to change in specific energy of the saturated field from mass inflows, to the reference pressure. Ψ_5 is the ratio of pressure change, due to change in specific energy of the saturated field from mass outflows, to the reference pressure. Ψ_6 is the ratio of pressure change, due to change in specific energy of the saturated field from heat transfer, to the reference pressure. Ψ_{11} is the ratio of pressure change, due to change in specific volume of the saturated field from volumetric flow, to reference pressure. And finally, Ψ_{13} is defined as the ratio of net mass flow to the reference system mass. The reference mass is the RCS mass at the beginning of the phase. This selection makes Ψ_{13} the fraction of RCS mass lost during the phase.

The specific volume and internal energy of the mixture, v_m and u_m in the equations represent the RCS-averaged values, which are determined by the saturated fluid properties as follows:

$$v_m = x v_g + (1-x) v_f \quad (6.4\text{-}27)$$

$$u_m = x u_v + (1-x) u_f \quad (6.4\text{-}28)$$

6.4.2.4 Scaling Analysis Results

The nondimensional groups characterize the normalized response in the RCS mass and pressure, and the scalability of the test facility to the actual plant is quantitatively examined by comparing the nondimensional groups. Table 6.4-1 lists the reference values used to obtain the nondimensional groups in order to examine the scalability between the US-APWR 7.5-in CLB and the ROSA/LSTF SB-CL-18 test. Regarding the RCS mass and pressure, *M* and *P*, the reference values are defined **[**

]. The break flow rate, SI flow rate, and heat source are important in determining the mass and pressure transient responses, and these references are defined by the values around **[** **]**, both for the US-APWR and ROSA. These reference values tend to represent their average behaviors during the boil-off phase. Similarly, the reference values for the pressure-derivative parameters, C_{1m}, and C_{2m}, are also defined by the values around **[** **]**. Table 6.4-1 also lists the evaluated nondimensional groups for the US-APWR 7.5-in CLB and for the ROSA/LSTF SB-CL-18 test. These nondimensional groups are calculated based on the reference values selected above. Since the pumped safety injection was intentionally not actuated, Ψ_4 was not

evaluated for the ROSA test. The normalized RCS mass and pressure reproduced by using the reduced equations, (6.4-8) and (6.4-9), are graphically compared between the plant and test facility in Figure 6.4-20 and Figure 6.4-21, respectively.

As for the ranking of nondimensional groups, the significant group is Ψ_6 for both systems. And the relative contribution for Ψ_5 and Ψ_{11} is the same order for both systems. These results indicate the similitude of these two systems is reasonable. Table 6.4-2 shows the scaling ratios of the evaluated nondimensional groups between the ROSA/LSTF SB-CL-18 test and the US-APWR 7.5-in CLB. Because no SI flow was actuated during the boil-off phase for the ROSA/LSTF SB-CL-18 test, the nondimensional group Ψ_4, pressure change due to the inflow energy, and its scaling ratio cannot be evaluated. The mechanism represented by the ψ_4 group is condensation caused by ECC injection. The lack of this mechanism in ROSA is consistent with the slower depressurization rate in ROSA relative to the US-APWR. In addition, the difference in the SI induces a scaling distortion, particularly, in the RCS mass inventory. Specifically, there appears a distortion in the nondimensional group Ψ_{13}, which represents the net mass flow change. The scaling ratio of Ψ_{13} is **[ ]**.

The scaling ratio of Ψ_5, which represents the pressure change due to the break flow energy, is **[ ]**, and shows no significant difference between the US-APWR and ROSA. This is reasonable because the ROSA break size is relatively close to the 7.5-in CLB postulated in the US-APWR. The scaling ratio of Ψ_6, the pressure change due to the heat source, is **[ ]**. Finally, the scaling ratio of Ψ_{11}, the pressure change due to change in the specific volume, is **[ ]**.

Similar to the approach described above, the reduced equations are applied to the US-APWR 1-ft^2 CLB, and the reference values selected for the evaluation and the resultant nondimensional groups are listed in Table 6.4-3. The reference values for *M* and *P* are defined **[ ]**, and the other reference values are obtained from the average values during the boil-off phase. The normalized mass and pressure of the reduced model are compared with those obtained for the ROSA/LSTF IB-CL-02 in Figure 6.4-22 and Figure 6.4-23, respectively.

As for the ranking of nondimensional groups, no significant groups are recognized for both systems. And the relative contribution is the same order for both systems. These results indicate the similitude of these two systems is reasonable. The evaluated scaling criteria are arranged in Table 6.4-4. Because no safety coolant is injected at the time selected to determine the reference incoming flow rate, the nondimensional group Ψ_4 is not evaluated for either the US-APWR 1-ft^2 CLB or the ROSA test. Furthermore, contribution of the inflow to the system response is relatively smaller for larger break cases. The normalized mass reduction for the US-APWR is faster than that for the ROSA test because of the relatively larger break flow rate. Thus, the net mass reduction is larger in the US-APWR 1-ft^2 CLB, and the scaling ratio for Ψ_{13} is **[ ]**. The scaling ratio of Ψ_5, which represents the pressure change due to the break flow energy, is **[ ]**. The scaling ratio of Ψ_6, the pressure change due to the heat source, is **[ ]**. Finally, the scaling ratio of Ψ_{11}, the pressure change due to change in the specific volume, shows a slightly lower as **[ ]**.

Table 6.4-1 Comparison of Physical Values and Nondimensional Groups between US-APWR 7.5-in CLB and ROSA/LSTF SB-CL-18 for Boil-off Phase

Reference Parameters	US-APWR 7.5in CLB	ROSA/LSTF SB-CL-18	Notes
t_0 (sec)			Time period
M_0 (kg)			Initial RCS mass
P_0 (MPa)			Initial RCS pressure
$\dot{q}_{net0}$ (MW)			Net heat source at middle period
$\dot{m}_{break,0}$ (kg/s)			Break flow rate at middle period
$\dot{m}_{SI,0}$ (kg/s)			SI flow rate at middle period
$h_{break,0}$ (kJ/kg)			Break enthalpy at middle period
$h_{SI,0}$ (kJ/kg)			SI enthalpy at middle period
$u_{m,0}$ (kJ/kg)			Reactor internal energy at middle period
$v_{m,0}$ (m^3/kg)			Reactor specific volume at middle period
$C_{1m,0}$ (Pa/J)			
$C_{2m,0}$ (Pa/m^3)			
Nondimensional Group			
Ψ_4			
Ψ_5			
Ψ_6			
Ψ_{11}			
Ψ_{13}			
Ranking groups in the depressurization equation			
ψ_5/ψ_6			
ψ_{11}/ψ_6			

Table 6.4-2 Scaling Criteria between US-APWR 7.5-in CLB and ROSA/LSTF SB-CL-18 for Boil-off Phase

Scaling Parameters	$\frac{\Psi_{i,ROSA}}{\Psi_{i,US-APWR}}$	Definitions
$\frac{\Psi_{4,ROSA}}{\Psi_{4,US-APWR}}$		Ratio of pressure change, due to change in specific energy of the saturated field from mass inflows, to reference pressure
$\frac{\Psi_{5,ROSA}}{\Psi_{5,US-APWR}}$		Ratio of pressure change, due to change in specific energy of the saturated field from mass outflows, to reference pressure
$\frac{\Psi_{6,ROSA}}{\Psi_{6,US-APWR}}$		Ratio of pressure change, due to change in specific energy of the saturated field from heat transfer, to reference pressure
$\frac{\Psi_{11,ROSA}}{\Psi_{11,US-APWR}}$		Ratio of pressure change, due to change in specific volume of the saturated field from volumetric flow, to reference pressure
$\frac{\Psi_{13,ROSA}}{\Psi_{13,US-APWR}}$		Ratio of integrated mass flow to reference mass

Table 6.4-3 Comparison of Physical Values and Nondimensional Groups between US-APWR 1-ft^2 CLB and ROSA/LSTF IB-CL-02 for Boil-off Phase

Reference Parameters	US-APWR 1-ft^2 CLB	ROSA/LSTF IB-CL-02	Notes
t_0 (sec)			Time period
M_0 (kg)			Initial RCS mass
P_0 (MPa)			Initial RCS pressure
$\dot{q}_{net0}$ (MW)			Net heat source averaged in this phase
$\dot{m}_{break,0}$ (kg/s)			Break flow rate averaged in this phase
$\dot{m}_{SI,0}$ (kg/s)			SI flow rate averaged in this phase
$h_{break,0}$ (kJ/kg)			Break enthalpy averaged in this phase
$h_{SI,0}$ (kJ/kg)			SI enthalpy averaged in this phase
$u_{m,0}$ (kJ/kg)			Reactor internal energy averaged in this phase
$v_{m,0}$ (m^3/kg)			Reactor specific volume averaged in this phase
$C_{1m,0}$ (Pa/J)			
$C_{2m,0}$ (Pa/m^3)			
Nondimensional Group			
Ψ_5			
Ψ_6			
Ψ_{11}			
Ψ_{13}			
Ranking groups in the depressurization equation			
ψ_5/ψ_6			
ψ_{11}/ψ_6			

Table 6.4-4 Scaling Criteria between US-APWR 1-ft^2 CLB and ROSA/LSTF IB-CL-02 for Boil-off Phase

Scaling Parameters	$\frac{\Psi_{i,ROSA}}{\Psi_{i,US-APWR}}$	Definitions
$\frac{\Psi_{4,ROSA}}{\Psi_{4,US-APWR}}$	[ ]	Ratio of pressure change, due to change in specific energy of the saturated field from mass inflows, to reference pressure
$\frac{\Psi_{5,ROSA}}{\Psi_{5,US-APWR}}$		Ratio of pressure change, due to change in specific energy of the saturated field from mass outflows, to reference pressure
$\frac{\Psi_{6,ROSA}}{\Psi_{6,US-APWR}}$		Ratio of pressure change, due to change in specific energy of the saturated field from heat transfer, to reference pressure
$\frac{\Psi_{11,ROSA}}{\Psi_{11,US-APWR}}$		Ratio of pressure change, due to change in specific volume of the saturated field from volumetric flow, to reference pressure
$\frac{\Psi_{13,ROSA}}{\Psi_{13,US-APWR}}$		Ratio of integrated mass flow to reference mass

Figure 6.4-20 Comparison of Normalized RCS Mass between US-APWR 7.5-in CLB and ROSA/LSTF SB-CL-18 for Boil-off Phase

Figure 6.4-21 Comparison of Normalized RCS Pressure between US-APWR 7.5-in CLB and ROSA/LSTF SB-CL-18 for Boil-off Phase

Figure 6.4-22 Comparison of Normalized RCS Mass between US-APWR 1-ft^2 CLB and ROSA/LSTF IB-CL-02 for Boil-off Phase

Figure 6.4-23 Comparison of Normalized RCS Pressure between US-APWR 1-ft^2 CLB and ROSA/LSTF IB-CL-02 for Boil-off Phase

6.4.2.5 Validation of Scaling Results

In the process of the present top-down scaling analysis, accuracy of the reduced model must be verified to ensure the reliability of the results evaluated in the preceded section. In order to accomplish this purpose, the normalized mass and pressure responses reproduced by the reduced model are compared with results from the M-RELAP5 calculations (US-APWR SBLOCAs) and experimental measurements (ROSA/LSTF SB-CL-18 and IB-CL-02).

Prior to discussing validity of the obtained results, status of the variables used to determine the nondimensional parameters M^* and P^* for the ROSA/LSTF SB-CL-18 test is described. The incoming and outgoing flow rates are based on the measured break and SI flow rates. Similarly, SI coolant temperature is from the test specification. On the other hand, the break flow enthalpy, and the SG and hot wall heat transfer were extracted from the M-RELAP5 calculation because there are no available measured data. It is noted that an agreement for the nondimensional RCS mass inventory M^* between the measurement and the reduced model is reasonable, because the measured break flow rate was commonly used to derive M^* from the measurements and to evaluate M^* in the reduced model using Equation (6.4-8). Similarly, a good agreement can be found in M^* for the US-APWR SBLOCAs.

The reduced model is able to provide the temporal changes for the normalized RCS mass and pressure by numerically evaluating the reduced equations, (6.4-8) and (6.4-9). The equations were evaluated using M-RELAP5 results or experimental data for the terms on the right hand side of the equations. The results are compared with those calculated by M-RELAP5 in Figure 6.4-24 for the normalized mass and in Figure 6.4-25 for the normalized pressure during the US-APWR 7.5-in CLB boil-off phase. The same comparisons are depicted in Figure 6.4-26 and Figure 6.4-27 for the US-APWR 1-ft^2 CLB. The comparisons with the ROSA/LSTF measurements are shown in Figure 6.4-28 and Figure 6.4-29 for the ROSA/LSTF SB-CL-18 test and in Figure 6.4-30 and Figure 6.4-31 for the IB-CL-02. These comparisons demonstrate that the reduced model accurately reproduces the code-calculated boil-off or code-calculated responses. Therefore, it can be concluded that the evaluated scaling results are sufficiently reliable.

6.4.2.6 Evaluation for Scaling Distortions

The apparent scaling distortion due to no pumped SI in the ROSA test is shown in the comparison of normalized RCS mass response between the US-APWR 7.5-in CLB and ROSA test, in Figure 6.4-20. As might be expected from this scaling analysis result, a significant core uncovery occurred during the boil-off phase of the ROSA/LSTF SB-CL-18 test. In contrast, the HHIS delivers a sufficient amount of safety coolant to the RCS, which prevents the core from experiencing a significant uncovery and heat-up during the boil-off phase of the US-APWR 7.5-in CLB. Consequently, the ROSA test was more severe than the US-APWR 7.5-in CLB, even though the break size of the ROSA test was comparable to the US-APWR 7.5-in break. Considering the differences in HHIS operation between the US-APWR and ROSA test, the apparent differences in the RCS mass responses are easily explained, and are not a critical scaling concern. The lack of pumped ECC flow in ROSA makes the ROSA results conservative relative to the US-APWR.

The US-APWR 1-ft^2 CLB undergoes a slightly larger mass reduction than the ROSA test. This was caused by a larger contribution of break flow rate which is at least partially caused by the use of the Appendix K break flow model in M-RELAP5 which overestimates the mass flow out the break. The effect of this distortion needs to be addressed for evaluating the code applicability to IETs.

The scaling analysis results also show that the pressure response in the ROSA tests is well scalable to the US-APWR 7.5-in CLB, the 1-ft^2 CLB. This indicates that the governing mechanism for the boil-off phase is common between the US-APWR and the ROSA/LSTF, although effects of some local phenomena and processes, such as the break flow rate and the hot wall heat transfer, are being emphasized more in the 1-ft^2 CLB than in the other break sizes. This similarity of pressure behavior is important, since the depressurization rate directly affects the pumped SI flow rate (if available) and the accumulator actuation.

To this end, it is judged that the ROSA/LSTF SB-CL-18 and IB-CL-02 tests are appropriate integral effects tests for assessing code applicability to the US-APWR SBLOCA boil-off phase. Similitude of the test data is quantitatively evaluated as listed in Table 6.4-1 through Table 6.4-4, where no significant scaling distortions are found.

Figure 6.4-24 Comparison of Normalized RCS Mass between M-RELAP5 and Reduced Model for US-APWR 7.5-in CLB Boil-off Phase

Figure 6.4-25 Comparison of Normalized RCS Pressure between M-RELAP5 and Reduced Model for US-APWR 7.5-in CLB Boil-off Phase

Figure 6.4-26 Comparison of Normalized RCS Mass between M-RELAP5 and Reduced Model for US-APWR 1-ft^2 CLB Boil-off Phase

Figure 6.4-27 Comparison of Normalized RCS Pressure between M-RELAP5 and Reduced Model for US-APWR 1-ft^2 CLB Boil-off Phase

Figure 6.4-28 Comparison of Normalized RCS Mass between Measurement and Reduced Model for ROSA/LSTF SB-CL-18 Boil-off Phase

Figure 6.4-29 Comparison of Normalized RCS Pressure between Measurement and Reduced Model for ROSA/LSTF SB-CL-18 Boil-off Phase

Figure 6.4-30 Comparison of Normalized RCS Mass between Measurement and Reduced Model for ROSA/LSTF IB-CL-02 Boil-off Phase

Figure 6.4-31 Comparison of Normalized RCS Pressure between Measurement and Reduced Model for ROSA/LSTF IB-CL-02 Boil-off Phase

6.4.3 Bottom-up Scaling Analysis

During the boil-off phase, CHF/dryout, uncovered heat transfer, and two-phase mixture level are identified as the important phenomena and processes affecting the PCT. These phenomena and processes are localized, and the relevant thermal-hydraulic models and correlations are usually assessed by using the experimental data obtained in the separate effects test (SET) facilities. One approach in evaluating scalability of the SET facility is to define a nondimensional parameter characterizing the thermal-hydraulic phenomena and processes of interest, like the Nusselt number for the heat transfer, which are compared between the experimental and actual plant conditions. In the other approach, the primary geometric dimensions affecting the important phenomena and processes are identified, and similitude of the dimensions is evaluated between the test facility and actual plant. Simultaneously, the primary thermal-hydraulic conditions, including power and pressure are compared between the experimental test and actual plant, and it is confirmed that the experimental conditions reasonably cover the plant conditions. In the present bottom-up scaling evaluation, the latter approach is adopted.

6.4.3.1 CHF/Dryout

The CHF/dryout model in M-RELAP5 has been assessed by using the test data obtained in the ORNL/THTF test facility[6-19]. The THTF is an electrically heated bundle test loop configured to produce conditions similar to those in the representative SBLOCA. The 3.09.10 test series, which was performed to obtain the void profile and uncovered heat transfer data, is selected, because the code ability to predict the dryout region can be validated using the test data. Details of the test facility are described in Reference 6-20.

The THTF test facility was designed to represent 1/4 of the cross section of a 17x17 PWR fuel assembly. Table 6.4-5 identifies the primary geometric dimensions related to the CHF/dryout, and lists their scalability between the ORNL/THTF test facility and US-APWR. As shown in the table, the primary design parameters are also well scaled to the US-APWR fuel design. This is natural because there is no significant scaling distortion between the PWR 17x17 and US-APWR 17x17 fuel assemblies except for the active heated length. The heated length of US-APWR fuel is increased to 14-ft so as to reduce the linear heat generation rate compared with the existing fuel with the12-ft heated fuel length. However, the grid span, which plays an important role in the CHF behavior, is consistent between the US-APWR 14-ft fuel and the existing 12-ft fuel. Therefore, it is judged that CHF/dryout behavior obtained in the ORNL/THTF test facility is applicable to the US-APWR code assessment from the geometric viewpoint.

Table 6.4-6 lists the primary experimental conditions in the ORNL/THTF test. Since the core inlet temperature is saturated and the flow rate is stagnant during the boil-off phase, the pressure range selected for the test is important. Figure 6.4-32 compares the experimental pressure with the range possible during the US-APWR SBLOCAs. The figure contains the experimental data for the ORNL/THTF reflood test and the ROSA/LSTF void profile test, which were used in the M-RELAP5 code assessment. The figure shows the US-APWR SBLOCA conditions are well covered by the experimental pressure range.

Similarly, the experimental power range (linear heat generation rate) is compared with that of the US-APWR SBLOCAs in Figure 6.4-33. In the US-APWR SBLOCAs, the onset of

dryout appears during the loop seal clearance or core recovery phase, specifically 120 to 150 seconds after the reactor scram. The linear heat generation in that time period is around 1kW/m, and well covered by the test conditions selected for the ORNL/THTF test.

As described above, the test facility and experimental conditions are well scalable to the US-APWR SBLOCAs from the viewpoint of the geometric and experimental conditions.

The heat-up observed in the ORNL/THTF was mainly caused by dryout mechanism governed by hydraulic conditions. The applicability of CHF model is considered to be more important during the blowdown phase. The assessment for the CHF model has been performed by using the ROSA/LSTF transient tests and no heat-up was predicted as in the tests during the blowdown phase. In order to ensure the applicability of CHF model in M-RELAP5 to the US-APWR, the comparison of the database range of the CHF model against the flow conditions during the blowdown phase was performed as shown in Figure 6.4-34. The transient conditions during the blowdown phase in the US-APWR are well covered by the database range.

6.4.3.2 Uncovered Heat Transfer

With respect to the uncovered heat transfer, M-RELAP5 has been validated based on the same test data obtained in the ORNL/THTF test facility, as well as done for the CHF/dryout model[6-1]. Therefore, scalability of the test facility and experimental conditions are to be referred to Section 6.4.3.1. Applicability of the uncovered heat transfer model in M-RELAP5 under the transient conditions is to be addressed within the framework for the reflood phase.

6.4.3.3 Two-Phase Mixture Level

Accuracy of the code-calculated two-phase mixture level, which is affected by the void distribution, is primarily dependent on the interfacial shear model implemented in the code. The related model of M-RELAP5 has been validated by using the void profile test obtained in the ROSA/LSTF[6-21] and ORNL/THTF[6-19] test facilities, which were conducted under representative SBLOCA conditions. As for the ORNL/THTF test, the test series of 3.09.10 is selected for the assessment experimental data. Therefore, scalability of the test facility is referred to Section 6.4.3.1.

The ROSA/LSTF test facility is an integral effects test (IET) facility developed to simulate LOCAs and anticipated operational transients in the representative 4-loop PWR. The core consists of 24 fuel assemblies having 7x7 electric heater rods simulating the 17x17 PWR fuel design. In the framework for the natural circulation experiment in the SBLOCAs, the test facility provided the void fraction measurements. The core and fuel bundle geometric dimensions of interest are identified in Table 6.4-7, which are compared with that of US-APWR. As shown in the table, the geometric volume scaling factor of the test facility is **[ ]** to the US-APWR, and there is no significant distortion between the test facility and plant.

The experimental conditions of the ROSA/LSTF test, power and pressure, are also compared with that of US-APWR SBLOCAs in Figure 6.4-32 and Figure 6.4-33, respectively. Although the test data selected from the ROSA/LSTF is limited to a small number, it can be confirmed that the US-APWR SBLOCA conditions are well covered by the combined ROSA/LSTF and ORNL/THTF test data.

Hence, the SET data used in code assessment for the two-phase mixture level are scalable to US-APWR and adequately cover the range of conditions expected in the US-APWR SBLOCAs.

Table 6.4-5 Scaling of ORNL/THTF Test Facility Dimensions to US-APWR

Item	THTF	US-APWR	US-APWR/ THTF
No. of Assemblies per Core	1	257	–
Rod Array per Assembly	8×8	17×17	–
Total No. of Rods per Assembly	64	289	4.52
No. of Heated Rods per Assembly	60	264	4.40
No. of Unheated Rods per Assembly	4	25	6.25
Heated-to-Unheated Rod No. Ratio	15	10.56	0.70
No. of Grid Spacers	6	[ ]	
Active Length (m)	3.66		
Heated Rod Diameter (m)	0.0095	0.0095	1.00
Unheated Rod Diameter (m)	0.0102	0.0097	0.95
Rod Pitch (m)	0.0127	0.0126	0.99
Flow Area per Assembly (m^2)	0.0062	[ ]	
Hydraulic Diameter (m)	0.0106		

Table 6.4-6 ORNL/THTF Uncovered Heat Transfer and Level Swell Test Conditions

Test No.	Power (kW)	Pressure (MPa)	Mass Flux (kg/m^2s)	Inlet Temperature (K)	Outlet Temperature (K)
3.09.10I	487.19	4.50	29.76	473.0	774.1
3.09.10J*	234.82	4.20	12.93	480.3	728.4
3.09.10K*	70.23	4.01	3.13	466.5	935.0
3.09.10L	476.22	7.52	29.11	461.3	715.6
3.09.10M*	223.85	6.96	13.38	474.4	746.5
3.09.10N*	103.14	7.08	4.60	473.1	947.9
3.09.10AA*	278.71	4.04	21.15	450.9	547.0
3.09.10BB*	140.45	3.86	9.44	458.2	540.8
3.09.10CC*	72.42	3.59	7.22	467.6	531.6
3.09.10DD*	283.10	8.09	19.82	453.4	595.4
3.09.10EE*	140.45	7.71	11.00	455.9	581.0
3.09.10FF*	70.23	7.53	4.83	451.4	565.8

* Test selected for M-RELAP5 assessment.

Table 6.4-7 Scaling of ROSA/LSTF Test Facility Dimensions to US-APWR

Item	THTF	US-APWR	US-APWR/ THTF
No. of Assemblies per Core	24	257	–
Rod Array per Assembly	7×7	17×17	–
Total No. of Rods per Core	1168	74273	63.59
No. of Heated Rods per Core	1064	67848	63.77
No. of Unheated Rods per Core	104	6425	61.78
Heated-to-Unheated Rod No. Ratio	10.23	10.56	1.03
No. of Grid Spacers	9	[ ]	
Active Length (m)	3.66		
Heated Rod Diameter (m)	0.0095	0.0095	1.00
Unheated Rod Diameter (m)	0.0122	0.0097	0.79
Rod Pitch (m)	0.0126	0.0126	1.00
Flow Area per Assembly (m^2)	0.0982	[ ]	
Hydraulic Diameter (m)	0.0110		

Table 6.4-8 ROSA/LSTF Void Profile Test Conditions

Test No.	Power (MW)	Heat Flux (kW/m^2)	Pressure (MPa)	Exit Velocity J_g (m/s)
ST-VF-01A*	0.5	4.5	1.0	0.425
ST-VF-01B*	1.0	9.1	1.0	0.851
ST-VF-01C*	2.0	148.2	1.0	1.702
ST-VF-01D*	3.5	31.8	1.0	2.978
ST-NC-08E	1.426	13.0	2.4	0.566
ST-NC-01*	3.57	30.7	7.3	0.553
ST-NC-06E*	3.95	34.0	7.3	0.612
SB-CL-16L*	5.0	43.0	7.3	0.774
ST-SG-04	7.17	61.7	7.35	1.104
ST-VF-01E	1.0	9.1	15.0	0.091
ST-VF-01F	0.5	4.5	15.0	0.045
ST-VF-01G	2.0	18.2	15.0	0.182
ST-VF-01H	4.0	36.3	15.0	0.363
TR-LF-03	0.94	7.2	17.2	0.080

* Test selected for M-RELAP5 assessment.

Figure 6.4-32 Comparison of Pressure Range between ORNL/THTF Test and US-APWR/SBLOCA

Figure 6.4-33 Comparison of Power Range between ORNL/THTF Test and US-APWR/SBLOCA

Figure 6.4-34 Comparison of flow conditions during blowdown phase between the database range of CHF model in M-RELAP5 and the US-APWR/SBLOCA

6.4.4 Summary

The RCS mass and pressure responses during the boil-off phase are important, because they determine the core liquid level depression, the pumped SI flow rate, and the accumulator actuation, which affect the core heat-up behavior. Therefore, similarity of the global responses with respect to the RCS mass and pressure was investigated between the US-APWR SBLOCA and the IETs, ROSA/LSTF SB-CL-18 and IB-CL-02 tests, using the top-down approach. Regarding the local thermal-hydraulic phenomena and processes of interest, the SETs provide a set of experimental data used for the code assessment. In the present study, the ORNL/THTF uncovery heat transfer and two-phase mixture level swell tests, and the ROSA/LSTF void profile test are examined to validate their scalability to the US-APWR based on the bottom-up approach.

The top-down scaling analysis demonstrated that the ROSA/LSTF SB-CL-18 test is well scaled to the US-APWR 7.5-in CLB. The dominant Ψ group is the same between the two systems and the order of ranking of Ψ group is similar. This means that the global processes observed both in the US-APWR SBLOCA and ROSA test are essentially identical. No significant distortions appear in the resultant boil-off behavior between the plant and test facility.

The top-down scaling analysis of the 1-ft^2 break using the ROSA/LSTF IB-CL-02 test showed good agreement of the individual Ψ groups and similar rankings of the Ψ groups for the depressurization equation. The similar rankings for the depressurization equation indicate the same process is dominant in both facilities and that the phenomena interactions are also similar. For the mass conservation equation similar fractions of system mass were lost in both facilities. The mass fraction lost was somewhat larger in the US-APWR response. This larger mass fraction is at least partially caused by the use of the Appendix K break flow model in M-RELAP5 which overestimates the mass flow out the break.

The CHF/dryout, uncovered heat transfer, and two-phase mixture level are identified as the important phenomena and processes during the boil-off phase. In the M-RELAP5 code assessment, the models related to the above phenomena and processes have been validated by using test data obtained in the ORNL/THTF and ROSA/LSTF test facilities. The present study evaluated the geometrical scaling of the test facility to the US-APWR, and showed no significant distortion. Simultaneously, the experimental test conditions, pressure, temperature, flow rate, and power, were compared with those expected under the various US-APWR SBLOCAs, showing that the US-APWR SBLOCAs conditions were well covered by the selected experimental tests.

6.5 Core Recovery

6.5.1 Phenomena and Applied Test Facility

The core recovery phase starts at the end of the boil-off phase, and ends when the fuel cladding is fully quenched and/or when the core is completely recovered. From this definition, the SI flow rate, including the accumulator, exceeds the break flow rate at the beginning of the recovery phase. The vessel mass inventory then increases, and core recovery is established, resulting in rewetting and quench at the dryout portion of fuel cladding. Therefore, the core reflooding and rewetting are important from the viewpoint of the local thermal-hydraulic behavior, whereas the RCS mass response is of interest in investigating the similitude between the plant and test facility.

The 7.5-in CLB is selected as a typical US-APWR SBLOCA. Since the limiting PCT occurs during the core recovery phase in the 1-ft^2 CLB, this case is also of interest in investigating the applicability of the experimental data. The IETs, the ROSA/LSTF SB-CL-18 and IB-CL-02 tests, used for the M-RELAP5 code assessment, are examined in terms of their scalability to these representative US-APWR SBLOCAs selected above.

Test data to address the reflooding processes and rewet phenomena are provided from the ORNL/THTF high-pressure reflood test and the FLECHT-SEASET forced-reflood test. Scalability of these separate effects tests (SETs) is examined based on the bottom-up approach as was done for the boil-off phase.

6.5.2 Top-Down Scaling Analysis

6.5.2.1 Transient Behavior of Interest

As the RCS pressure decreases, the flow rate injected by the HHIS increases, and then the accumulator starts delivering additional safety coolant when the pressure falls below its actuation level. This behavior can be expected both in the US-APWR SBLOCAs and in the ROSA/LSTF SB-CL-18 and IB-CL-02 tests, although the pumped SI was intentionally not functional in the ROSA SB-CL-18 test. After the accumulator starts injecting a large amount of water, some of the steam accumulated in the RCS is condensed, and the core reflooding starts. The coolant entering the core suppresses the fuel cladding temperature excursion, and the hot cladding is rewetted and quenched. Therefore, the RCS mass response is a primary global behavior of interest, which is addressed by the top-down scaling approach. The RCS pressure response is no longer critical after the accumulator starts injecting safety coolant in the scenarios for the US-APWR SBLOCAs.

For the US-APWR 7.5-in CLB, the RCS mass starts recovering just after actuation of the advanced accumulator[6-17]. As shown in Figure 6.4-1, the beginning of the RCS mass recovery is **[ ]** after the break. The core liquid level turns to be minimum at **[ ]** which is defined as the beginning of recovery phase in this study. Then, the RCS pressure is well stabilized and the core is sufficiently recovered at **[ ]**, which is defined as the end of the recovery phase.

For the 1-ft^2 CLB, the accumulator starts injecting safety coolant around **[ ]**, prior to the HHIS, because the RCS pressure rapidly falls to the level at which the

accumulator becomes operable. It should be noted also that the pumped SI flow is delayed due to the loss-of-offsite power assumption. Then, the HHIS begins delivering coolant at about **[ ]**. Although the RCS mass inventory and the downcomer liquid level begin to recover at **[ ]**, the obvious core reflooding starts around **[ ]**, as explained in the end of Section 6.4.2.1. For the present analysis, the start time is the end of boil-off phase when the core liquid level is minimum, **[ ]**. The end time was judged from the core liquid level is almost saturated after the initiation of reflooding, **[ ]**. In the ROSA/LSTF IB-CL-02 test the core recovery started at **[ ]** and the core liquid level was almost saturated at **[ ]**.

The RCS pressure during the core recovery phase is lower in the 1-ft^2 CLB than in the other cases (the 7.5-in CLB and the ROSA/LSTF SB-CL-18). The difference in pressure level will be addressed by the bottom-up approach, and its effect is to be examined in investigating the code scale-up capabilities.

6.5.2.2 Governing Conservation Equations

The transient of interest during the recovery phase is the global mass response. Hence, this response is mathematically expressed by the mass conservation equation for the lumped volume filled with the two-phase mixture as was done for the natural circulation and boil-off phases.

Mass conservation equation:

$$\frac{d\left(\rho_\ell V_\ell + \rho_v V_v\right)}{dt} = \frac{d\rho_m V}{dt} = \dot{m}_{SI} + \dot{m}_{ACC} - \dot{m}_{break} \tag{6.5-1}$$

6.5.2.3 Nondimensional Equations and Groups

Similarly to the boil-off phase, the nondimensional equation and group can be derived as follows.

Nondimensionalized mass equation:

$$\frac{dM^*}{dt^*} = \Psi_{13}\left(\dot{m}^*_{SI} + \dot{m}^*_{ACC} - \dot{m}^*_{break}\right) \tag{6.5-2}$$

where m_{SI}, m_{ACC}, and m_{break} are the SI, accumulator and break flow rates, respectively. The nondimensional group Ψ_{13}, which is defined as the ratio of net mass flow to the reference system mass, is defined by

$$\Psi_{13} = \frac{\dot{m}_0 t_0}{M_0} \tag{6.5-3}$$

The values for the system reference mass are the RCS mass at the beginning of the phase. This makes the value of Ψ_{13} the fraction of system mass added during the phase.

6.5.2.4 Scaling Analysis Results

Table 6.5-1 compares the reference values used in evaluating the nondimensional groups and the resultant nondimensional groups between the US-APWR 7.5-in CLB and ROSA/LSTF SB-CL-18 test. The scaling criteria, ratios of the evaluated nondimensional

groups between the US-APWR 7.5-in CLB and ROSA are listed in Table 6.5-2. Similarly, Table 6.5-3 and Table 6.5-4 compares the ROSA/LSTF IB-CL-02 scaling analysis results with the US-APWR 1-ft^2 CLB results. The reference values for *M* and *P* are defined at the beginning of the core recovery phase. For the other variables, the reference values are extracted from the data around **[ ]**, which are the representative conditions during the period when the core reflooding begins to cool and rewet the hot cladding. Figure 6.5-1 and Figure 6.5-2 give comparisons between the US-APWR SBLOCAs and the ROSA tests.

The global mass responses for the US-APWR 7.5-in CLB and the ROSA/LSTF SB-CL-18 test were similar, as shown in Figure 6.5-1. This can be quantitatively recognized by comparing the values for the nondimensional group Ψ_{13}, and the resultant scaling ratio of **[ ]**. Although the pumped SI was not used for the ROSA test, the accumulator flow rate is the dominant inflow factor during the core recovery phase for both the US-APWR and ROSA, resulting in the small scaling distortion with respect to Ψ_{13}.

As also for the US-APWR 1-ft^2 CLB, the evaluated scaling ratio for Ψ_{13} remains at **[ ]** and the temporal change of mass inventory is very similar between the two systems as shown in Figure 6.5-2.

Table 6.5-1 Comparison of Physical Values and Nondimensional Groups between US-APWR 7.5-in CLB and ROSA/LSTF SB-CL-18 for Core Recovery Phase

Reference Parameters	US-APWR 7.5-in CLB	ROSA/LSTF SB-CL-18	Notes
t_0 (sec)	[	]	Time period
M_0 (kg)			RCS mass at middle period
$\dot{m}_{break,0}$ (kg/s)			Break flow rate at middle period
$\dot{m}_{SI,0}$ (kg/s)			SI flow rate at middle period
$\dot{m}_{ACC,0}$ (kg/s)			
Nondimensional Group			
Ψ_{13}	[	]	

Table 6.5-2 Scaling Criteria between US-APWR 7.5-in CLB and ROSA/LSTF SB-CL-18 for Core Recovery Phase

Scaling Parameters	$\frac{\Psi_{i,ROSA}}{\Psi_{i,US-APWR}}$	Definitions
$\frac{\Psi_{13,ROSA}}{\Psi_{13,US-APWR}}$	[ ]	Ratio of integrated mass flow to reference mass

Table 6.5-3 Comparison of Physical Values and Nondimensional Groups between US-APWR 1-ft^2 CLB and ROSA/LSTF IB-CL-02 for Core Recovery Phase

Reference Parameters	US-APWR 1-ft^2 CLB	ROSA/LSTF IB-CL-02	Notes
t_0 (sec)	[	]	Time period
M_0 (kg)			Initial RCS mass
$\dot{m}_{break,0}$ (kg/s)			Break flow rate averaged in this phase
$\dot{m}_{SI,0}$ (kg/s)			SI flow rate averaged in this phase
$\dot{m}_{ACC,0}$ (kg/s)			ACC flow rate averaged in this phase
Nondimensional Group			
Ψ_{13}	[	]	

Table 6.5-4 Scaling Criteria between US-APWR 1-ft^2 CLB and ROSA/LSTF SB-CL-18 for Core Recovery Phase

Scaling Parameters	$\frac{\Psi_{i,ROSA}}{\Psi_{i,US-APWR}}$	Definitions
$\frac{\Psi_{13,ROSA}}{\Psi_{13,US-APWR}}$	[ ]	Ratio of integrated mass flow to reference mass

Figure 6.5-1 Comparison of Normalized RCS Mass between US-APWR 7.5-in CLB and ROSA/LSTF SB-CL-18 for Core Recovery Phase

Figure 6.5-2 Comparison of Normalized RCS Mass between US-APWR 1-ft^2 CLB and ROSA/LSTF IB-CL-02 for Core Recovery Phase

6.5.2.5 Validation of Scaling Results

The normalized RCS mass response from the reduced model is compared with those of the M-RELAP5 calculations for the US-APWR SBLOCAs and with measured results for the ROSA/LSTF SB-CL-18 and IB-CL-02 tests in Figure 6.5-3 through Figure 6.5-6. These comparisons are necessary to verify the accuracy of the developed reduced models and scaling results addressed in the preceded section.

The reduced models assume that fluid remains at the saturated condition. This simplification is a potential concern because there is a small amount of subcooling in the core inlet liquid during the core recovery phase, particularly for the US-APWR 1-ft^2 CLB as shown in Figure 6.4-16. However, Figure 6.5-3 through Figure 6.5-6 demonstrate that the reduced model applied here is capable of reproducing the references accurately, for the US-APWR 1-ft^2 CLB and the ROSA/LSTF IB-CL-02 test. Therefore, it is judged that the reduced model is applicable to the scaling analysis for the core recovery phase. It is noted the agreement between the nondimensional RCS mass inventory for the measurement and that by the reduced model is reasonable, because the reduced model uses the measured break and SI flow rates to derive the nondimensional value as was done to determine the nondimensional mass based on the measurements.

6.5.2.6 Evaluation for Scaling Distortions

In the US-APWR 7.5 inch break, the core recovery is eventually accomplished by the advanced accumulator in addition to the HHIS, whereas the standard accumulator alone worked for the ROSA/LSTF SB-CL-18 test. The difference in the SI operation conditions was a probable concern inducing a scaling distortion into the RCS mass response. The lack of pumped ECC flow in the ROSA/LSTF SB-CL-18 test makes the test results conservative relative to the US-APWR response. The scaling analysis results, however, quantitatively demonstrate that the RCS mass response of the ROSA/LSTF SB-CL-18 test is scalable to that of the US-APWR 7.5-in CLB SBLOCA, as indicated by the good agreement of the nondimensional group Ψ_{13} between the plant and test.

For the 1-ft^2 break case, a larger ratio of mass inflow against the initial system mass was attained for the US-APWR compared to the ROSA/LSTF. This was mainly caused by the less initial system mass attained by the adoption of Appendix K break flow model in M-RELAP5. As discussed in Section 6.1.3, the break flow model tends to overestimate the break flow rate for this break size and the tendency corresponds to the smaller initial system mass. The larger break flow rate is a result of the Appendix K treatment.

Figure 6.5-3 Comparison of Normalized RCS Mass between M-RELAP5 and Reduced Model for US-APWR 7.5-in CLB Core Recovery Phase

Figure 6.5-4 Comparison of Normalized RCS Mass between M-RELAP5 and Reduced Model for US-APWR 1-ft^2 CLB Core Recovery Phase

Figure 6.5-5 Comparison of Normalized RCS Mass between Measurement and Reduced Model for ROSA/LSTF SB-CL-18 Core Recovery Phase

Figure 6.5-6 Comparison of Normalized RCS Mass between Measurement and Reduced Model for ROSA/LSTF IB-CL-02 Core Recovery Phase

6.5.3 Bottom-up Scaling Analysis

If a significant core uncovery occurs during the boil-off phase, during the core recovery phase, the fuel cladding temperature excursion can be suppressed by increasing the vapor and/or liquid flow entering the core. As the mass of liquid in the core increases, the steam cooled region of the core moves into the film boiling, and then to the transition boiling heat transfer mode, before finally rewetting. From the safety assessment point of view, the reflooding and rewet are the phenomena and processes of interest during the core recovery phase, and scalability of the SETs is examined by the bottom-up approach.

6.5.3.1 Reflood

The reflooding phenomena have been addressed using the IET data obtained in the ROSA/LSTF facility as was done in the top-down scaling. In the M-RELAP5 code assessment, the ability to predict the fuel cladding temperature behavior during the core recovery phase is validated by using SET data obtained from the forced reflooding conditions, specifically the ORNL/THTF high-pressure reflooding test[6-22] and the FLECHT-SEASET forced-reflood test[6-23].

The primary dimensions of the ORNL/THTF test facility are described in Section 6.4.3.1. The FLECHT-SEASET test was conducted to obtain the cladding temperature behavior under low-pressure reflooding conditions. The test section consisted of electric heater rods, which simulated the 17x17 PWR fuel. Table 6.5-5 lists the scaling ratios of the FLECHT-SEASET facility dimensions to US-APWR, and shows the test facility is well scaled to the US-APWR.

Fluid pressure, inlet temperature and velocity vary over a wide range in the SBLOCA conditions, because the onset of reflooding is dependent on the accident scenario, particularly on the break size postulated. The experimental pressure, inlet temperature and velocity are shown in Table 6.5-6 and Table 6.5-7 for the ORNL/THTF and FLECHT-SEASET tests, respectively. The ORNL/THTF test was performed under high-pressure reflood conditions, whereas the FLECHT-SEASET test originally simulated the large break LOCA reflooding under low-pressure conditions. By employing these two tests, the code assessment matrix covers a wide range of reflooding assessment data. Although the experiments mainly correspond to the core recovery phase, the experimental set also covers the state when the significant core uncovery occurs during US-APWR SBLOCAs. As shown in Figure 6.5-7 through Figure 6.5-9, the experimental conditions adequately cover the expected range of US-APWR SBLOCA conditions.

The comparisons described above demonstrate that the experimental data used in the M-RELAP5 code assessment are well scaled and applicable to the US-APWR SBLOCAs.

6.5.3.2 Rewet

Since rewetting occurs during the core reflood, the rewet model implemented in the code is usually assessed by using the reflooding test data as described in the preceding section. Also in the M-RELAP5 assessment, the ORNL/THTF high-pressure reflooding test and the FLECHT-SEASET forced-reflood test are used to validate the code. The maximum cladding temperature is of interest in validating the code capability. The experimental

range for the maximum cladding temperature is up to 1600 °F, which is sufficiently higher than the limiting PCT expected for US-APWR SBLOCAs. Therefore, as concluded in Section 6.5.3.1, these two test facilities provide experimental data that are well scaled to US-APWR SBLOCAs.

Table 6.5-5 Scaling of FLECHT-SEASET Test Facility Dimensions to US-APWR

Item	FLECHT-SEASET	US-APWR	US-APWR/ F-S
No. of Assemblies per Core	1	257	–
Type of Assembly	17x17	17×17	–
Total No. of Rods per Assembly	177	289	1.63
No. of Heated Rods per Assembly	161	264	1.61
No. of Unheated Rods per Assembly	16	25	1.56
Heated-to-Unheated Rod No. Ratio	10.06	10.56	1.05
No. of Grid Spacers	7	[ ]	
Active Length (m)	3.66		
Heated Rod Diameter (m)	0.0095	0.0095	1.00
Unheated Rod Diameter (m)	0.0108	0.0097	0.90
Rod Pitch (m)	0.0126	0.0126	1.00
Flow Area per Assembly (m^2)	0.0156	[ ]	
Hydraulic Diameter (m)	0.0097		

Table 6.5-6 ORNL/THTF High-Pressure Reflood Test Conditions

Test No.	Pressure (MPa)	Initial mass flux (kg/m^2s)	Initial inlet subcooling (K)	Max Initial Temperature (K)	Linear heat power (kW/m)	Flooding velocity (cm/s)
3.09.10O	3.88	25.36	74	1055	2.03	12.2
3.09.10P*	4.28	12.19	65	1089	0.997	9.2
3.09.10Q*	3.95	12.68	66	1027	1.02	5.9
3.09.10R	7.34	27.64	113	1033	2.16	11.7
3.09.10S	7.53	13.82	105	1077	1.38	10.2

* Test selected for M-RELAP5 assessment.

Table 6.5-7 FLECHT-SEASET Forced-Reflood Test Conditions

Test	Pressure (psia)	Inlet Subcooling (F)	Max Initial Temperature (F)	Linear heat power (kW/ft)	Flooding velocity (in/s)
31504	40	144	1507	0.7	0.97
31701	40	141	1640	0.7	6.10
32013	60	141	1555	0.7	1.04

Figure 6.5-7 Comparison of Pressure Range between Reflooding Experiment and US-APWR/SBLOCA

Figure 6.5-8 Comparison of Inlet Temperature Range between Reflooding Experiment and US-APWR/SBLOCA

Figure 6.5-9 Comparison of Inlet Velocity Range between Reflooding Experiment and US-APWR/SBLOCA

6.5.4 Summary

The RCS mass response and the core reflooding behavior are of interest for the core recovery phase. Scalability of the IET data from the ROSA/LSTF SB-CL-18 test was examined using the top-down approach to demonstrate the applicability of the test data to the global behavior of the US-APWR. On the other hand, the local thermal-hydraulic behavior was addressed using the bottom-up approach. In the present analysis, the ORNL/THTF high-pressure reflooding test and FLECHT-SEASET forced-reflooding test provide the data necessary to assess the reflooding and rewetting models implemented in M-RELAP5.

The top-down scaling analysis showed that the ROSA/LSTF SB-CL-18 and IB-CL-02 tests are able to be used as scalable tests with respect to the RCS mass response of the US-APWR SBLOCAs with different break sizes. It is noted that the Appendix K break flow model of M-RELAP5 results in a smaller mass inventory for the US-APWR 1-ft^2 CLB.

In the bottom-up scaling analysis, the present study shows that the primary dimensions of the SET facilities employed here are well scaled to the US-APWR design, and the experimental test conditions adequately cover the range of conditions expected for the US-APWR SBLOCAs.

6.6 References

6-1 Mitsubishi Heavy Industries, Ltd., 'Small Break LOCA Methodology for US-APWR,' MUAP-07013-P (R1),May 2010.

6-2 The ROSA-IV Group, 'ROSA-IV Large Scale Test Facility (LSTF) System Description,' JAERI-M 84-237, January 1985.

6-3 H. Kumamaru et al., 'ROSA-IV/LSTF 5% Cold Leg Break LOCA Experiment Run SB-CL-18 Data Report,' JAERI-M 89-027, March 1989.

6-4 JAEA, "Experimental Report on Simulated Intermediate Break Loss-of-Coolant Accident using ROSA/LSTF," March 2010 (*in Japanese, proprietary*).

6-5 S. Banerjee et al., 'Top-Down Scaling Analyses Methodology for AP600 Integral Tests,' INEL-96/0040, May 1997.

6-7 M. Ishii and I. Kataoka, 'Similarity Analysis and Scaling Criteria for LWRs under Single-Phase and Two-Phase Natural Circulation,' NUREG/CR-3267, March 1983.

6-8 J. N. Reyes, Jr. and L. Hochreiter, 'Scaling Analysis for OSU AP600 Test Facilities (APEX),' Nuclear Engineering and Design, 186, pp53-109 (1998).

6-9 N. Zuber, 'Problems in Modeling of Small Break LOCA,' NUREG-0724, October 1980.

6-10 C.L. Tien & C.P. Liu," Survey on Vertical Two-Phase Countercurrent Flooding," EPRI NP-984, Feb. 1979.

6-11 C. Vallee et al., "Counter-current Flow Limitation Experiments in a Model of the Hot Leg of a Pressurized Water Reactor – Comparison between Low Pressure Air/Water Experiments and High Pressure Steam/Water Experiments," The 13th Int. Topical Meeting on Nuclear Reactor Thermal Hydraulics (NURETH-13), N13P1107, Sep. 2009.

6-12 H. J. Richter, 'Flooding in Tubes and Annuli,' *Int. J. Multiphase Flow*, Vol. 7, No. 6, pp. 647-658, 1981.

6-13 G. B. Wallis, 'One-Dimensional Two-Phase Flow,' McGraw-Hill, 1969.

6-14 Y. Kukita, Y. Anoda, and K. Tasaka, 'Summary of ROSA-IV LSTF First-Phase Test Program – Integral Simulation of PWR Small-Break LOCAs and transients -,' *Nucl. Eng. Design*, Vol. 131, pp 101-111, 1991.

6-15 J. Liebert and R. Emmerling, 'UPTF Experiment Flow Phenomena during Full-scale Loop Seal Clearing of a PWR,' *Nucl. Eng. Design*, 179, pp. 51-64, 1998.

6-16 Mitsubishi Heavy Industries, Ltd., 'Small Break LOCA Sensitivity Analyses for US-APWR,' MUAP-07025-P (R1), May 2010.

6-17 Mitsubishi Heavy Industries, Ltd., 'The Advanced Accumulator,' MUAP-07001-P (R2), September 2008.

6-18 Mitsubishi Heavy Industries, Ltd., Design Control Document for US-APWR Chapter 15,' MUAP-DC015 Revision 2, November 2009.

6-19 T. M. Anklam et al., 'Experimental Investigations of Uncovered-Bundle Heat Transfer and Two-Phase Mixture-Level Swell under High-Pressure Low-Heat-Flux Conditions,' NUREG/CR-2456, ORNL-5848, March 1982.

6-20 D. K. Felde, et al., 'Facility Description – THTF MOD3 ORNL PWR BDHT Separate-Effects Program,' NUREG/CR-2640, ORNL/TM-7842, September 1982.

6-21 Y. Anoda et al., 'Void Fraction Distribution in Rod Bundle under High Pressure Conditions,' HTD-Vol.155, Am. Soc. Mech. Eng., Winter Annual Meeting, Dallas, November 25-30, 1990.

6-22 C. R. Hyman et al., 'Experimental Investigations of Bundle Boiloff and Reflood under High-Pressure Low Heat Flux Conditions,' NUREG/CR-2455, ORNL-5846, 1982.

6-23 M.J. Loftus et al., 'PWR FLECHT-SEASET Unblocked Bundle Forced and Gravity Reflood Task Data Report,' NUREG/CR-1532, WCAP-9699, 1980.

7. CODE SCALE-UP CAPABILITIES

7.1 Reviews for Code Governing Equations and Numerics

The governing equations in M-RELAP5[7-1] are identical to those in RELAP5-3D[7-2], which has been widely verified and validated in its application to the existing light water reactor accident analyses including the PWR loss-of-coolant accidents (LOCAs). The basic field equations for the two-fluid nonequilibrium model in M-RELAP5 and RELAP5-3D consist of two phasic continuity equations, two phasic momentum equations, and two phasic energy equations. The phase change model between the phases is calculated from the interfacial and wall heat and mass transfer models. Combined with the interfacial models, the two-fluid model is able to mechanistically and accurately simulate the complicated two-phase phenomena and processes occurring in each reactor component of the US-APWR., e.g. boiling, condensation, co-current and counter-current flow in the various flow regimes. State relationship equations and constitutive equations make up closure relations for the system of basic field equations. The adequacy of the constitutive models and correlations is discussed in Section 7.2.

The basic numerical approaches to solve the hydrodynamic and other equations for M-RELAP5 are described in Reference 7-2, with some additional detail added in Reference 7-3. However, the fundamental mathematical basis for the hydrodynamic equations is provided in Reference 7-4. As discussed in Sections 8.1 and 8.2 of Reference 7-2, two important numerical approaches are used in the hydrodynamic solution to ensure the accuracy of the time step advancement: time step control and mass/energy error mitigation. Other numeric techniques, as well as a discussion of the mathematical basis for the hydrodynamic partial differential equations are provided in Reference 7-4. The topics included in Reference 7-4 that are not discussed further here are (a) the characteristics of the two-phase flow equations, (b) a detailed discussion of the semi-implicit and nearly implicit time advancement schemes including a discussion of the regions of stability, accuracy, and convergence, (c) truncation and linearization errors, (d) time smoothing, and (e) single to two-phase transitions. The time steps are controlled to ensure the accuracy and stability of the calculations. Several factors are used including the fluid Courant limit, mass error checks, a limit on the extrapolation of state properties in meta-stable regions, phase appearance and disappearance checks, and a limit on the pressure change in a volume where a non-condensable appears.

A review of the code governing equations and numerics for an earlier version of RELAP5 is described in Reference 7-5. The review concluded that the governing equations and numerics were generally applicable for simulating SBLOCAs. M-RELAP5 is based on RELAP5-3D, which has been improved substantially compared to the code version reviewed in Reference 7-5. However, the primary improvements result from the new models and features that have been added to the code, including multi-dimensional hydrodynamic and reactor kinetics models, additional working fluids, new hydrodynamic components such as feedwater heaters and compressors, and code coupling capability. The basic hydrodynamic and point kinetics models have not been changed from those used in the code version described in Reference 7-5. The M-RELAP5 model of the US-APWR does not utilize the new models included in RELAP5-3D. Furthermore, the transient behaviors of interest occurring under the US-APWR SBLOCAs, including local phenomena and processes, are very similar to those in the conventional PWRs. Therefore, the review of the code governing equations and numerics described in Reference 7-5 is

applicable to M-RELAP5.

7.2 Evaluation of Code Model and Correlation Scale-up Capability

In this section, applicability of important closure models and correlations for predicting the US-APWR SBLOCA high-ranked phenomena to the US-APWR SBLOCA analysis are individually assessed. Code models and correlations applicability are assessed through evaluations of: (1) model pedigree, (2) the parameter ranges for which the model was originally developed, over which it is applied in M-RELAP5, over which it has been assessed and those required for the US-APWR SBLOCA analysis, (3) the fidelity with which the code model or correlation can replicate appropriate experimental data, and (4) the scalability of the model to US-APWR plant geometry and SBLOCA conditions. Seventeen phenomena are selected as high-ranked phenomena for the US-APWR SBLOCA analysis. Code models or correlations are not required to predict some phenomena like fuel rod local power or three-dimensional core power distribution. Some phenomena, like water level in SG outlet piping and loop seal formation and clearance, are complex behaviors related to interactions between systems, processes and various parameters, and are more appropriately assessed through integral code assessment rather than individual code model and correlation assessment. The phenomena finally selected for the assessment of code models and correlations in this section are eight as listed with underline in Table 7.2-1.

Table 7.2-1 Assessment Basis in Examination for Code Scale-up Capabilities

Model/Correlation	Assessment Basis	Scaling Examination
Fuel Rod		
Decay Heat	-	Described in Section 7.2.1
Local Power	-	Conservative assumption
Core		
CHF/Dryout	SET	Described in Section 7.2.2
Uncovered Heat Transfer	SET	Described in Section 7.2.3
Rewet	SET	Described in Section 7.2.4
Mixture Level	SET	Described in Section 7.2.5
3-D Power Distribution	-	Conservative assumption
Steam Generator		
CCFL in SG Inlet	SET	Described in Section 7.2.6
CCFL in SG U-Tubes	SET	Described in Section 7.2.6
Primary Side Heat Transfer	IET	Described in Section 7.2.7
Secondary Side Heat Transfer	IET	Described in Section 7.2.7
Crossover Leg		
Water Level	SET/IET	Examined in Section 7.3
Loop Seal Formation and Clearance	IET	Examined in Section 7.3
Downcomer		
Mixture Level/Void Distribution	IET	Examined in Section 7.3
DVI/SI Water Flow rate	-	Conservative assumption
Break		
Critical Flow	SET	Described in 7.2.8
Break Flow Enthalpy	SET	Described in 7.2.8

7.2.1 Decay Heat

7.2.1.1 Fission Product Decay Heat

Fission product decay heat is evaluated with the ANS standard 1971 plus 20% uncertainty required by Appendix K[7-6]. The ANS standard 1971 was based on the curve recommended by K. Shure for infinite irradiation of uranium fuel. Though the ANS standard 1971 ignores individual factors which affect the fission product decay heat, the uncertainty factor of 20% conservatively envelopes these effects. Then, its applicability to US-APWR SBLOCA analyses is obvious.

Fission product decay heat is evaluated as part of the point kinetics model in M-RELAP5, which allows energy yields and decay constants for groups of fission products. Energy yields and decay constants of 11 groups were obtained by fitting the ANS standard 1971 curve with 20% uncertainty. The comparison of the ANS standard 1971 with the resulting M-RELAP5 decay heat model is shown in the topical report of SBLOCA methodology for US-APWR[7-1].

The fission product decay heat model was developed for uranium-fueled thermal reactors. Therefore, its scaling is not a concern.

7.2.1.2 Actinide Decay Heat

Actinide decay heat of ^{239}U and ^{239}Np produced from neutron capture by ^{238}U is considered in M-RELAP5. The released energy from the decay and the decay constant of the actinides shown in the ANS/ANSI 5.1-1979 standard as the default values, which are accepted in NUREG-0800[7-7], are used in US-APWR analyses. The yield of ^{239}U produced per a nuclear fission (a conversion factor) is required to obtain the actinide decay heat. The value of 1.0 is used in US-APWR SBLOCA analyses. This value is sufficiently conservative for the fuel type and burn up considered in the US-APWR nuclear design.

The actinide decay heat model was also developed for uranium-fueled thermal reactors. Therefore, its scaling is not a concern.

7.2.2 CHF

The 1986 AECL-UO CHF lookup table[7-8] is used in M-RELAP5. This lookup table was developed from the wide range of the tube data, and was compared with the CHF data in INEL bank under “Critical Heat Flux”[7-9].

Geometrical scaling is primarily accounted for by selection of an appropriate diameter, and so on in the lookup table. The lookup table was assessed in the range of tube diameter from 0.001 to 0.0375 m which covers the US-APWR fuel assembly hydraulic diameter of 0.011m. The lookup table was developed for a wide range of pressure (0.1 to 20 MPa), mass flux (0.0 to 7500 kg/m^2-s), and equilibrium quality (-0.5 to 1.0) that exceeds the range needed for SBLOCA analyses of the US-APWR. The range of pressure and mass flux in SBLOCA analyses of the US-APWR is described in Section 6.4.3 of this report.

The 1986 AECL-UO CHF lookup table can be adequately applied to the bundle geometry

using the bundle factor. The CHF lookup table including the bundle factor is validated by the ORNL/THTF Uncovered-Bundle Heat Transfer Tests, which simulate the rod diameter and the rod pitch of the US-APWR fuel assembly. The scalabilities in terms of the facility dimensions and experimental conditions are examined in Section 6.4.3.1, and no scaling concern is identified.

As the applicable ranges of geometrical parameter and coolant conditions of the CHF lookup table cover those of the US-APWR, and the CHF lookup table is also assessed against the ORNL/THTF tests, which simulate the US-APWR fuel assembly geometry, it can be applied to US-APWR SBLOCA analyses.

7.2.3 Uncovered Heat Transfer

Heat transfer by the transition boiling, the film boiling and the vapor convection regimes occurs in order above the core mixture level during the core boil-off phase. The dominant heat transfer mechanism for fuel rod temperature transients during SBLOCAs is due to vapor convection heat transfer. The modified Dougall-Rohsenow correlation[7-10] is used for two-phase conditions and the Dittus-Boelter correlation[7-11] is used for single-phase vapor conditions in M-RELAP5. The Dittus-Boelter correlation was developed from tube heat transfer data in turbulent conditions. Vapor velocity obtained with a homogeneous two-phase flow assumption is used in the modified Dougall-Rohsenow correlation. Then, the modified Dougall-Rohsenow correlation is an expanded correlation of the Dittus-Boelter correlation to the two-phase conditions. In the modified Dougall-Rohsenow correlation, the physical properties of vapor are evaluated at the film temperature rather than the bulk temperature. And the vapor temperature from a non-equilibrium model, rather than the saturated temperature, is used to evaluate wall heat flux in M-RELAP5. These treatments give smaller heat transfer than expected as described in the topical report of SBLOCA methodology for US-APWR[7-1].

Geometrical scaling is accounted for by a tube diameter in these correlations. The value of the constant 0.023 was found by McAdams[7-12] from the experimental data of a wide range of tube diameter which covers the US-APWR fuel assembly hydraulic diameter. As the modified Dougall-Rohsenow is theoretically introduced from the Dittus-Boelter correlation, its applicable range of diameter is same as the Dittus-Boelter correlation and then it can be applied to US-APWR fuel assembly.

The constant C of the Dittus-Boelter correlation for a bundle is given by Weisman with

$$C = 0.042(s/D) - 0.024$$

where s is a tube pitch and D is a tube diameter.[7-13] The constant for the US-APWR fuel assembly is 0.032, and is greater than the value of 0.023 for a tube. Then, the Dittus-Boelter correlation using the value of 0.023 for M-RELAP5 can be conservatively applied to the US-APWR fuel assembly.

The applicability of the Dittus-Boelter and the modified Dougall-Rohsenow correlations to the US-APWR core boil-off transients is assessed against the ORNL/THTF Uncovered-Bundle Heat Transfer Tests, which simulate the rod diameter and the rod pitch of the US-APWR fuel assembly. The scalabilities in terms of the facility dimensions and experimental conditions are examined in Section 6.4.3.1, and no scaling concern is

identified.

As the applicable range of geometrical parameter of the Dittus-Boelter and the modified Dougall-Rohsenow correlations covers those of US-APWR, and these correlations are assessed against the ORNL/THTF tests, which simulate the US-APWR fuel assembly, they can be applied to US-APWR SBLOCA analyses.

7.2.4 Rewet

The cladding temperature decreases as the core mixture level increases and finally rewets during the core recovery phase. Dominant heat transfer in this phase is due to film boiling heat transfer at low void conditions and the transition boiling heat transfer above the core mixture level. The reflood model[7-3], which considers enhanced cooling above the quench front and axial heat conduction in the heater rod, is not applied to the US-APWR SBLOCA analysis. This approach is conservative.

The conduction heat transfer through vapor film, the convection heat transfer to vapor and the radiation heat transfer to droplets and vapor are considered in the film boiling heat transfer. A dominant heat transfer mechanism for the rewet phenomenon is the conduction heat transfer through vapor film by the Bromley correlation[7-14]. Minimum critical wave length, rather than tube diameter, is used as the length term of the Bromley correlation in M-RELAP5. As the minimum critical wave length depends on fluid properties, the correlation is therefore independent of geometrical scale and can be applied to the US-APWR fuel assembly.

The Chen correlation[7-15], which is assessed using tube data, is used for the transition boiling heat transfer. The geometrical scaling parameter of the Chen correlation is a tube diameter. The correlation is assessed in the range of tube diameter from 0.00488 to 0.02 m, which covers the US-APWR fuel assembly hydraulic diameter of 0.011m. The heat flux by contact between the liquid and wall is evaluated by a complex three step model in the original Chen correlation. This heat flux is replaced by the critical heat flux calculated with the 1986 AECL-UO CHF lookup table in M-RELAP5 to simplify the computational process. This modification under-predicts especially the low quality data, which are typical of the rewet phenomena as described in the topical report of SBLOCA methodology for US-APWR[7-1]. Then the transition boiling heat transfer correlation can be conservatively applied to the rewet phenomenon.

The applicability of the film boiling and transition boiling correlations to the US-APWR rewet phenomena is assessed against the ORNL/THTF High-Pressure Reflood Tests[7-16], which simulate the rod diameter and the rod pitch of the US-APWR fuel assembly. In addition, the code assessment has been expanded to the lower pressure range by using the test data obtained in the FLECHT-SEASET test facility[7-17]. Scalabilities of these SET facilities are examined in Section 6.5.3.1. M-RELAP5 conservatively predicts the rewet time. Therefore, the heat transfer model related to the rewet phenomena can be conservatively applied to US-APWR SBLOCA analyses.

7.2.5 Core Mixture Level

The two-phase mixture level swell can be related to the void profile below the two-phase

mixture level. Prediction of the void profile is strongly dependent on the accuracy of the liquid-vapor interfacial shear model implemented in the code, and M-RELAP5 employs the Chexal-Lellouche model[7-18] for the rod bundle geometry in the core. The original correlation was developed for the drift-flux void model, and the interfacial shear is correlated with the drift-flux parameters in its implementation in RELAP5-3D and M-RELAP5 which employ the two-fluid non-equilibrium boiling model[7-2].

The accuracy of the Chexal-Lellouch correlation has been verified and validated by using a wide range of void measurement data[7-18]. In addition, the applicability to the US-APWR SBLOCAs is demonstrated by using the ROSA/LSTF and ORNL/THTF void measurements in the framework of M-RELAP5 code assessment[7-1]. Scalability of the facility dimensions and experimental conditions to the US-APWR is examined in Section 6.4.3.3, where no scaling concern is identified.

The M-RELAP5 assessments using the ROSA/LSTF and ORNL/THTF test data demonstrated that the code is capable of reproducing the void distribution accurately. M-RELAP5 tends to predict the two-phase mixture level slightly lower than the measurements as shown in Figure 8.1.2-30 of the topical report[7-1]. In addition, an even more conservative prediction is being recognized in the sensitivity calculation where the heater rod power is multiplied by 1.2 as required by Appendix K (Figure 8.1.2-32[7-1]).

Through the above investigation, it is judged that the M-RELAP5 two-phase mixture model is applicable to the US-APWR SBLOCA analyses without any scaling concern.

7.2.6 CCFL

The CCFL phenomena strongly depend on the geometry, like the flow path diameter, orientation, end effects and so on. The CCFL model in M-RELAP5 can apply to various geometries by adjusting several parameters in the model to fit specified geometries.

In SBLOCAs, the most important locations for CCFL are the SG U-tubes uphill side and the hot leg because water accumulation in these locations acts to depress the core liquid level during the loop seal period. The geometry of SG U-tubes is characterized by a small diameter vertical pipe without end effects and that of hot leg is characterized by a large diameter horizontal pipe connected to an inclined riser. In the US-APWR analyses, the Wallis J*-type correlation is applied to the bottom of SG U-tubes and the Kutateladze Ku*-type correlation is applied to the junction between SG inlet plenum and riser of hot leg.

The J* correlation is based on the study by Wallis[7-19] and the applicability was assessed using the Dukler Air-Water test reported in Reference 7-1. The scaling discussion between the Dukler test and the US-APWR is given in Section 6.3.3. In that section, the scalability of the J* correlation was confirmed for the effects on the flow path diameter, the flow path length, the fluid combination and the pressure.

The Ku* correlation was derived from the UPTF data (flow path diameter: 0.75m) as reported in Ref. 7-1. Since the Ku number is not dependent on the flow path diameter, the adaptability of the UPTF correlation to the US-APWR (0.787m) is considered to be high as already discussed in Section 6.3.3. As for the pressure scaling, there is an uncertainty in the scalability of UPTF to the US-APWR because the UPTF test was performed at 15 bar

or less and the loop seal period of US-APWR occurs at about 90bar.

The effect of pressure was recently reported in NURETH-13 by the Dresden group[7-20]. The hot leg geometry of the Dresden group is simulated using a rectangular duct of 5 cm in width and 25 cm in height and high-pressure steam-water experiments were conducted at 15 bar, 30 bar and 50 bar. The CCFL data under different pressures were correlated reasonably well with Ku. However, it is recognized that the Ku for water down-flow rate at a steam flow rate tends to be larger with pressure. This tendency means that the UPTF correlation derived at 15 bar or less gives conservative results under higher pressure because more water accumulates around the SG inlet plenum when using the UPTF correlation than would be expected. The additional water accumulation reduces the liquid level in the core during the loop seal period, which increases the likelihood of a core dryout.

Since the CCFL correlation strongly depends on the flow-path geometry, the Ku relationship by the Dresden group using the rectangular geometry cannot apply directly to the US-APWR. However, the qualitative tendency of the pressure on the liquid down-flow is considered to be relevant to the US-APWR. Therefore, the use of the CCFL correlation derived from the UPTF data is considered to be conservative in the M-RELAP5 SBLOCA analyses.

7.2.7 Steam Generator Heat Transfer

The SG heat transfer model was not validated using the SET data, but was examined in the code assessment using the IET data from the ROSA/LSTF, LOFT and Semiscale test facilities. The code assessment results are reported in Reference 7-1.

For example, dynamic behaviors in terms of the SG secondary side pressures, primary system pressure are compared between calculations and measurements as shown in Figures 8.2.1-83, -84, and -82 of Reference 7-1. The results show that the model mechanistically simulating the SG secondary system is able to reproduce the measured SG secondary side pressures with reasonable accuracy. The predicted integral of SG outlet steam mass agrees with the measurement within 10% as shown in Figure 8.2.1-99 of Reference 7-1. Furthermore, the calculated core differential pressure is conservative in comparison with the measurement (Figure 8.2.1-92 of Reference 7-1). Similar code accuracy was confirmed against the other tests, SB-CL-09 (10% break) and IB-CL-02 (17% break), obtained in ROSA/LSTF, and also against LOFT L3-1 (2.5% break) and Semiscale S-LH-1 tests. There is no significant dependency on the break size and on the test facility in terms of the code predictability.

Referring to Section 5.1 of the present report, the SG heat transfer is identified as an important phenomenon and process from the blowdown to loop seal clearance phases. Top-down scaling analysis results in Sections 6.1 to 6.3 indicate that there is no significant scaling distortion due to the SG heat transfer between the US-APWR SBLOCA and ROSA/LSTF SB-CL-18 test.

7.2.8 Break Flow

7.2.8.1 Critical Flow

Appendix K requires that the Moody break flow model be used. Therefore, a demonstration of the capability of the Moody model to represent the effects of scale is not required. However, its applicability to the various small break tests is assessed using IET data in the M-RELAP5 topical report[7-1], where the model appropriately or conservatively predicts the break flow rate compared with the measurements obtained in the different test facilities. The Moody critical flow model was developed for two-phase conditions upstream of the break and is not applicable for subcooled conditions. M-RELAP5 uses the Henry-Fauske model to calculate critical flow for subcooled conditions. M-RELAP5 also uses the Henry-Fauske model to calculate critical flow for superheated conditions upstream of the break. Section 7.1.6 of the topical report[7-1] gives the method to combine the Moody critical flow model with the Henry-Fauske, and the implementation into M-RELAP5 is verified in Appendix C of the same topical report.

The Henry-Fauske critical flow model and its implementation into RELAP5 are described in Reference 7-3. The capability of the Henry-Fauske critical flow model to represent the effects of scale was studied extensively in an earlier version of RELAP5 as described in Reference 7-5. The critical flow results summarized in the references are still applicable to M-RELAP5 as long as it can be shown that the implementation of the Moody model has not affected the results from the Henry-Fauske model. The assessment of the Henry-Fauske model is described in the section 7.6.5 of the Models and Correlation manual of M-RELAP5[7-21].

7.2.8.2 Break Flow Enthalpy

Chapter 15.6.5 of the standard review plan (SRP) requires sensitivity calculations with respect to the effect of break orientation (circumferential location of piping, top, side, or bottom) in the spectrum analysis determining the limiting SBLOCA consequence. This requirement arises because the steam quality of the break flow affects the mass and energy removed from the RCS and because the steam quality depends on the break orientation during stratified flow in horizontal piping with the break. This phenomenon is explicitly modeled by using the offtake/pullthrough model in M-RELAP5, which is identical to that in RELAP5-3D[7-3].

The offtake/pullthrough model has been developed based on the experimental database obtained in different scaled facilities with different fluid conditions[7-22,7-23,7-24,7-25]. The experiments cover a range of diameter of the main horizontal pipe, of operating pressure, and of offtake diameter and orientation. There are no scale effects observed in the data due to the ratio of the diameters of the offtake and the main pipe. In addition, the offtake/pullthrough model has been also validated by applying to the LOFT LP-SB-02 test analysis, which simulated a break of 29.4-mm diameter in the hot leg piping (286-mm diameter) in Reference 7-3.

Independent from the verifications and validations performed for the model development, M-RELAP5 with the offtake/pullthrough model has been assessed using the small break test data obtained in ROSA/LSTF, LOFT, and Semiscale facilities. ROSA test, in particular,

simulated the side-orientation break (SB-CL-18 and SB-CL-09) and the top-orientation break (IB-CL-02). Although the break sizes are different among the tests, the code assessment results show that M-RELAP5 is able to predict the break flow rate appropriately or conservatively. It is noted that M-RELAP5 tends to predict the primary system depressurization faster than the measurement following the loop seal clearance. This indicates there is a possibility that the code tends to estimate discharge flow enthalpy higher than the measurement. However, the resultant PCTs predicted by M-RELAP5 are conservative.

In its application to the safety analysis, the spectrum analysis for the break orientation is performed to determine the limiting accident case as well as for the break size. Therefore, uncertainty due to the break flow enthalpy can be excluded from the safety analysis results.

7.3 Evaluation of Integrated Code Scale-up Capability

M-RELAP5's capability to analyze the SBLOCA behavior was confirmed by the validation analyses with the IETs and SETs focused on the models related to the important phenomena identified in the PIRT. M-RELAP5 was also assessed by the comparison with the ROSA/LSFT SBLOCA integral tests (SB-CL-18 and IB-CL-02) for confirmation of the integral system behavior. The top-down and bottom-up scaling analyses for test facilities performed in the previous section assure that the important phenomena or processes in the integral and separate effects tests are appropriately scaled to US-APWR SBLOCA behavior. Therefore, it can be concluded that M-RELAP5 has scale-up capability to US-APWR and can be applied to US-APWR SBLOCA analyses.

In this section, M-RELAP5 scale-up capability to US-APWR is assessed with a different approach. In this assessment, the nondimensional reduced equations developed in the top-down scaling analysis for test facilities are used. Each nondimensional reduced equation is a governing equation for important transient behaviors developed based on conservation laws and first principles. It is validated against scaled IET data. By assessing the applicability of an actual plant calculation results to the nondimensional reduced equation, it can be confirmed that important phenomena and processes considered in the nondimensional reduced equation are reproduced in the actual plant calculation and that the code has a scale-up capability to the plant. This assessment study is performed using US-APWR SBLOCA calculation results obtained by M-RELAP5, and scale-up capability of M-RELAP5 to US-APWR is confirmed.

7.3.1 Blowdown

The RCS depressurization initiated by the break is a dominant global phenomenon during the blowdown phase. The RCS depressurization can be represented using the mass and energy equations which accounts for the system behavior by macroscopically dividing the RCS into the subcooled and saturated regions. The nondimensional reduced equation derived from the above equations can be used to assess a scale-up capability of M-RELAP5 to US-APWR during the blowdown phase.

The comparison between the integrals of the left hand side (LHS) and the right hand side (RHS) of equation ((6.1-9)) using the experimental data of ROSA/LSTF (SB-CL-18) is shown in Figure 7.3-1. As the plot of the both side values obtained from the experimental data agrees reasonably well with the line of the theoretical equation with 45 degree slope, it is concluded that the nondimensional reduced equation adequately reproduces the RCS pressure behavior. The comparison between the LHS values and RHS values using the calculation results by M-RELAP5 for the ROSA experiment analysis and US-APWR 7.5-in cold leg break (CLB) analysis are also shown in Figure 7.3-1. Both plots of the calculation results agree reasonably well with the theoretical equation. From these comparisons, it is concluded that the important phenomena considered in the nondimensional reduced equation are reproduced in the US-APWR calculation as well as in the ROSA calculation.

Similarly, the plots for the ROSA/LSTF IB-CL-02 and US-APWR 1-ft^2 CLB are shown in Figure 7.3-2 and a reasonable agreement is also confirmed for the relatively large break case. The plots for the ROSA experimental data, in particular, deviate from the theoretical equation. This probably is caused by an uncertainty in the measured break flow rate which

was experimentally determined from the liquid level change in the blowdown storage tank downstream of the break unit. As shown in Figure 6.1-4 (SB-CL-18) and Figure 6.1-12 (IB-CL-02), a time delay and oscillatory behavior are observed in the measured break flow rate.

The same comparisons for the RCS inventory, based on the nondimensional reduced equation (6.1-8) are shown for the ROSA/LSTF SB-CL-18 and IB-CL-02 in Figure 7.3-3 and Figure 7.3-4, respectively. The plots of the corresponding US-APWR SBLOCA case are compared with the experimental case in each figure. All plots agree reasonably well with the theoretical equation. Therefore, it is concluded that the nondimensional reduced equation adequately reproduces the RCS inventory behavior and the important phenomena related to the RCS inventory considered in the nondimensional reduced equation are reproduced in the US-APWR calculation as well as in the ROSA calculation.

Regression coefficients and correlation coefficients for linear regression equations between the RHS values and LHS values of each comparison are shown in Table 7.3-1 for the smaller break case and in Table 7.3-2 for the larger break case, respectively. The maximum uncertainty of the regression coefficient (slope) due to approximation of the nondimensional reduced equation and imperfect instrumentation was estimated to be -40% to +65% in the evaluation of RELAP5/MOD3 for simulating AP600 SBLOCA analysis[7-5]. As the nondimensional reduced equations with the first order approximation which consider only the most important term and neglects the other terms are used in the evaluation for AP600, the uncertainty of the regression coefficient is considered to be large compared with of the nondimensional reduced equations used in this study which consider all terms. Therefore, the allowable limit of the regression coefficient error is set to be -20% to +30% in this study. The US-APWR calculation results for the RCS pressure and inventory satisfy this criterion.

As discussed above, the nondimensional parameters derived from the experimental data and/or the M-RELAP5 calculations behave similarly between the tests and US-APWR SBLOCAs. The important transients considered in the nondimensional reduced equation can be reproduced in the US-APWR calculate on as well as in the ROSA calculation. The nondimensional parameters from the experimental data, ROSA M-RELAP5 calculation, and US-APWR SBLOCA M-RELAP5 calculation, acceptably agree with those by the theoretical equations. Therefore, it is concluded that M-RELAP5 has a scale-up capability to US-APWR during the blowdown phase.

7.3.2 Natural Circulation

The RCS pressure remains almost constant during the natural circulation phase because the SG secondary acts as an effective heat sink for removal of core decay heat, while the energy outflow from the break is restricted because of the low quality break flow. Therefore, the dominant parameter during this phase is the RCS inventory. A scale-up capability of M-RELAP5 to US-APWR during the natural circulation phase is assessed using the nondimensional reduced equation (6.2-8) for the RCS inventory. It is noted that an idealized natural circulation period does not appear in the larger break cases such as in the ROSA/LSTF IB-CL-02 test as discussed in Section 6.2.2.1.

The comparisons between the integrals of the LHS and the RHS values of equation (6.2-8) using the ROSA SB-CL-18 experimental data, ROSA M-RELAP5 calculation result

and US-APWR M-RELAP5 calculation result are shown in Figure 7.3-5. All plots agree with the line of the theoretical equation with 45 degree slope. Also the deviation of the regression coefficient of every comparison from the theoretical equation is less than 1% as shown in Table 7.3-1. The reason for the favorable agreement of the ROSA experimental data with the theoretical equation is as follows. Though the LHS value of the RCS inventory ought to be calculated based on the measured differential pressure in the individual components, the LHS value is calculated extracting the break flow rate which is used to calculate the RHS value from the initial RCS inventory in the present calculation. And the reason for the favorable agreement of M-RELAP5 calculation result with the theoretical equation is that the RCS inventory depends on only the break flow rate and this obvious relation between the RCS inventory and the break flow rate is not affected by scaling of the system. The scale-up capability of M-RELAP5 during the natural circulation phase is dependent on the scale-up capability of the break flow model, and its scale-up capability to US-APWR is already discussed in Section 7.2.

It is concluded that M-RELAP5 has a scale-up capability to US-APWR during the natural circulation phase, because the important transients considered in the nondimensional reduced equation are reproduced in the US-APWR calculation as well as in the ROSA calculation and the applicability of the break flow model to US-APWR is confirmed.

7.3.3 Loop Seal Clearance

The RCS pressure remains almost constant during the loop seal clearance phase similar to the natural circulation phase discussed previously. As the liquid is distributed around the RCS, including some upper regions such as the U-tubes, during the loop seal clearance phase, the core cooling condition can not be judged directly from the RCS inventory. Therefore, an important parameter during the loop seal clearance phase is the core collapsed water level as well as the RCS mass inventory. A scale-up capability of M-RELAP5 to US-APWR during the loop seal clearance phase is assessed using the nondimensional reduced equation (6.3-12) for the core and upper plenum collapsed water level. Figure 6.3-7 shows the applicability of M-RELAP5 to the measurement and Figure 6.3-15 shows the validity of the reduced equation comparing the measurement. M-RELAP5 corresponds well to the reduced equation because both comparisons in Figure 6.3-7 and Figure 6.3-15 indicate reasonable agreements each other.

The comparisons for the RCS mass inventory between the integrals of the LHS and the RHS of equation (6.3-13) using the ROSA experimental data, ROSA M-RELAP5 calculation result and US-APWR M-RELAP5 calculation result are shown in Figure 7.3-6. Every plot agrees well with the line of the theoretical equation with 45 degree slope. Also the deviation of the regression coefficient from the theoretical equation is small as shown in Table 7.3-1.

It is concluded that M-RELAP5 has a scale-up capability to US-APWR during the loop seal clearance phase because the important transients considered in the nondimensional reduced equation are reproduced in the US-APWR calculation as well as in the ROSA calculation and the applicability of the break flow model and the CCFL model to the US-APWR is confirmed.

7.3.4 Boil-Off

The dominant parameters during the boil-off phase are the core collapsed water level, which affects the core heat-up behavior and the RCS pressure, which affects the ECCS flow rate and the core heat transfer. The core collapsed water level is well correlated with the RCS inventory during the boil-off phase, because almost all the liquid is in the reactor vessel and the liquid accumulates in the lower part of the reactor vessel due to the gravity. Therefore, a scale-up capability of M-RELAP5 to US-APWR during the boil-off phase is assessed using the nondimensional reduced equation (6.4-8) for the RCS inventory and equation (6.4-9) for the RCS pressure.

In Section 6.4.2, two representative limiting cases are investigated for US-APWR SBLOCAs, 7.5-in and 1-ft^2 CLB cases, in examining the scalability of ROSA/LSTF SB-CL-18 and IB-CL-02. The top-down scaling results quantitatively demonstrated that the ROSA tests are individually scalable to the corresponding case from the viewpoint of the global RCS inventory and pressure change.

The comparisons between the integrals of the LHS and the RHS of the RCS inventory equation (6.4-8) using the ROSA experimental data, ROSA M-RELAP5 calculation result and US-APWR M-RELAP5 calculation result are shown in Figure 7.3-7 for the smaller break case and in Figure 7.3-8 for the larger break case, respectively. All plots agree with the line of the theoretical equation with 45 degree slope. And also the deviation of the regression coefficient of every comparison from the theoretical equation is less than 1% as shown in Table 7.3-1. The reason for the favorable agreement with the theoretical equation is described in the previous section for the natural circulation. The RCS inventory during the boil-off phase is dependent on only the break flow rate and the SI flow rate, and this direct relation between the RCS inventory and the break flow rate and the SI flow is not affected by scaling of the system. Therefore, the scale-up capability of M-RELAP5 during the boil-off phase is dependent on the scale-up capability of the break flow model, and its scale-up capability to US-APWR is already confirmed.

The same comparisons for the RCS pressure, based in reduced equation (6.4-9), are shown in Figure 7.3-9 for the smaller break case and in Figure 7.3-10 for the larger break case. All plots agree reasonably well with the theoretical equation. Also the deviations of the regression coefficient from the theoretical equation are within the allowable error band as shown in Table 7.3-1 for the smaller break case and in Table 7.3-2 for the larger break case. This indicates that the energy and mass balances and responses are similar between the US-APWR SBLOCA and ROSA test, and that M-RELAP5 is able to accurately predict the US-APWR SBLOCAs with various break sizes.

It is concluded that M-RELAP5 has a scale-up capability to US-APWR during the boil-off phase because the important phenomena during the boil-off phase considered in the nondimensional reduced equation are reproduced in the US-APWR calculation.

7.3.5 Core Recovery

The dominant parameters during the core recovery phase are the RCS inventory and the RCS pressure, which are same as during the boil-off phase. However, the RCS pressure is no longer of interest from the safety assessment point of view, since the accumulator is already injecting safety coolant during this phase in the US-APWR SBLOCAs. Therefore,

a scale-up capability of M-RELAP5 to US-APWR during the core recovery phase addresses the transient behavior of RCS inventory using the nondimensional reduced equation (6.5-2) in the present section.

Similar to the boil-off phase, the top-down scaling analysis in Section 6.5.2 addresses both the 7.5-in and 1-ft^2 CLB cases in examining the scalability of ROSA/LSTF SB-CL-18 and IB-CL-02 tests, respectively. The transient of interest is limited to the RCS inventory transient for the core recovery phase, which is dominated by the mass balance consisting of the SI and break flow rates from the global point of view.

The comparisons for the RCS inventory are shown in Figure 7.3-11 for the smaller break and in Figure 7.3-12 for the larger break, respectively. All plots agree with the line of the theoretical equation with 45 degree slope. And also the deviation of the regression coefficient of every comparison from the theoretical equation is within 5% as shown in Table 7.3-1 for the smaller break and in Table 7.3-2 for the larger break.

It is concluded that M-RELAP5 has a scale-up capability to US-APWR during the core recovery phase because the important phenomena during the core recovery phase considered in the nondimensional reduced equation are reproduced in the US-APWR calculation.

7.3.6 Summary

M-RELAP5 scale-up capability to US-APWR SBLOCA analysis is assessed using the nondimensional reduced equations developed in the top-down scaling analysis for test facilities. The primary nondimensional parameters obtained from the experimental data and/or M-RELAP5 calculations behave similarly between the ROSA test and US-APWR SBLOCA. This indicates that the important transient responses can be appropriately reproduced by the nondimensional reduced equations, and that the responses are similar between the test and US-APWR SBLOCA. As for the primary nondimensional parameters, the deviations from the theoretical equation were quantitatively evaluated, and the agreements are reasonably acceptable for the ROSA experiment data, ROSA M-RELAP5 calculation, and US-APWR SBLOCA M-RELAP5 calculation, throughout the SBLOCA transient. In conclusion, M-RELAP5 has a scale-up capability to US-APWR SBLOCA analysis.

Table 7.3-1 Quantitative Evaluation of Agreement with the Nondimensional Regression Equation for 7.5-in CLB case

Phase	Parameter	Scenario	Regression Coefficient	Correlation Coefficient	Deviation from Theory (%)
Blowdown	RCS Pressure	ROSA-Exp			
		ROSA-R5			
		US-APWR-R5			
	RCS Mass	ROSA-Exp			
		ROSA-R5			
		US-APWR-R5			
Natural Circulation	RCS Mass	ROSA-Exp			
		ROSA-R5			
		US-APWR-R5			
Loop seal	RCS Mass	ROSA-Exp			
		ROSA-R5			
		US-APWR-R5			
Boil-off	RCS Pressure	ROSA-Exp			
		ROSA-R5			
		US-APWR-R5			
	RCS Mass	ROSA-Exp			
		ROSA-R5			
		US-APWR-R5			
Recovery	RCS Mass	ROSA-Exp			
		ROSA-R5			
		US-APWR-R5			

Table 7.3-2 Quantitative Evaluation of Agreement with the Nondimensional Regression Equation for 1-ft^2 CLB case

Phase	Parameter	Scenario	Regression Coefficient	Correlation Coefficient	Deviation from Theory (%)
Blowdown	RCS Pressure	ROSA-Exp			
		ROSA-R5			
		US-APWR-R5			
	RCS Mass	ROSA-Exp			
		ROSA-R5			
		US-APWR-R5			
Boil-off	RCS Pressure	ROSA-Exp			
		ROSA-R5			
		US-APWR-R5			
	RCS Mass	ROSA-Exp			
		ROSA-R5			
		US-APWR-R5			
Recovery	RCS Mass	ROSA-Exp			
		ROSA-R5			
		US-APWR-R5			

Figure 7.3-1 Blowdown Phase: Normalized RCS Pressure for 7.5-in CLB case

Figure 7.3-2 Blowdown Phase: Normalized RCS Pressure for1-ft^2 CLB case

Figure 7.3-3 Blowdown Phase: Normalized RCS Inventory for 7.5-in CLB case

Figure 7.3-4 Blowdown Phase: Normalized RCS Inventory for1-ft^2 CLB case

Figure 7.3-5 Natural Circulation Phase: Normalized RCS Inventory for 7.5-in CLB case

Figure 7.3-6 Loop Seal Clearance Phase: Normalized RCS Inventory for 7.5-in CLB case

Figure 7.3-7 Boil-off Phase: Normalized RCS Inventory for 7.5-in CLB case

Figure 7.3-8 Boil-off Phase: Normalized RCS Inventory for1-ft^2 CLB case

Figure 7.3-9 Boil-off Phase: Normalized RCS Pressure for 7.5-in CLB case

Figure 7.3-10 Boil-off Phase: Normalized RCS Pressure for1-ft^2 CLB case

Figure 7.3-11 Core Recovery Phase: Normalized RCS Inventory for 7.5-in CLB case

Figure 7.3-12 Core Recovery Phase: Normalized RCS Inventory for1-ft^2 CLB case

7.4 Summary

This chapter evaluated the M-RELAP5 code scale-up capability with respect to the code governing equations and numerics, specific models or correlations, and the code integral predictability for the specific transient.

The M-RELAP5 code governing equations and numerics are basically the same as those in the original RELAP5-3D and are concluded to be applicable to the US-APWR SBLOCAs. For the specific models and correlations, the phenomena listed in Table 7.2-1 were evaluated and all the models/correlations are concluded to be applicable to the phenomena.

For the integral evaluation, the M-RELAP5 scale-up capability was assessed using the nondimensional reduced equations developed in the top-down scaling analysis for test facilities. It is concluded that M-RELAP5 has a scale-up capability to US-APWR SBLOCA analysis because the important phenomena during SBLOCA transients considered in the nondimensional reduced equations are reproduced in the US-APWR calculations with M-RELAP5.

7.5 References

7-1 Mitsubishi Heavy Industries, Ltd., 'Small Break LOCA Methodology for US-APWR,' MUAP-07013-P (R1), May 2010.

7-2 'RELAP5-3D Code Manual, Code Structure, System Models, and Solution Methods,' Vol. 1, INEEL-EXT-98-00834, Revision 2.4, June 2005.

7-3 'RELAP5-3D Code Manual, Models and Correlations,' Vol. 4, INEEL-EXT-98-00834, Revision 2.4, June 2005.

7-4 A. S. Shieh et al., 'RELAP5/MOD3 Code Manual, Validation of Numerical Techniques in RELAP5/MOD3,' Vol. 6, NUREG/CR-5535, EGG-2596, October 1994.

7-5 C. D. Fletcher et al., 'Adequacy Evaluation of RELAP5/MOD3, Version 3.2.1.2 for Simulating AP600 Small Break Loss-of-Coolant Accidents,' INEL-96/0400, April 1997 (Non-Proprietary Version).

7-6 'Decay Energy Release Rates Following Shutdown of Uranium-Fueled Thermal Reactors,' Approved by Subcommittee ANS-5, ANS Standards Committee, October 1971.

7-7 NUREG-0800 : STANDARD REVIEW PLAN "9.2.5 ULTIMATE HEAT SINK" Revision 2, July 1981.

7-8 D. C. Groenveld et al., '1986 AECL-UO Critical Heat Flux Lookup Table,' Heat Transfer Engineering, 7, 1-2, pp46-62,1986.

7-9 R. Shumway, New Critical Heat Flux Method for RELAP5/MOD3 Completion Report, EGG-EAST-8443, January 1989.

7-10 M. S. Dougall and W. M. Rohsenow, 'Film Boiling on the Inside of Vertical Tubes with Upward Flow of a Fluid at Low Qualities,' MIT-ME 9079-26, 1963.

7-11 F. W. Dittus and M. K. Boelter, 'Heat Transfer in Automobile Radiators of the Tubular Type,' Publications in Engineering, 2, University of California, Berkley, 1930, pp.443-461.

7-12 W. H. McAdams, 'Heat Transmission', 3rd Edition, New York McGraw-Hill, 1954.

7-13 L. S. Tong and J. Weisman, 'Thermal Analysis of Pressurized Water Reactors,' 2nd Edition, American Nuclear Society, 1979.

7-14 L. A. Bromley, 'Heat Transfer in Stable Film Boiling,' Chemical Engineering Progress, 46, pp.221-227, 1950.

7-15 J. C. Chen et al., 'A Phenomenological Correlation for Post-CHF Heat Transfer', NUREG-0237, June 1977.

7-16 C. R. Hyman et al., 'Experimental Investigations of Bundle Boiloff and Reflood under High-Pressure Low Heat Flux Conditions,' NUREG/CR-2455, ORNL-5846, 1982.

7-17 M.J. Loftus et al., 'PWR FLECHT-SEASET Unblocked Bundle Forced and Gravity Reflood Task Data Report,' NUREG/CR-1532, WCAP-9699, 1980.

7-18 B. Chexal and G. Lellouche, 'A Full-Range Drift-Flux Correlation for Vertical Flow (Revision 1),' EPRI NP-3989-SR, September 1986.

7-19 G. B. Wallis, 'One Dimensional Two Phase Flow,' McGraw-Hill, 1969.

7-20 C. Vallee et al., "Counter-current Flow Limitation Experiments in a Model of the Hot Leg of a Pressurized Water Reactor – Comparison between Low Pressure Air/Water Experiments and High Pressure Steam/Water Experiments," The 13th Int. Topical Meeting on Nuclear Reactor Thermal Hydraulics (NURETH-13), N13P1107, Sep. 2009.

7-21 Mitsubishi Heavy Industries, Ltd., 'M-RELAP5 Code Supplementary Manual Volume IV: Models and Correlations,' 6AS-1E-UAP-090071(R0), UAP-HF-09564,

December 2009.
7-22 C. Smoglie, 'Two-Phase Flow Through Small Branches in a Horizontal Pipe with Stratified Flow,' KfK 3861, Kernforschungszentrum Karlsruhe GmbH (KfK), Karlsruhe, FRG, December 1984.
7-23 T. Maciaszek and A. Menponteil, 'Experimental Study on Phase Separation in a Tee Junction for Steam-Water Stratified Inlet Flow,' Paper C2, European Two-Phase Flow Working Group Meeting, Munich, FRG, June 10-13, 1986.
7-24 V. E. Schrock, et al., 'Small Break Critical Discharge - The Role of Vapor and Liquid Entrainment in a Stratified Two-Phase Region Upstream of the Break,' NUREG/CR-4761, LBL-22024, Lawrence Berkeley Laboratory, December 1986.
7-25 J. L. Anderson and R. L. Benedetti, 'Critical Flow Through Small Pipe Breaks,' EPRI NP-4532, Idaho National Engineering Laboratory, May 1986.

8. EVALUATIONS

This chapter summarizes the overview of all phases analyzed in Chapter 6 and important thermal-hydraulic phenomena identified in each phase based on the top-down and the bottom-up scaling analyses.

Table 8-1 shows the summary of definition of phase boundary and applied scaling approach among the US-APWR two break cases and the ROSA/LSTF two IETs. In the smaller break size case where the loop seal PCT was observed, all the typical phases for the SBLOCAs are realized and the same mechanism can be applied for the transition of each phase boundary of the two systems. On the other hand for the 1-ft^2 break case, core heat up and quenching during depleting the liquid head along loop seal were not observed and the PCT occurred during the boil-off phase. In this report, MHI judged that no natural circulation or loop seal clearance phases existed for the 1-ft^2 break case and the time period after the blowdown phase was analyzed as the boil-off phase. The boundary was defined as the transition from subcooled discharge at break to saturated.

Figure 8-1 compares the relation between P* vs. M* which are the RCS pressure and mass inventory nondimensionalized using the initial value for all the cases. The trajectories for each break size follow similar paths down to M* of about 0.3. After that there are differences attributed to differences in break flow and ECC flow. In the blowdown phase, the pressure decreasing rate of the US-APWR 1-ft^2 CLB just after the break initiation is lower and the difference relative to the ROSA/LSTF was caused by a larger q_{net}. The scaling distortion including this difference was discussed in Section 6.1.2.6 and no significant impacts on the safety issues were observed. In the period around the boundary between the boil-off and the recovery phases, the trajectory is somewhat scattered. This is mainly caused by the different assumption for ECCS activation, for example', that no high pressure SI was assumed in the ROSA/LSTF SB-CL-18.

Table 8-2 relates the high-ranked phenomena and processes with the applied scaling approach, and with the experimental test data used in the M-RELAP5 code assessment.

For the blowdown phase, the US-APWR PIRT table (Table 5.1-1) identifies the break flow and the SG heat transfer as important phenomena and processes. Scaling of the break flow in the ROSA/LSTF SB-CL-18 and IB-CL-02 tests is addressed by the top-down approach for the blowdown phase and the scaling distortion just after the break initiation was discussed in Section 6.1.2.6. The applicability of the M-RELAP5 break flow model was also examined using the ROSA/LSTF measurements in the bottom-up scaling Section 6.1.3. It was confirmed from the analyses that no significant safety concerns result from the distortion. The SG heat transfer is addressed in the top-down scaling based on the mass and energy conservations along with the break flow. Although the contribution of q_{net} (q_{core} – q_{SG}) is slightly different between the US-APWR and the ROSA/LSTF, no significant impacts were identified. The top-down scaling analysis showed that the blowdown behavior in the US-APWR SBLOCAs is scalable to that observed in the ROSA test, which is used in validation for the M-RELAP5 SG heat transfer model.

For the natural circulation phase, the SG heat transfer is also addressed in the top-down scaling based on the mass and energy conservations along with the break flow, which demonstrated that the RCS mass inventory and pressure behaviors in the ROSA/LSTF SB-CL-18 test are scalable to those in the US-APWR SBLOCAs. In addition, similitude of

the momentum balance, including the downcomer and lower plenum static head, between the ROSA test and US-APWR SBLOCA was assessed based on the top-down approach.

The complicated behaviors expected during the US-APWR loop seal clearance phase were examined both by the top-down and bottom-up approach. The loop seal clearing behavior was addressed with static pressure and mass balances over the RCS using the top-down approach. The important local phenomena and processes such as the flooding limit in the SG U-tubes were investigated using the bottom-up approach by examining scalabilities for the facility geometry and experimental conditions.

For the boil-off phase, scaling of the global RCS mass and pressure responses were addressed using the top-down approach based on the mass and energy conservation, while scaling of the other local important phenomena and processes was examined using the bottom-up approach. The ROSA/LSTF test results were assessed to be representative of the US-APWR response. The CHF and post CHF heat transfer, and the two phase mixture level response were evaluated using bottom-up scaling and used data from the THTF test facility. The THTF heat transfer and level conditions were found to cover the range of conditions expected in the US-APWR.

For the recovery phase the top-down approach based on the mass conservation was applied to the scaling analysis for the RCS mass inventory response. The recovery responses in the ROSA/LSTF tests were found to be scalable to the US-APWR responses. The bottom-up approach was used to examine scalability of the rewetting and reflood processes using data from the THTF and FLECHT-SEASET test facilities. The experimental conditions in those facilities were shown to cover the range of conditions in the US-APWR recovery phase response.

All these scaling results showed that the ROSA/LSTF SB-CL-18 and IB-CL-02 tests can be scaled to the US-APWR SBLOCA, and the other Separate Effects Tests are also applicable to US-APWR SBLOCAs from the viewpoint of the test facility geometry and experimental conditions. It is noted that several important phenomena and processes such as the local power were not addressed for the present phase, since these are applied to the plant analysis with conservative assumptions.

From the code scale-up capability point of view, all the primary constitutive models and correlations were independently examined by the bottom-up approach, while the integrated code applicability was quantitatively investigated by the top-down approach. These demonstrated that there is no significant concern on M-RELAP5 application to US-APWR SBLOCA analyses.

Table 8-1 Summary of Definition of Phase Boundary and Applied Scaling Approach among US-APWR two break cases and ROSA/LSTF two IETs

Table 8-2 Relation between PIRT/AM and Applied Scaling Method (Governing Equations in Top-Down Scaling)

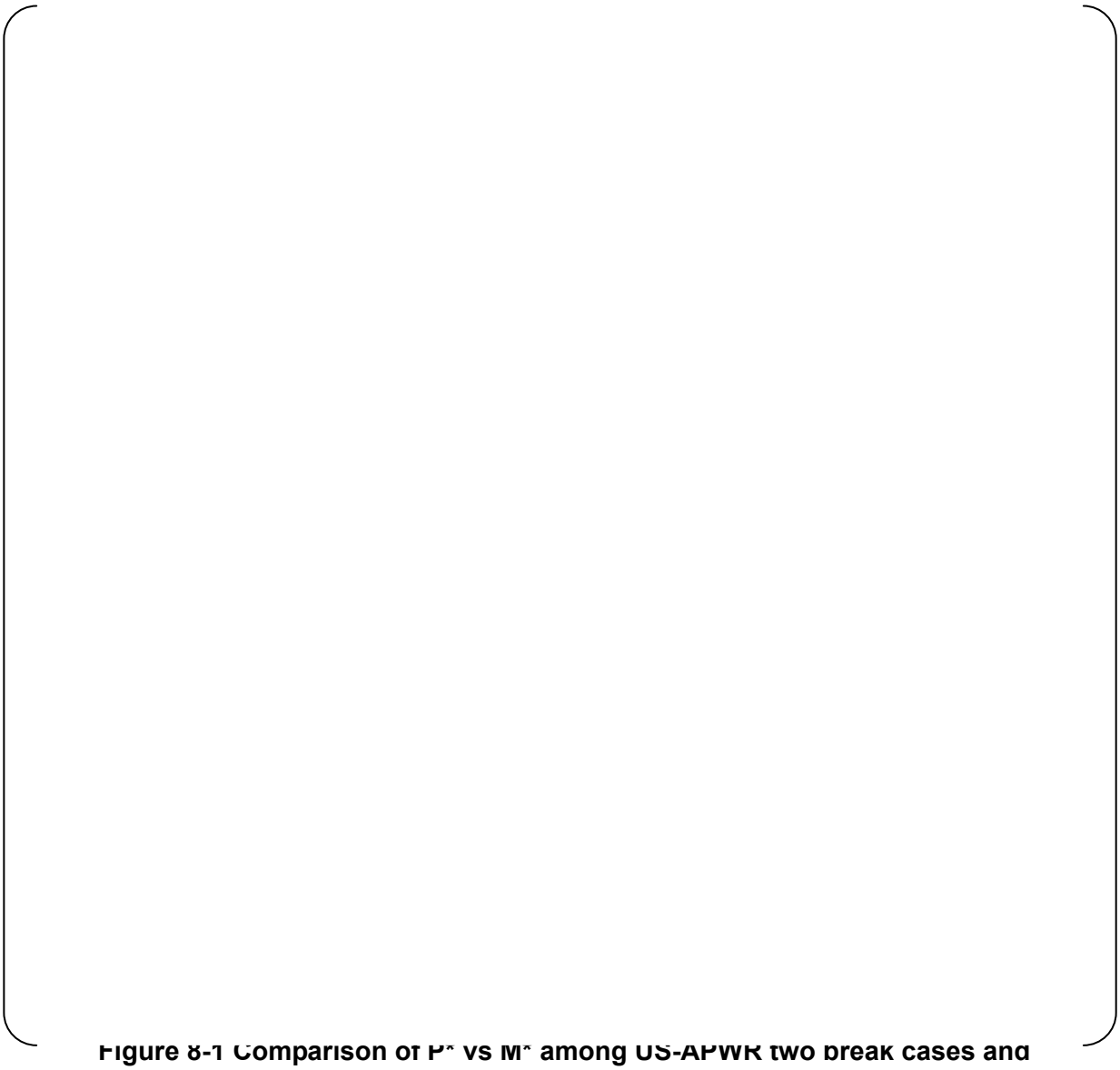

Figure 8-1 Comparison of P^* vs M^* among US-APWR two break cases and ROSA/LSTF two IETs (Measurement)

9. SUMMARY AND CONCLUSIONS

Quantitative scaling analyses based on the hierarchical two-tiered scaling (H2TS) methodology have been performed to complete the M-RELAP5 development and assessment which is required in EMDAP. Specifically, the IET and SET facilities and experimental data were evaluated by the top-down and bottom-up approaches to respond to Step 6 in Element 2 of EMDAP "*Perform Scaling Analysis and Identify Similarity Criteria*", which demonstrates whether similar thermal-hydraulic behaviors expected in US-APWR are also observed in the scaled test facilities. Here, the top-down scaling approach evaluated the global system behaviors and system interactions from ROSA/LSTF, and addressed the similarity between the ROSA/LSTF and US-APWR. On the other hand, the bottom-up scaling analyses addressed the issues raised in the plant- and transient-specific PIRT related to localized behaviors, where SETs in the code assessment matrix are examined.

Blowdown phase
The depressurization characteristic is important and the US-APWR depressurization is primarily controlled by the outflow from the break for a smaller break size where the loop seal PCT is likely to occur. And the outflow from the break and the net heat input from the core and the SG becomes significant under 1-ft^2 break case where the boil-off PCT is important. The same mechanism is also dominant in the ROSA/LSTF test. This similitude was evaluated by the ranking of the relevant nondimensional group, whether most important parameter is the same and the order of ranking is similar, resulting in the conclusion that the ROSA/LSTF is a scalable test facility to the US-APWR during the blowdown phase.

Natural circulation phase
The mass inventory is important and the significant nondimensional groups relating break flowrate and break flow enthalpy were identified and quantified, showing the ROSA/LSTF is a scalable test facility to the US-APWR during the natural circulation phase. Similarly, the integral momentum balance through the system was quantified both for the US-APWR and ROSA/LSTF, which demonstrated that the similarity is acceptable.

The bottom-up approach was simultaneously employed for the steam generation in core, two-phase flow regime and time scale in the piping for the US-APWR and ROSA/LSTF and the bottom-up scaling showed that there are no significant scaling distortion.

Loop seal clearance phase
The core liquid level is important and the liquid level behavior in the US-APWR was examined and compared with that in the ROSA/LSTF using nondimensional equations to quantitatively evaluate the scalability between the two systems. The core liquid level was primarily controlled by the CCFL induced liquid head in the uphill side of SG U-tubes and inlet plena, and by the head balance caused by the distribution of liquid along the loop seal. The same mechanisms are dominant for both the US-APWR and ROSA/LSTF test, but the core liquid level is likely to be more depressed in ROSA/LSTF compared to the US-APWR. This different characteristic is mainly caused by the geometrical difference in the depth of loop seal. The scalability of the CCFL along the uphill side of SG U-tubes was confirmed through the bottom-up scaling evaluation. The adequacy of loop seal behavior predicted for the US-APWR was also confirmed by the assessment for the residual water prediction in UPTF tests.

Boil-off phase

The mass inventory and pressure responses are important. The top-down scaling analysis demonstrated that the controlling mechanism for both responses are the same for the ROSA/LSTF and the US-APWR and the similitude between the two systems was confirmed comparing the order of magnitude of nondimensional parameters.

The bottom-up approach was simultaneously employed for CHF/dryout, uncovered heat transfer, and two-phase mixture level. In the M-RELAP5 code assessment, the models related to the above phenomena and processes have been validated by using test data obtained in the ORNL/THTF and the ROSA/LSTF. The present study evaluated the geometrical scaling of the test facility to the US-APWR, and showed no significant distortion. Simultaneously, the experimental test conditions, pressure, temperature, flowrate, and power, were compared with those expected in the various US-APWR SBLOCAs, showing that the US-APWR SBLOCAs conditions were well covered by the selected experimental tests.

Core recovery phase

The mass inventory and the core reflooding behavior are important and the former parameter was examined using the top-down approach and the latter local thermal-hydraulic behavior was assessed using the bottom-up approach. The top-down scaling analysis showed that the ROSA/LSTF is a scalable test facility with respect to the mass response of the US-APWR. In the bottom-up scaling analysis, the present study showed that the primary dimensions of the SET facilities employed here are well scaled to the US-APWR design, and the experimental test conditions adequately cover the range of conditions expected for the US-APWR.

Code scale-up capability

The M-RELAP5 code scale-up capability was examined by the bottom-up and top-down approaches and was confirmed to be applicable to the US-APWR SBLOCAs through the examination. The scalability of the governing equations and numerics, specific models or correlations were evaluated, and the scalability of the integrated code predictability both for the US-APWR SBLOCAs and ROSA/LSTF was also assessed from the top-down point of view using reduced equations for each phase.

From the above evaluations, it was concluded that the IET and SET experimental data are adequate to assess the M-RELAP5 applicability to US-APWR SBLOCAs without any significant scaling distortions, and that M-RELAP5 possesses scale-up capabilities from the experimental tests to the plant transient.

Appendix A TABELS OF USEFUL US-APWR AND ROSA/LSTF PARAMETERS

Tables of geometric and operational parameters for the US-APWR and the ROSA/LSTF facility are included in this appendix. Primary design parameters of the plant/test facility are summarized in Table A-1. Component elevation and component fluid volume are indicated in Table A-2 and Table A-3, respectively. Table A-4 shows hydraulic resistances where the value is relatively large.

Table A-1 Primary Parameters of the Plant/Test Facility

Parameters/Components	US-APWR	ROSA/LSTF	Ratio
Primary volume (m^3)		6.000	
Initial pressurizer pressure (MPa)	15.5	15.5	1.0
Initial hot leg temp (K)	598.15	599	0.999
Initial cold leg temp (K)	561.25	A:563,B:564	A:0.997, B:0.995
Initial RCS flowrate (kg/s)		48.7	
Initial core bypass flowrate (kg/s)		N/A	
Initial core power (MW)	4451	10	445.1
Reactor Vessel			
Inside diameter (m)		0.640	
Core height (m)		3.66	
Lower plenum max height (m)		2.361	
avg. height from volume (m)		1.901	
Upper plenum height (m)		2.126	
Upper head max height (m)		2.126	
avg. height from volume (m)		1.585	
Downcomer gap (m)		0.053	
Core heated flow area (m^2)		0.1134 (below spacer)	
Core bypass flow area (m^2)		N/A	
Downcomer flow area (m^2)		0.09774	
Hot Legs			
Inner diameter (m)		0.207	
Length (m)		3.686	
Cold Legs			
Inner diameter (m)		0.207	
Length (m)		3.438	

Table A-1 Primary Parameters of the Plant/Test Facility (Cont'd)

Parameters/Components	US-APWR	ROSA/LSTF	Ratio
Steam Generators			
Total plenum volume (m^3)		0.348 (0.695:incl. filler block)	
Plenum height (m)		0.706 (1.823:incl. filler block)	
Tube-sheet thickness (m)		0.322	
Tube ID (mm)		19.6	
Tube wall thickness (mm)		2.9	
Number of tubes		141	
Height of the tallest tube bend above tube sheet (m)		10.620	
Height of the shortest tube bend above tube sheet (m)		9.156	
Tube volume (m^3)		0.8384	
Secondary pressure (MPa)		A: 7.3,B: 7.4	
Heat transfer rate (MW)		35.7	
Pressurizer			
Tank ID (m)		0.6	
Volume (m^3)		1.147	
Height (m)		4.187	
Surge line ID (mm)		66.9	
Surge line length (m)		20.15	
Surge line volume (m^3)		0.07081	
Liquid level (m)		2.7	
DVI/HHIS			
Inlet line ID (mm)		N/A	
Inlet line length (m)		N/A	
Number		N/A	
Accumulator			
Tank volume (m^3)		4.8	
Discharge line ID (mm)		97.1	
Discharge line length (m)			

Table A-2 Component Elevations of Plant/Test Facility (m)
(Relative to Hot Leg Center Line)

Components	US-APWR	ROSA/LSTF
Bottom of lower plenum	[redacted]	-7.864
Downcomer bottom	[redacted]	-5.503
Downcomer top	[redacted]	1.693
Bottom of heated length	[redacted]	-5.503
Top of heated length	[redacted]	-1.843
Bottom of upper head	[redacted]	0.9712
DVI nozzle centerline	[redacted]	N/A
Hot leg centerline	[redacted]	0
Cold leg centerline	[redacted]	0
Pressurizer bottom	[redacted]	11.79
Pressurizer top	[redacted]	15.99
Top of SG tubesheet	[redacted]	2.461
Top of U-tubes (tall)	[redacted]	13.08
Top of U-tubes (short)	[redacted]	11.62
Bottom of accumulator	[redacted]	3.000
Crossover leg centerline	[redacted]	-3.718
Top of accumulator	[redacted]	10.04

Table A-3 Component Fluid Volume Distributions of Plant/Test Facility (m^3)

Component	US-APWR	ROSA/LSTF
Downcomer		0.693
Lower plenum		0.580
Core heated part		0.408
Core bypass region (inc. NR)		0
Upper plenum		0.484 0.5472(incl. Endbox)
Upper head		0.510
Hot leg (1/4)		0.124
Crossover leg (1/4)		0.212
Cold leg (1/4)		0.116
RCP(1/4)		0.024
Accumulator (1/4)		4.8
Accumulator (1/4) (liquid)		3.188
Pressurizer		1.147
Pressurizer(liquid)		0.763
PZR surge line		0.0708
Total (include ACC tank) (+PZR)		12.02
Total (include ACC liquid) (+PZR)		7.981
Total (no ACC) (+PZR)		7.217
Total (include ACC tank)		10.80
Total (include ACC liquid)		6.763
Total (no ACC)		6.000

Table A-4 Hydraulic Resistances of Plant/Test Facility

Components*	US-APWR (m^{-4})	ROSA/LSTF (m^{-4})
CL nozzles		A: 1.755e+2 B: 1.774e+2
Downcomer		3.912e+2
Lower plenum		2.618e+2
Core inlet		2.257e+2
Core		1.215e+3
Core outlet		3.043e+2
Upper plenum		Small
HL nozzles		A: 1.188e+3 B: 8.096e+2
SG U-tubes		A: 3.845e+3 (Average) B: 4.003e+3 (Average)
Crossover leg		A: 2.261e+3 B: 2.435e+3

*Hydraulic resistance defined below:

$$R = \frac{\Delta P \cdot \rho}{m^2}$$

ΔP : Differential pressure (Pa)
ρ : Density (kg/m^3)
m : Mass flow rate (kg/s)